

Phonon excitations in quasicrystals

M. Quilichini

Laboratoire Léon Brillouin, (CEA-CNRS) Commissariat à l'Energie Atomique de Saclay,
91191 Gif-sur-Yvette, France

T. Janssen

Institute for Theoretical Physics, University of Nijmegen, 6525ED, Nijmegen,
The Netherlands

Recent progress concerning lattice dynamics in quasicrystals, both theoretical and experimental, is discussed. The theory deals with the general description, which differs from that for ordinary crystals, and with model calculations and rigorous results for one-, two-, and three-dimensional systems. Experimental results are restricted mainly to quasicrystals with icosahedral symmetry.
[S0034-6861(97)00201-8]

CONTENTS

I. Introduction	277
II. Theoretical Considerations	278
A. The problem	278
B. Quasicrystals	281
C. Scaling properties	286
D. Studies with one-dimensional models	287
E. Electrons in quasicrystals	289
F. Two-dimensional phonon models	290
G. Icosahedral structures	292
H. Three-dimensional models	293
III. Experimental Results	297
A. Neutron scattering from icosahedral quasicrystalline phases measured with a three-axis spectrometer: Introduction	297
B. Results for $Al_{63}Cu_{25}Fe_{12}$	300
C. Results for $Al_{60.3}Cu_{10.5}Li_{29.2}$	300
D. Results for $Al_{68.7}Pd_{21.7}Mn_{9.6}$	302
E. Conclusions from three-axis experiments	305
F. Ultrasonic and Brillouin measurements	307
1. Introduction	307
2. $Al_{5.1}CuLi_3$	307
3. $Al_{68.7}Mn_{9.6}Pd_{21.7}$	307
4. Brillouin spectroscopy experiments	308
G. Time-of-flight experiments	308
1. Introduction	308
2. Generalized vibrational density of states and total dynamic structure factor	308
3. "Phason hopping"	311
IV. Concluding Remarks	312
Acknowledgments	312
References	313

I. INTRODUCTION

Quasicrystals, which were discovered in 1984, have aroused great excitement because they are a challenge to crystallographic analysis, showing at the same time sharp diffraction peaks and a point-group symmetry that is incompatible with lattice periodicity. One central question concerns the way in which their remarkable structural characteristics affect physical properties. The purpose of the present paper is to describe theoretical and experimental results concerning the lattice dynamics of quasicrystals.

Quasicrystals were first encountered in AlMn alloys obtained by rapid solidification from the melt. Shechtman *et al.* (1984) reported electron-diffraction patterns that consisted of sharp Bragg peaks and that displayed an icosahedral point-group symmetry. The former showed that there was long-range order, whereas the latter excluded lattice translation symmetry. Since this first experiment, quasicrystalline phases have been found in many metallic alloys, but very often the degree of quasicrystallinity was low due to the existence of a second phase and of a high density of (phason) defects. Besides quasicrystals with icosahedral symmetry, others have been found with octagonal, decagonal, dodecagonal, or tetrahedral point-group symmetries. New stable icosahedral alloys with a high degree of quasicrystallinity have been discovered by Tsai and coworkers (Tsai *et al.*, 1987a, 1987b) in AlCuTM (TM=V, Cr, Fe, Ru, Os) ternary alloys. And recently a stable quasicrystalline phase in AlMnPd and AlPdRe alloys has been reported (Tsai *et al.*, 1990). On the basis of thermodynamic data, it is presumed that strong chemical-order bonding between Pd and Al or Mn prevents the $Al_{70}Pd_{20}Mn_{10}$ quasicrystal from generating atomic disorder and phason strains during solidification.

The quasicrystalline structure seems to be very close in energy to other structures. Therefore, depending upon the preparation conditions, the composition, and the thermal history, AlFeCu alloys can be observed, even at room temperature, either in a perfect quasicrystalline state without any indication of phason strain (static disorder) or in a microcrystalline twin state with an overall pseudo-icosahedral symmetry, and indeed have been observed by Audier and Guyot (1990), Calvayrac *et al.* (1990), and Denoyer *et al.* (1990), and Dubois *et al.* (1991). The periodic microcrystalline structure has a rhombohedral unit cell. The coherent microdomains have orientational relationships that have been identified in AlFeCu by high-resolution microscopy and that create a perfect mean icosahedral orientational order.

Since the discovery of quasicrystals, significant progress has been made in determining their structural and static properties (Boudard *et al.*, 1992; Corner-Quiquandon *et al.*, 1991; Elcoro *et al.*, 1994; Janot *et al.*,

1989) even though atomic positions are not yet precisely known. However, the understanding of their dynamical properties is still rather limited. Because quasicrystals are often presented as an intermediate state between a periodic and a random system, one of the first questions that arises is how waves propagate in these quasiperiodic systems. In this paper we shall focus on lattice vibrations in a quasiperiodic medium and we shall review what is known up to now theoretically for specific models and experimentally for three well-studied systems, AlFeCu, AlCuLi, and AlMnPd. These all have icosahedral symmetry. It has not yet been possible to synthesize quasicrystals with other symmetries of sufficiently large size for study. A brief review on the dynamical properties of the icosahedral AlMnPd system has already been given by Suck (1993b).

This paper is organized as follows. First, in Sec. II, we define the problem we are facing and the questions that arise when one deals with the dynamics of quasiperiodic structures; then the results of some specific models are presented. In Sec. III, we review the experimental results available up to now—for the most part from neutron experiments. Finally, we summarize our review with some concluding remarks.

II. THEORETICAL CONSIDERATIONS

A. The problem

For ordinary lattice periodic crystals, the oscillations of the atoms around their equilibrium positions can be described in terms of elementary excitations, the phonons. These are propagating waves with a well-defined frequency and wave vector. The number of degrees of freedom in each unit cell is finite, three times the number s of particles in the unit cell. Although the atoms are all coupled together, the infinite-dimensional lattice-vibration problem is reduced to a finite-dimensional one if one uses the lattice periodicity. The modes are characterized by a wave vector, which can be restricted to the first Brillouin zone, and a branch label. The spectrum consists of bands. The $3s$ -dimensional dynamical matrices for different wave vectors decouple. The motion of particles connected by a lattice translation and moving in one mode differ only by a phase factor in going from one unit cell to another. Therefore the vibrations are extended, in contrast to the localized modes one sometimes finds in disordered systems.

In recent decades, systems without lattice periodicity, but with a great deal of (quasiperiodic) ordering have been studied. We call a system quasiperiodic if its diffraction pattern has sharp Bragg peaks at positions that are linear integer combinations of a finite number of basis vectors:

$$\vec{H} = \sum_{j=1}^n h_j \vec{a}_j^*, \quad h_j \in \mathbb{Z}. \quad (2.1)$$

In other words, the peaks can be indexed by a finite number of integers. If this number is 3 and the three

basis vectors \vec{a}_j^* are not in one plane, this is a lattice periodic structure; otherwise it is not. If there is no lattice periodicity, there is no proper Brillouin zone. This leads immediately to the question of whether in such systems there are also propagating waves, and what the difference is in dynamics between lattice periodic systems and aperiodic (but quasiperiodic) systems. In particular, one can ask about the character of the spectrum and the existence of extended and localized modes. The existence of systems without lattice periodicity has been known for a longer time in the case of incommensurately modulated crystal (IC) phases. A review of experimental and theoretical results for phonons in IC phases was given by Currat and Janssen (1988). We give here a short summary and later compare the situation with that in quasicrystals.

An IC phase can be described as a lattice periodic structure with a periodic deformation. For the simplest case of a displacively modulated IC phase, this means that the positions of the atoms are given by

$$\vec{r}_{nj} = \vec{n} + \vec{r}_j + \vec{f}_j(\vec{Q} \cdot \vec{n}), \quad (2.2)$$

where \vec{n} is a lattice vector, \vec{r}_j the position of the j th atom in the unit cell, f_j a periodic function with period 2π , and \vec{Q} a vector with irrational components with respect to the reciprocal lattice. Typically, such a phase originates at a temperature T_i via a soft mode with wave vector \vec{Q} and branch label ν . Then, for T decreasing towards T_i , the frequency $\omega_{\vec{Q}\nu}$ goes to zero, and just below T_i one has

$$\vec{f}_j(\vec{Q} \cdot \vec{n}) = X_{\vec{Q}\nu} e^{i\vec{Q} \cdot \vec{n}} \vec{\epsilon}(\vec{Q}\nu|j) + \text{c.c.} \quad (2.3)$$

for an eigenmode $(\vec{Q}\nu)$ with eigenvector $\vec{\epsilon}(\vec{Q}\nu)$ and normal coordinate $X_{\vec{Q}\nu}$. For lower temperatures the modulation function f_j gets higher harmonics as well. Very often there is a new phase transition at T_c towards a commensurate phase. Near T_c , the modulation can be described as an arrangement of nearly periodic domains separated by domain walls called discommensurations. The distance between these is such that there is no overall lattice periodicity and that, as in the case of sinusoidal modulation [Eq. (2.3)], the diffraction pattern shows peaks at positions $K + m\vec{Q}$, where K is a reciprocal lattice vector of the basic structure and m an integer. The existence of a soft mode is an idealization that is seldomly realized. However, such soft modes have indeed been observed in a number of compounds, such as biphenyl (Cailleau, 1985) and ThBr₄ (Bernard *et al.*, 1983).

In the incommensurate phase there are new types of excitations that do not occur in lattice periodic crystals. Because of the incommensurability, the position of the modulation wave is irrelevant: one may shift the wave with respect to the lattice without changing the energy. This implies that there is, besides the three ordinary infinite-wavelength excitations of zero frequency, another zero-frequency mode, called the phason. At T_i the modes with wave vector near \vec{Q} have for the lowest branch a parabolic dispersion: $\omega \approx \alpha(k - \vec{Q})^2$. Since the branches near \vec{Q} and $-\vec{Q}$ are degenerate and coupled,

the new eigenmodes are symmetric and antisymmetric combinations of the old ones. For $T < T_i$ there is a branch starting at $k - \vec{Q} = 0$ with zero frequency, the phason branch, and a branch with higher frequency, the amplitude branch. These correspond, respectively, to fluctuations in the phase and the amplitude of the modulation function. The minimum of the latter has zero frequency only at T_i . The phason branch starts at zero as long as the IC phase is in the sinusoidal region (see, for example, Moussa *et al.*, 1987). There has been a long discussion in the literature about the existence of a phason gap (Blinic *et al.*, 1986). Some experiments seem to indicate that the phason branch does not completely go to zero, but stops at a nonzero frequency. NMR measurements give an indication for a value of 70 GHz or more for the phason gap. Only in smectic liquid crystals has a vanishing gap been shown unambiguously (Blinic *et al.*, 1986).

These branches are the only ones that change qualitatively. For the other branches, one may see the modulation as a perturbation, with the modulation amplitude as a parameter. Because modes of the old system become coupled by the modulation if their wave vectors differ by a multiple of \vec{Q} , there are quantitative changes, but the overall picture remains the same. One can use the Brillouin zone of the basic structure for the characterization of the eigenmodes. The difference is that the pseudo-momentum is not a good quantum number (there is coupling with other modes differing by a multiple of \vec{Q} in the wave vector), and the dispersion curves are not smooth, but show gaps.

This can be seen in the dynamic structure factor $S(\vec{q}, \omega)$. Above T_i there are acoustic branches starting from every reciprocal-lattice point. Below T_i new branches appear starting at $\omega = 0$ and $\vec{q} = m\vec{Q}$ (modulo reciprocal-lattice vectors of the basis structure). Near T_i where the amplitude of the modulation is small and only first-order satellites ($m = \pm 1$) are observed, the relevant new branches start at $\omega = 0$ and $\vec{q} = \pm \vec{Q}$. Near the lock-in transition at T_c , however, the coupling between the modes becomes stronger, higher-order satellites appear, and many new branches can be observed for $|m| > 1$ in $S(\vec{q}, \omega)$ (Janssen and Currat, 1987). The function $S(\vec{q}, \omega)$ then has a very complicated structure: its non-negligible values are not restricted to a small number of curves in the (\vec{q}, ω) plane but appear everywhere (Fig. 1).

Because *a priori* the lattice dynamics of quasiperiodic IC phases are different from those of periodic systems, researchers have studied the behavior of simple models. The idea is that, if there is a fundamental difference in phonon characteristics between lattice periodic and quasiperiodic systems, this should show up already in such models. The simplest are linear-chain models. If $u_n \exp(i\omega t) + \text{c.c.}$ is the displacement of the n th particle in a chain, and the n th and $(n-1)$ th particles are connected by a spring with constant α_n , the equations of motion read

$$m_n \omega^2 u_n = \alpha_n (u_n - u_{n-1}) + \alpha_{n+1} (u_n - u_{n+1}). \quad (2.4)$$

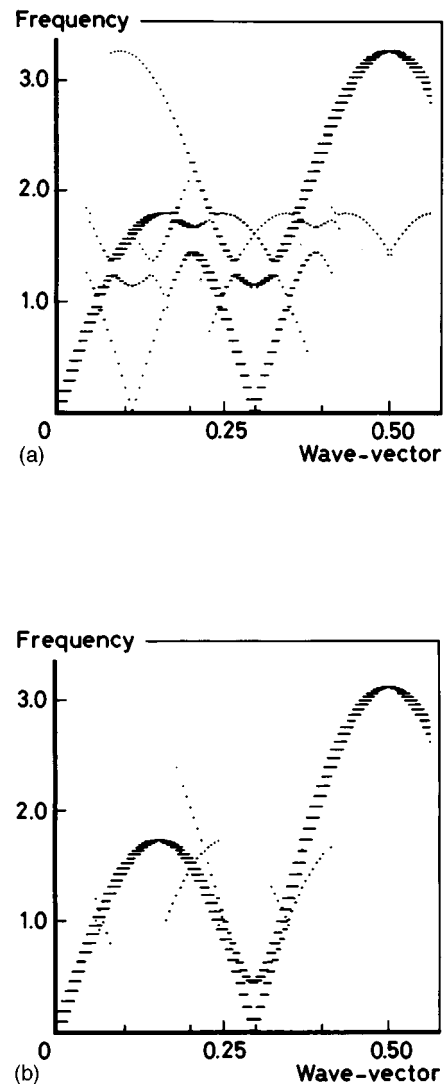


FIG. 1. Dynamic structure factor for an IC phase: (a) for sinusoidal modulation of small amplitude; (b) in the discommensuration regime. The modulus of the dynamic structure factor is indicated by the length of the horizontal strokes. If one plots this vertically one obtains a surface $S(q, \omega)$ above the q - ω plane. Compare this with the $S(q, \omega)$ for a quasicrystal in Fig. 9. Wave vectors are in units of the basis of the reciprocal lattice of the basic structure. Frequencies in a.u.

The sequence $\{\alpha_n\}$ or $\{m_n\}$ is taken to be quasiperiodic. Because the idea is that the periodic modulation influences the spring constants, this is a model for an IC phase. For each value of ω there are two solutions, but they are only physically allowed if the solution u_n does not grow faster than a polynomial as n goes to $\pm\infty$. A value of ω for which there is an allowed solution is said to belong to the spectrum. For a lattice periodic chain this is only the case when u_n is bounded. The number of degrees of freedom for a quasiperiodic system is infinite, and this number is not reduced by the n -dimensional translation symmetry. Therefore the determination of the eigenvibrations comes down to the eigenvalue problem of an infinite-dimensional matrix. A number of techniques have been used to attack this problem. The first

one is the use of periodic approximants. In this approach, one considers a series of rational numbers L_n/N_n tending to the irrational value $Q/2\pi$ of the modulation. For each periodic approximant, one can determine the spectrum and the eigenvectors by solving an N_n -dimensional problem. If these quantities tend to a limit when n tends to infinity, the limit is supposed to be the value for the incommensurate case.

Alternatively, one may use finite clusters from the quasiperiodic structure and let the size of these clusters go to infinity. For the periodic and cluster approximants, the dimension of the dynamical matrix grows exponentially. On the other hand, the matrix is sparse—it has many zeros. This fact is used in the moment method (Benoit *et al.*, 1990), the Lanczos method and its variations (Cullum and Willoughby, 1985), and the recursion method (Haydock *et al.*, 1980).

A third technique, which can be used for chains, uses a transfer matrix. If the Hamiltonian is written as

$$H = \sum_n \left\{ \frac{p_n^2}{2m_n} + \frac{\alpha_n}{2} (u_n - u_{n-1})^2 \right\}, \quad (2.5)$$

the equations of motion are given by Eq. (2.4). Consider first the case in which the incommensurability is in the coupling constants ($m_n = m$); we introduce $Q_n = \alpha_n(u_n - u_{n-1})$. Then one has the relation

$$Q_{n-1} - 2Q_n + Q_{n+1} + \frac{m\omega^2}{\alpha_n} Q_n = 0. \quad (2.6)$$

Notice that the first three terms correspond to a discrete version of the second derivative. When one expresses Q_{n+1} in terms of Q_n and Q_{n-1} , one can write

$$\begin{pmatrix} Q_{n+1} \\ Q_n \end{pmatrix} = T_n \begin{pmatrix} Q_n \\ Q_{n-1} \end{pmatrix}, \quad T_n = \begin{pmatrix} 2 - m\omega^2/\alpha_n & -1 \\ 1 & 0 \end{pmatrix}. \quad (2.7)$$

Such a matrix T_n is a transfer matrix. From the relation above follows the relation

$$\begin{pmatrix} Q_{n+N+1} \\ Q_{n+N} \end{pmatrix} = \prod_{p=1}^{N+1} T_{n+p-1} \begin{pmatrix} Q_n \\ Q_{n-1} \end{pmatrix}. \quad (2.8)$$

Every value of ω for which the displacements u_n remain bounded—which is the case if the trace of the product of T_n 's remains between -2 and $+2$ —is in the spectrum. In principle, this gives a way to determine the spectrum. This method is especially useful for one-dimensional systems.

When the incommensurability is in the masses ($\alpha_n = \alpha$), one may derive from Eq. (2.4) the recurrence relation

$$u_{n+1} = (2 - m_n\omega^2/\alpha)u_n - u_{n-1}, \quad (2.9)$$

which gives the mapping

$$\begin{pmatrix} u_{n+1} \\ u_n \end{pmatrix} = T_n \begin{pmatrix} u_n \\ u_{n-1} \end{pmatrix}, \quad T_n = \begin{pmatrix} 2 - m_n\omega^2/\alpha & -1 \\ 1 & 0 \end{pmatrix}, \quad (2.10)$$

and one can determine the spectrum in the same way as in the case of the modulated spring constants. Of course, this is nothing but the general duality between two harmonic chains with nearest-neighbor coupling, one with masses m_n and spring constants α_n , and one with masses a^2/α_n and spring constants a^2/m_n (Toda, 1966).

The simplest modulated-chain model takes $m_n = m$ and

$$\alpha_n = \alpha[1 + \delta \cos(Qn + \phi)] \quad (2.11)$$

in Eq. (2.4), with δ being the modulation amplitude. Numerically, researchers have observed the appearance of an infinite number of gaps in the dispersion curve (de Lange and Janssen, 1981). If one develops $Q/2\pi$ in a continued fraction expansion, the main gaps correspond to those one finds in truncating this series after a few terms; smaller gaps correspond to higher orders.

The gaps tend rapidly to zero and the spectrum has a limit. In the limit spectrum one finds a scaling behavior: a part of the spectrum is a scaled-down version of the whole spectrum (de Lange and Janssen, 1981). For example, if one multiplies the lowest part of the spectrum for the n th approximant by the appropriate factor, one finds the lower part of the $(n-1)$ th approximant. This shows that there are gaps at arbitrarily low frequencies, but the size of the gaps goes exponentially to zero. This scaling behavior (Figs. 2 and 3) is very similar to that in the spectrum of an electron in a crystal in an external magnetic field (Hofstadter, 1976). The analysis of spectral properties will be discussed later on.

Because of Bloch's theorem, one knows that in one mode, the motion of particles connected by a lattice translation differs only in the phase. This excludes localized states in perfect lattice periodic crystals. Therefore the modes in the rational approximants are strictly extended, but their limit behavior may be different. For low frequencies and small δ , the eigenvectors are still extended, but a careful multifractal analysis for the case $\delta=1$ (and $\phi=\pi/2$) shows that the states are neither extended nor (exponentially) localized (Janssen and Kohmoto, 1988). Their character is termed critical. Contrary to the periodic case, allowed solutions of Eq. (2.4) for quasiperiodic systems can be extended, localized, and critical (or pseudolocalized—see, for example, de Lange and Janssen, 1984, where this characterization is given in superspace terms). We recall that generally a spectrum has three contributions: a point spectrum and a continuous spectrum, where for the latter one may distinguish an absolute continuous and a singular continuous spectrum. Eigenvectors that are normalizable belong to the point spectrum: they describe localized states. Allowed states belonging to the continuous spectrum are delocalized. If one considers the integrated density of states $I(\omega)$, i.e., the fraction of eigenmodes with frequency smaller than ω , these three parts correspond to a function consisting purely of jumps, a smooth continuous function, and a Cantor function, respectively. The corresponding states are sometimes called extended, localized, and critical in these three cases. A Cantor function is a continuous function that is constant

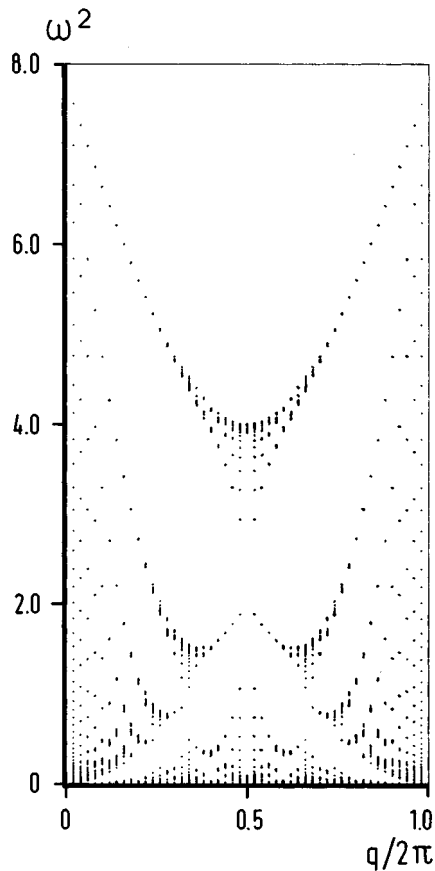


FIG. 2. Spectra for the modulated-chain model with spring constants $\alpha_n = \alpha[1 + 0.3 \cos(Qn + \phi)]$ as functions of the wave vector Q . Shown are the spectra for each approximant L/N of $Q/2\pi$, with $N < 50$. The main gaps can be obtained in first-order perturbation calculations, the other gaps in higher-order calculations. Frequencies: a.u.; Q in $2\pi/a$.

except at the points of a nowhere-dense set of points (see Fig. 4). This interesting class of functions often appears in discussions of quasiperiodic systems. Physicists usually call it a (complete) devil's staircase.

There are simple models in which a displacive IC phase transition occurs, for example, the discrete frustrated ϕ^4 (Diffour) model (Janssen and Tjon, 1982) or the Frenkel-Kontorova model (Frenkel and Kontorova, 1938)—see also Aubry and Le Daeron (1983). In such models the lattice dynamics have been studied as a function of temperature.

A quasiperiodic system can always be obtained from a periodic structure in higher-dimensional space. If n is the number of indices for the diffraction pattern, the basis vectors, which are of course linearly dependent in three dimensions if $n > 3$, can be seen as a projection from an n -dimensional reciprocal lattice Σ^* on physical space. This means that there is an n -dimensional periodic structure, the lattice Σ , for which Σ^* is the reciprocal lattice that in projection on the physical space gives the position of the diffraction spots. One can show that the physical quasiperiodic structure is just the intersection of the n -dimensional periodic system with physical

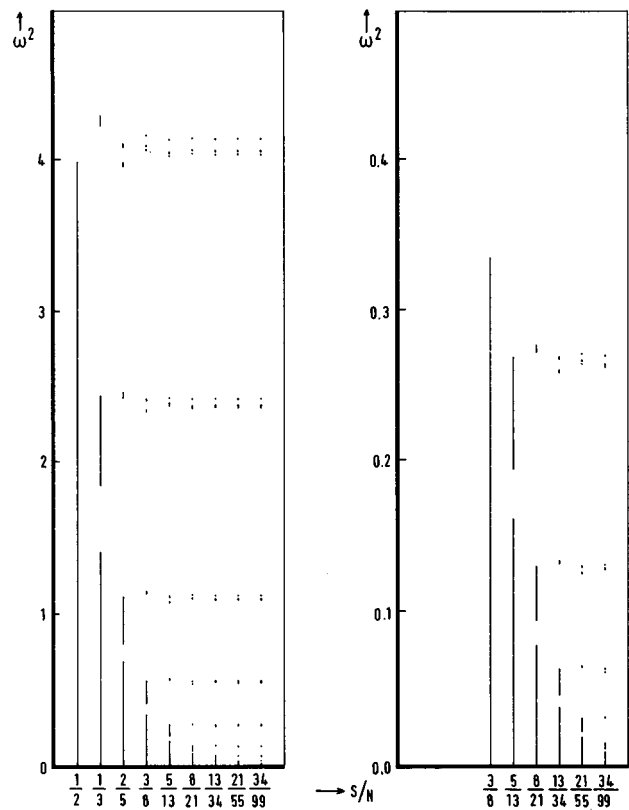


FIG. 3. The vibrational spectra in the low-frequency region for a number of commensurate approximants S/N up to $(3 - \sqrt{5})/2$, together with an enlarged version of them. This shows that the spectra have scaling behavior.

space, which is a hyperplane in the n -dimensional space. Therefore each point in “superspace” has coordinates in physical space and coordinates in the additional space, called internal or perpendicular space. For point atoms, the periodic n -dimensional systems consist of $(n-3)$ -dimensional hypersurfaces that intersect the physical space in the atom positions. These hypersurfaces are then called *atomic surfaces*. For a simple displacively modulated IC phase, for example, the atom positions are given by Eq. (2.2). They are the intersection of the lines

$$t \mapsto [\vec{n} + \vec{r}_j + \vec{f}_j(\vec{Q} \cdot \vec{n} + t), t] \quad (\text{real } t) \quad (2.12)$$

with the hyperplane $t=0$ (Fig. 5). The atomic surfaces are, in this case, lines in four dimensions.

B. Quasicrystals

Since 1984, we have known of a class of quasiperiodic systems termed quasicrystals (Shechtman *et al.*, 1984). Originally found in rapidly quenched AlMn, such phases have been discovered in a large number of binary and ternary alloys. It is characteristic that their diffraction patterns show sharp peaks and that the symmetry of these patterns is a point group that is incompatible with lattice periodicity in three dimensions. The latter follows from the fact that there are fivefold, eightfold, tenfold,

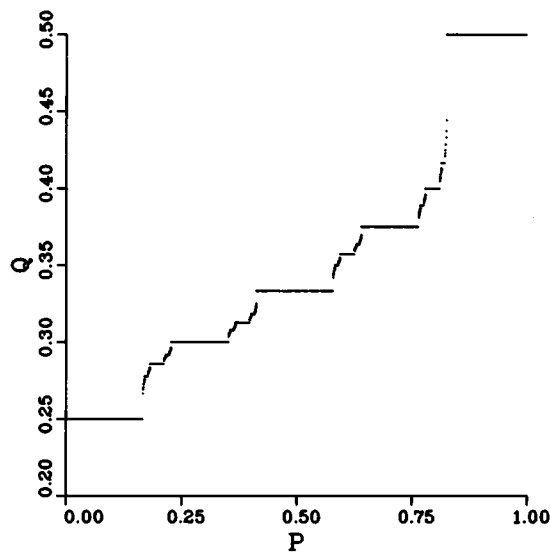


FIG. 4. Example of a Cantor function. It is a continuous non-decreasing function with plateaus at all rational values between $1/4$ and $1/2$.

or twelfold rotation symmetries. The diffraction patterns can be indexed with a finite number of integer indices, which shows that these structures are quasiperiodic. For compounds such as AlMn, AlMnPd, and AlCuFe, the rank n is equal to six. For other quasicrystals, like the decagonal and octagonal ones, it can be five.

The vibrational properties of quasicrystals have much in common with those of IC phases. The difference is that quasicrystals cannot be seen as a small deformation of a periodic structure. Therefore the vibrational properties are more like those in the discommensuration region (near T_c) of IC phases. The point-group symmetry implies that the topology of the interconnections is different: the coordination number of the atoms varies. Even if all interatomic interactions are the same, the vibration problem is by no means trivial.

On the other hand, the approaches used for the lattice vibration problem in IC phases can be used for quasicrystals as well: simple models for which one studies approximants or series of clusters, or uses transfer-matrix techniques.

Quasicrystals, in common with all quasiperiodic systems, can be embedded into a higher-dimensional space, such that the quasicrystal is obtained as the intersection of a lattice periodic n -dimensional structure with the three-dimensional physical space, which is given as $\tau = \text{constant}$ [we use here τ instead of t for the $(n-3)$ -dimensional perpendicular component] and is denoted by V_E . The additional space is V_I , sometimes called perpendicular space or internal space, and the n -dimensional space is termed the superspace. We suppose here that $n > 3$, which means that the three-dimensional structure is aperiodic. Its Fourier spectrum consists of δ peaks at positions

$$\vec{k} = \sum_{i=1}^n h_i \vec{a}_i^*, \quad h_i \in \mathbb{Z}. \quad (2.13)$$

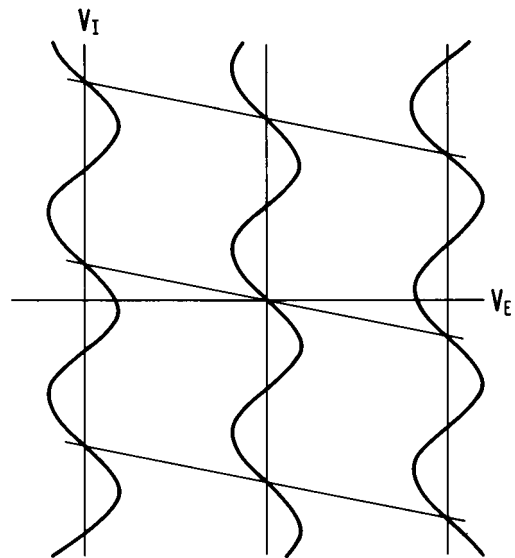


FIG. 5. Embedding of a sinusoidally modulated IC phase in superspace. The undulating lines are the atomic surfaces. The space V_E is the physical space, and V_I is the internal or perpendicular space. The intersections of the lines with the physical space yield the atomic positions in physical space.

All the vectors of this form belong to the Fourier module of the structure, which is denoted by M^* and is the projection of the n -dimensional reciprocal lattice Σ^* . This lattice is the reciprocal of a direct lattice Σ in n dimensions. One can view the quasiperiodic structure as the intersection of a periodic structure in n dimensions—with Σ as translation lattice—and the physical space V_E . One says that the n -dimensional structure is Σ -periodic.

There is a difference between the embedding of an IC phase and that of a quasicrystal. For the latter, the atoms in the physical space $\tau(\in V_I) = \text{constant}$ are the intersections of bounded atomic surfaces Ω_j at positions r_j in the n -dimensional unit cell. An atomic surface for an atom j at the position \vec{r}_s intersects the physical space if $\tau - \vec{r}_I$ belongs to Ω_j (Fig. 6). Therefore the positions in the physical space are $(n + r_j)_E$ for all $n \in \Sigma$ for which $\tau - n_I \in \Omega_j$.

Quasicrystals can often be modeled by quasiperiodic tilings in three dimensions. A tiling is an arrangement of copies of a finite number of three-dimensional objects, which fills space without gaps and without overlaps. The objects play the role of the unit cells for periodic crystals. They may contain a certain configuration of atoms (a decoration). For example, a three-dimensional (3D) Penrose tiling is a quasiperiodic arrangement consisting of rhombohedra of two types. The vertices are the intersection of physical space with a six-dimensional lattice periodic system consisting of three-dimensional triacontahedra (regular polytopes with 30 faces) positioned in the lattice points of a 6D lattice. A decoration of both rhombohedra with atoms gives a quasiperiodic 3D atom arrangement. The diffraction pattern is of rank six: one needs six integer indices.

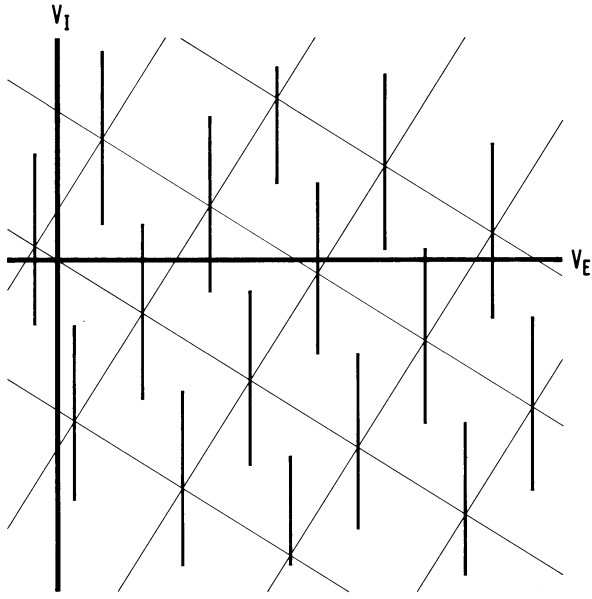


FIG. 6. Embedding of a quasicrystal in n -dimensional superspace. The vertical lines indicate the $(n-3)$ -dimensional atomic surfaces. An atomic surface Ω in the lattice point $n \in \Sigma$ intersects physical space if $\tau - n_I \in \Omega$.

If $(n + r_j)_E$ are equilibrium positions of the quasicrystal, vibrations around this equilibrium configuration are given by a displacement field $u_{nj\tau}$, which can be taken to be a vector field with only components parallel to the physical space. In the harmonic approximation, the vibrations for a single mode are $u_{nj\tau} \exp(i\omega t) + \text{c.c.}$ Moreover, because of the lattice periodicity in n dimensions, the modes are characterized by a wave vector in the n -dimensional Brillouin zone and a branch label ν . Then the mode

$$u_{nj\tau}^{q\nu} = \exp(iqn) U_j^{q\nu}(\tau - n_I), \quad (\tau - n_I \in \Omega_j) \quad (2.14)$$

has frequency $\omega_{q\nu}$. It is clear that the displacement is only defined if the atomic surface really intersects the physical space. Then the function $U_j^{q\nu}(x)$ is defined on the atomic surface Ω_j and has as values vectors parallel to physical space. This function can still be horribly complicated.

The function $U_j(\tau)$ is a Σ -periodic vector-valued function on the atomic surfaces Ω_j . Therefore, it can be developed in a Fourier series:

$$U_j^{q\nu}(\tau) = \sum_{K \in \Sigma^*} A_{K_j}^{q\nu} \exp(iK_I \tau). \quad (2.15)$$

This gives for the displacement field of a single mode

$$u_{nj\tau}^{q\nu} = \exp(iqn) \sum_{K \in \Sigma^*} A_{K_j}^{q\nu} \exp[iK_I(\tau - n_I)]. \quad (2.16)$$

Notice that the displacement for the real physical system is obtained by putting $\tau=0$. This means that the displacement field in physical space is not a Bloch wave but the product of a phase factor and a quasiperiodic function:

$$\begin{aligned} \vec{u}(\vec{r}) &= \exp(i\vec{k} \cdot \vec{r}) U(\vec{r}) \\ &= \exp(i\vec{k} \cdot \vec{r}) \sum_{K \in M^*} \vec{a}(K) \exp(iK \cdot \vec{r}). \end{aligned} \quad (2.17)$$

This is exactly as for IC phases (Currat and Janssen, 1988). For quasicrystals this has been discussed by Kitaev (1988). The infinite set of three-dimensional vectors $A_{K_j}^{q\nu}$ forms the equivalent of an eigenvector for the lattice dynamics of a three-dimensional lattice periodic crystal. There its number of components is three times the number of atoms in the unit cell. Here the number of components is infinite, because the number of degrees of freedom in the n -dimensional unit cell is infinite (all points of the s atomic surfaces). The dynamical matrix for a quasicrystal is, consequently, infinite dimensional as well.

The displacement field does not change if one replaces q by $q + Q$, with $Q \in \Sigma^*$. Consider then a fixed value for τ . Then

$$u_{nj\tau}^{q\nu} = e^{i(qn + Q_E n_E)} \sum_{K \in \Sigma^*} A_{K_j}^{q\nu} e^{iK_I \tau} e^{i(Q_I - K_I)n_I}. \quad (2.18)$$

Therefore the same displacement field in the hyperplane $\tau = \text{constant}$ is given for the wave vector $\vec{q} = q + (Q_E, 0)$ and the eigenvector

$$\vec{A}_{K_j}^{\vec{q}\nu} = A_{(K+Q)_j}^{q\nu} e^{iQ_I \tau}. \quad (2.19)$$

The description in terms of wave vector and eigenvector is not unique. This is well known already in the case of incommensurate crystal phases.

If the wavelength of the vibration is large with respect to the interatomic distances, one can consider a continuum approximation to the problem. This means that the time-dependent discrete displacement field $u_n(t)$ is replaced by a continuous function $u(x, t)$. In the harmonic approximation, the equations of motion become

$$\frac{\partial^2}{\partial t^2} u(x, t) = T(x) \frac{\partial^2}{\partial x^2} u(x, t), \quad (2.20)$$

where $T(x)$ is the average force constant α divided by the local mass density: $T(x) = \alpha/m(x)$. The mass distribution is quasiperiodic, and consequently the function $T(x)$ can be embedded into n dimensions, yielding $T(x, \tau)$, $x \in V_E, \tau \in V_I$. The harmonic approximation considers solutions $u(x, t) = U(x) \exp(i\omega t)$. The function $U(x)$ can also be considered as dependent on the perpendicular component τ . The equations of motion then become

$$-\omega^2 U(x, \tau) = T(x, \tau) \frac{\partial^2}{\partial x^2} U(x, \tau). \quad (2.21)$$

Because of the periodicity, the solutions can be written as Bloch waves, and the function $T(x, \tau)$ can be expanded in a Fourier series:

$$U(x, \tau) = \sum_{K \in \Sigma^*} c^q(K) e^{iqx + iK_E x + iK_I \tau}, \quad (2.22)$$

$$T(x, \tau) = \sum_{K \in \Sigma^*} A(K) e^{iK_E x + iK_I \tau}. \quad (2.23)$$

Substitution gives the eigenvalue problem

$$\omega^2 c^q(K) = \sum_{K'} (q + K_E + K'_E)^2 A(K') c^q(K - K'), \quad (2.24)$$

in which the squares of the frequencies are the eigenvalues of an infinite-dimensional operator. Because A is the Fourier transform of the inverse-mass distribution, its main contributions correspond to those wave vectors K for which the structure factor has strong peaks as well. As follows from Eq. (2.19), the wave vector q is not unique. The same displacement field may be described by $q + Q$ for every Q in the Fourier module.

This shows that the dispersion around the origin is repeated at every vector Q of the Fourier module. In an inelastic-scattering experiment with momentum transfer \vec{q} and energy transfer $\hbar\omega$ one also sees the mode at $\vec{q} - Q$, which has a component at \vec{q} because of the coupling between Fourier components. This is significant if $A(Q)$ is big. Hence waves with wave vectors differing by a vector Q from the Fourier module for which the static structure factor is big have a strong interaction. The result is the appearance of pseudo-Brillouin zone boundaries between such strong peaks. They appear halfway between two strong Bragg peaks. In general this is not a position belonging to the Fourier module, but rather the projection of a reciprocal-space vector with integer and half-integer coordinates with respect to the reciprocal lattice.

Such points again have a one-to-one correspondence between the three-dimensional vector and an n -dimensional vector. The points of the Fourier module correspond to the Γ points in reciprocal space, the points of the reciprocal lattice. The other special points are projections of points on the n -dimensional Brillouin zone. These special points have been investigated by Nizeki and Akamatsu (1990)—see also Niu and Nori (1990). Because they correspond to Brillouin-zone boundary points, at their projection in physical space one may expect to find the critical points for the phonon density of states.

The equations of motion for the quasicrystal are

$$\omega^2 u_{n\alpha} = \sum_{m\beta} \Phi \begin{pmatrix} n & m \\ \alpha & \beta \end{pmatrix} u_{m\beta}. \quad (2.25)$$

The solutions can be written as

$$\Psi = \sum_{n\alpha} u_{n\alpha} |n\alpha\rangle, \quad (2.26)$$

which are eigenfunctions of the operator H :

$$H\Psi = \omega^2 \Psi, \quad \langle n\alpha | H | m\beta \rangle = \Phi \begin{pmatrix} n & m \\ \alpha & \beta \end{pmatrix}. \quad (2.27)$$

For a basis

$$|k\alpha\rangle = \frac{1}{\sqrt{N}} \sum_n \exp(ikn) |n\alpha\rangle, \quad (2.28)$$

the equations for the coefficients $c(k\alpha)$ with respect to this basis are

$$\omega^2 c(k\alpha) = \sum_{k'\beta} \langle k\alpha | H | k'\beta \rangle c(k'\beta). \quad (2.29)$$

The matrix elements

$$\begin{aligned} \langle k\alpha | H | k'\beta \rangle &= \sum_s e^{ik's} \left[e^{i(k'-k)n} \Phi \begin{pmatrix} n & n+s \\ \alpha & \beta \end{pmatrix} \right] \\ &= \sum_s \exp(ik's) A_{s\alpha\beta}(k' - k) \end{aligned}$$

are only different from zero if $k' - k$ belongs to the Fourier module.

In a coherent inelastic-scattering experiment there is a momentum transfer $\hbar H$ and an energy transfer $\hbar\omega$ to the scattered neutron. (We use H for the scattering vector to avoid confusion with vectors Q from the Fourier module, such as the modulation wave vector for IC phases.) For general modes, the coherent differential scattering cross section is given by the expression

$$\begin{aligned} \left. \frac{\partial^2 \sigma}{\partial \Omega \partial E} \right|_{\text{coh}}(\vec{H}) &= \frac{k_f}{k_i} \sum_{q\nu} \sum_{K \in M^*} |F|^2 (n_{q\nu} + \frac{1}{2} \pm \frac{1}{2}) \\ &\quad \times \delta(\omega \pm \omega_{q\nu}) \delta(\vec{H} \pm \vec{q} - \vec{K}), \quad (2.30) \end{aligned}$$

where $n_{q\nu}$ is the temperature-dependent Bose-Einstein occupation factor, and F a matrix element that, for a quasicrystal with one atom per vertex, is given by

$$\begin{aligned} F &= \frac{\bar{b}}{\sqrt{m\omega_{q\nu}}} e^{-W(H)} \sum_n e^{iHn} C(\tau - n_I) \\ &\quad \times \sum_{Q \in \Sigma^*} H \cdot A_Q^{q\nu} e^{iqn + iQ_I(\tau - n_I)}. \quad (2.31) \end{aligned}$$

Here, $C(x)$ is the characteristic function on the atomic surface (with value unity on Ω and zero outside). This function can be developed in a Fourier integral,

$$C(x) = \int B_{-k} e^{ikx} dk. \quad (2.32)$$

Substitution of this integral, followed by the summation over n , yields

$$F = \frac{\bar{b}}{\sqrt{m\omega_{q\nu}}} e^{-W(H)} \sum_{Q \in \Sigma^*} B_{H_I - Q_I} e^{-iH_I \tau} H \cdot A_Q^{q\nu}. \quad (2.33)$$

The intensity of the scattering is, therefore, determined by two factors. One is the dynamic eigenvector $A_Q^{q\nu}$, while the other is the factor B , which corresponds to the static structure, because the static structure factor is

$$F_0(H) = \sum_n C(\tau - n_I) e^{iH_E n_E} = B_{H_I} e^{-iH_I \tau}. \quad (2.34)$$

The situation here is fully comparable with that in incommensurate crystal phases, where the dynamic scattering is also determined by these two processes. This implies that scattering is important only if the static structure factor is strong.

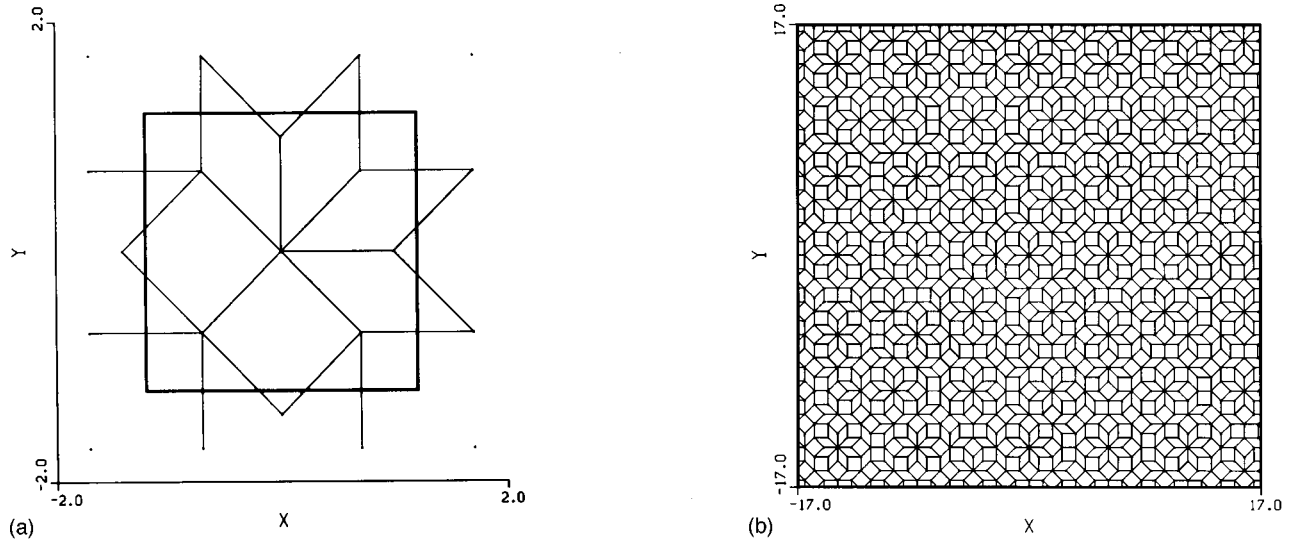


FIG. 7. Two approximants to the octagonal tiling: (a) with $L/N=1/1 \approx \sqrt{2}/2$, and (b) with $L/N=5/7$.

For the general case of more atomic surfaces per n -dimensional unit cell, Eq. (2.33) generalizes to

$$F = \sum_{j=1}^s \frac{\bar{b}_j}{\sqrt{m_j \omega_{qv}}} e^{-W_j(H)} e^{iHr_j} \times \sum_Q B_{H_I - Q_I}^j e^{-iH_I \tau H} \cdot A_{Q_I}^{qv}, \quad (2.35)$$

when the Fourier integral of the characteristic function of Ω_j is given by

$$B_k^j = \frac{1}{V_j} \int_{\Omega_j} dx e^{ikx}. \quad (2.36)$$

A quasiperiodic structure is the limit of a series of periodic approximants. If the lattice Σ of the embedded quasiperiodic structure has basis vectors $a_i = (a_{Ei}, a_{Ii})$, an approximant is obtained by replacing the irrational components of a_{Ii} by rationals. Then the intersection of Σ with V_E is a lattice, and the intersection of the n -dimensional structure with V_E is periodic. In the case of tilings, the form of the tiles remains the same if one keeps the components of a_{Ei} fixed. As an example, consider the octagonal tiling that is the result of intersecting V_E with a four-dimensional periodic structure with basis vectors $(\cos \pi j/4, \sin \pi j/4, \cos 3 \pi j/4, \sin 3 \pi j/4)$ ($j=1, \dots, 4$) and an atomic surface equal to the projection of the unit cell of Σ on V_I . The tiles are squares or rhombuses with an angle $\pi/4$. If one replaces the components $\sqrt{2}/2$ by a rational number L/N , Σ intersects V_E in a lattice with basis vectors $(L + N\sqrt{2}/2, L + N\sqrt{2}/2)$ and $(-L - N\sqrt{2}/2, L + N\sqrt{2}/2)$. The unit cell is composed of the same squares and rhombuses as the quasiperiodic tiling, but they are now arranged in a periodic fashion (Fig. 7). The diffraction pattern of this periodic approximant lives on a square reciprocal lattice, but the intensity distribution is very similar to that of the quasiperiodic octagonal tiling (Fig. 8).

The dynamic structure factor $S(q, \omega)$ for the quasiperiodic structure is the limit of that for the series of approximants,

$$S(q, \omega)_{L/N} \sim \sum_{kv} \left| \sum_{j=1}^s e^{iqr_j} q \cdot \epsilon_j(kv) \right|^2 \Delta(q - k) \times \delta(\omega - \omega_{kv}), \quad (2.37)$$

where j runs over the particles in the unit cell, and $\epsilon(kv)$ is the eigenvector for the mode kv . The sum over the exponential functions replaces, in Eq. (2.35), the contributions of $\exp(iHr_j)$ and $B_{H_I - Q_I}^j$, while the eigenvector

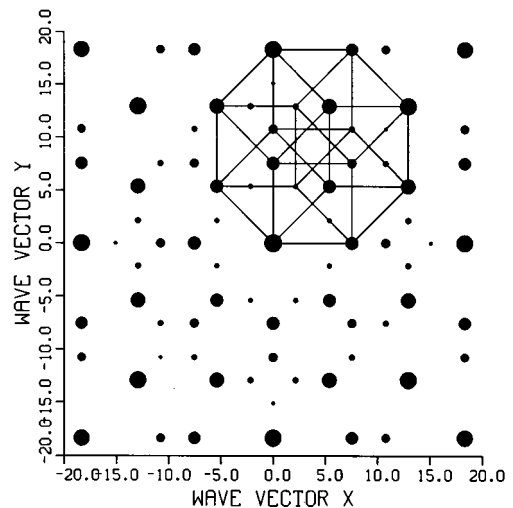


FIG. 8. The diffraction patterns for the $2/3$ approximant to the octagonal tiling. Strong Bragg peaks are near the positions of Bragg peaks of the quasiperiodic tiling. The four basis vectors of the Fourier module are the projections of four four-dimensional vectors that span a 4D Brillouin zone. The projection of this zone is shown. Wave vectors are in units of the reciprocal lattice basis vector.

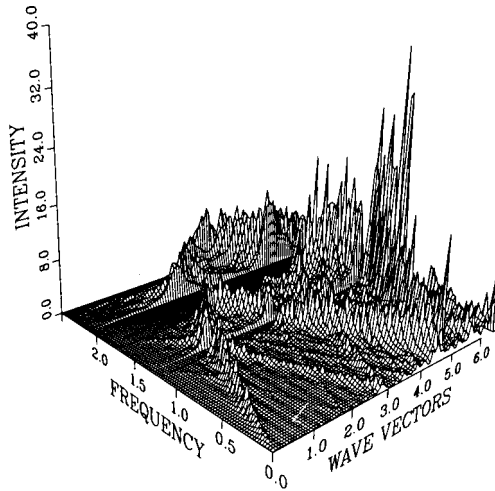


FIG. 9. The function $S(q, \omega)$ for the Fibonacci chain with two masses. There is a branch running from the origin to the first intense Bragg reflection near $q=4.8$. In between a branch starts at the less intense Bragg peak near $q=3.0$ (a.u.).

ϵ_j replaces $A_{Q_j}^{qv}$. Because of the function Δ (the sum of delta functions on the reciprocal lattice), a given mode contributes to the scattering with an infinite number of wave vectors q . The intensity, i.e., the value of $S(q, \omega)$, however, varies considerably. Therefore, even if for large values of L and N the mesh of the reciprocal lattice becomes finer and finer, there are no big changes in $S(q, \omega)$, just as the static structure factor does not change much from one approximant to another.

Consider, as an example, the Fibonacci chain. This is the intersection of a structure whose lattice is generated by $(1, -\tau)$ and $(\tau, 1)$ [$\tau = (\sqrt{5} + 1)/2$]. It is a 1D tiling with tiles of length 1 and τ . The atoms are at positions $m + n\tau$. If one replaces τ in the internal coordinate by F_{n+1}/F_n , where F_n are the Fibonacci numbers ($F_0 = F_1 = 1$, $F_n = F_{n-1} + F_{n-2}$), one obtains a periodic structure with unit cell of length $F_n + F_{n+1}\tau$. Consider the case in which there are atoms of mass m_1 at the right vertex of an interval of length 1, and m_2 for one at the end of an interval of length τ . Because the positions in the unit cell of an approximant are irrational, the function $S(q, \omega)$ is not periodic. For $\omega=0$, the only contributing mode is the acoustic $k=0$ mode, and for that mode $S(q, 0)$ is just the static structure factor, since this has Bragg peaks that are intense if $q = -h_1\tau + h_2 \approx 0$. The points of the Fourier module correspond to the Γ points for lattice periodic systems. The intensities at these Γ points are determined by the structure factor. The plots of $S(q, \omega)$ do not change much if one changes the approximant. An example is given in Fig. 9. Starting from a strong Bragg peak, there is an acoustic branch with significant intensity, whereas from other Bragg peaks, only very weak branches start. For higher frequencies, the branches starting from different peaks meet, and there is a parabolic behavior of the intensity maxima. For frequencies near the maximal frequency many neighboring q vectors differing by a reciprocal-lattice vector give a

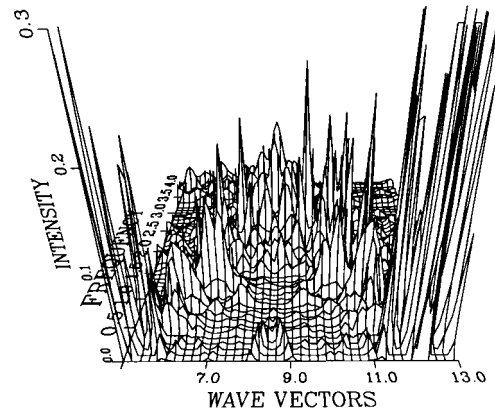


FIG. 10. $S(\vec{q}, \omega)$ for the 2/3 approximant to the octagonal tiling (41 atoms per unit cell). The path runs from $(5, 2)$ to $(5, 5)$ (a.u.).

strong contribution. This is partially due to the fact that the states at high frequency tend to be more localized. From Eq. (2.37), it follows then that there is a broad distribution of contributing q vectors. If the unit cell tends to infinity, and the reciprocal lattice meshes to zero, this will give a broadening of the measured peaks. In Fig. 9 one clearly can see the gaps in the spectrum as valleys with vanishing values of $S(q, \omega)$.

As a second example, we consider the octagonal tiling and its approximants (Fig. 8). With springs along the edges of the rhombuses and between the atoms that are closest together, one can calculate the eigenvalues, the eigenvectors, and the corresponding dynamic structure factor. In the case of an approximant to the octagonal tiling, one gets the picture of Fig. 10. Here the intensity is plotted for a path in reciprocal space from one strong Bragg peak Fig. 8 to another. Again, from both peaks originate narrow acoustic branches, which coalesce for higher frequencies. At still higher frequencies one observes a decrease of intensity and a broadening.

C. Scaling properties

The spectra for the modulated-spring model show self-similarity both as functions of energy and as functions of energy and modulation wave vector. The self-similarity for one given modulation wave vector can be seen if one compares spectra for various approximants to the incommensurate value. For example, if one considers approximants $1/2$, $2/3$, $3/5$, $5/8$, and so on, to the irrational number $\tau - 1 = (\sqrt{5} - 1)/2$, and compares the spectra for the modulated-spring model, the lower part of the spectrum for the approximant F_n/F_{n+1} is very similar to the whole spectrum for F_{n-1}/F_n , up to a scale factor.

In the limiting case of $\delta=1$ for the modulated-spring model [Eq. (2.11)] the total measure, meaning the sum of all bandwidths, goes to zero if the order of the approximant (n) goes to infinity. This approach occurs ex-

ponentially. If the bands in the n th approximation have widths $\Delta_i^{(n)}$, the total measure $B^{(n)} = \sum_i \Delta_i^{(n)}$ behaves as

$$B^{(n)} \sim \exp(-n\epsilon). \quad (2.38)$$

The number of particles N_n in the unit cell increases like λ^n , where λ is the scale factor [for Fibonacci $\lambda = (1 + \sqrt{5})/2$]. Therefore one has

$$\epsilon = - \lim_{n \rightarrow \infty} \frac{\ln B^{(n)}}{\ln N_n} \ln \lambda. \quad (2.39)$$

If this limit exists, it is called the spectral scaling index.

Such scaling behavior has also been found for the modulated-spring model with modulation function

$$\alpha_n = \begin{cases} \alpha & \text{if } 0 \leq n\tau \bmod 1 < \tau \\ \beta & \text{otherwise} \end{cases} \quad (2.40)$$

and for similar chains with a finite number of values for the coupling constants.

This scaling occurs even for the separate bands. If one plots the logarithm of the width of the top band against the order n of the approximant, or equivalently against the logarithm of the number of particles in the unit cell, one finds a straight line, i.e., exponential falling off of the width. The exponent, however, is different from the value of ϵ for the whole spectrum. Suppose that the bands show such a scaling behavior. That means that the widths decrease as a function of the order of the approximant as

$$\Delta_i^{(n)} \sim \exp(-n\epsilon_i).$$

The index i is not a good label, because a band at approximately the same energy gets a label that increases with increasing order n . However, if one normalizes the index on the interval $[0,1]$, one can write

$$\epsilon^{(n)}(i/N_n) = - \frac{\ln \Delta_i^{(n)}}{\ln N_n} \ln \lambda. \quad (2.41)$$

If this function on the unit interval converges, then at all energies there is scaling behavior. An example is given in Fig. 11. For the Fibonacci chain the function $\epsilon^{(n)}(x)$ is there plotted on the interval $[0,1]$ for three values of n . The peaks converge, albeit slowly, to a finite value. For example, for $x = 1 - \tau = (3 - \sqrt{5})/2$, there is a peak with a limiting value of 1.7 (for clarity only four low values of n are used in the figure).

In later subsections we shall see examples of scaling behavior in more than one dimension.

D. Studies with one-dimensional models

As for IC phases the lattice dynamics of quasicrystals have been studied on simple models. These consist usually of an n -dimensional ($n=1,2,3$) tiling with atoms at the vertices, at the center of a tile, or with another given location within each tile, and springs between neighboring atoms. As expected, the effects are the strongest for

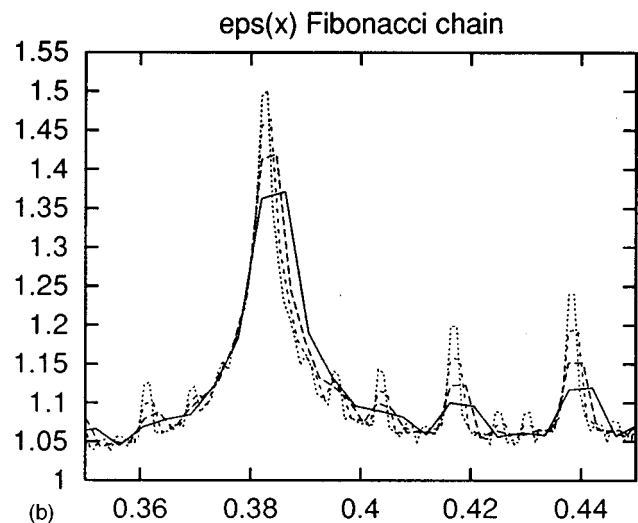
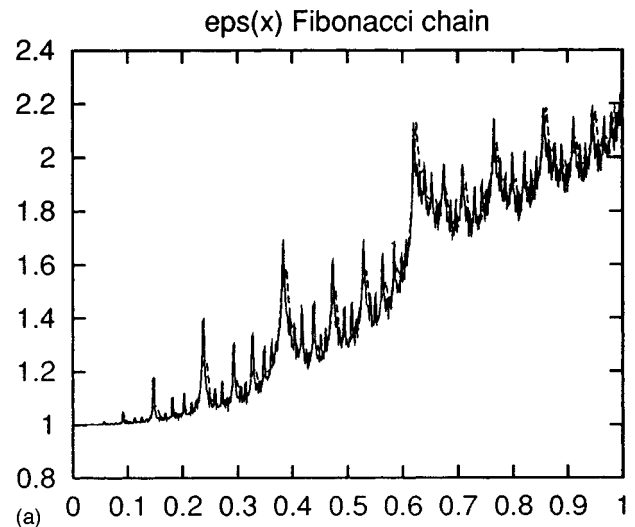


FIG. 11. The function $\epsilon^{(n)}$ for a number of approximants to the Fibonacci chain. (a) For $x \approx 0$, i.e., for long wavelengths, the waves are barely distinguishable from extended waves. (b) For the values $x = m + n\tau \pmod{1}$ the function converges, albeit slowly, to a limiting value (e.g., at $x = 2 - \tau \approx 0.38$).

one-dimensional systems, but for two- and three-dimensional quasicrystal models one also finds behavior that differs from that of ordinary periodic crystals.

One-dimensional quasiperiodic tilings can be considered to be modulated crystal phases, because there is an average structure, and the deviations from this structure can be interpreted by means of a modulation function. For the Fibonacci chain, the average lattice constant is $a = 3\tau - 4$, and the modulation function is the discontinuous function

$$f(x) = (\tau - 2) \text{Frac}(x - x_0). \quad (2.42)$$

[Here, $\text{Frac}(x) = x - \text{largest integer smaller than } x$.] Therefore it is not surprising that the results for one-dimensional quasicrystals are very similar to those for one-dimensional modulated chains (de Lange and Janssen, 1981). The vibrational properties of the Fibonacci chain have been studied by

several workers (e.g., Kohmoto and Banavar, 1986). The model is a linear chain with masses m_n and harmonic springs with coupling constants α_n . Usually the masses are taken to be equal and the force constants take two values, one for bonds across long intervals, and one for those over short intervals.

If one uses the transfer-matrix technique, the matrices T_n have only two forms, one with $\alpha_n=\alpha$ and one with $\alpha_n=\beta$. We denote them by T_a and T_b . In contrast to an IC phase, a quasiperiodic system often has scaling symmetry. We show this on the Fibonacci chain. It can be constructed in another way. If one considers the set of intervals (of length 1 and τ), one can transform the latter as follows. Replace a long interval by a long-short pair and a short interval by a long one. If one starts with a long interval and repeats the transformation, one arrives, after five steps, at the series $LSLLSLSLLSLLS$, and, in the limit of an infinite number of steps, at the Fibonacci chain. This process is equivalent to the following one. Start with two patches of intervals S_0 and S_1 . The n th patch S_n is obtained by putting S_{n-2} behind S_{n-1} . If one starts with $S_0=S$ and $S_1=L$, then $S_5=LSLLSLSL$ and again, in the limit, one obtains the Fibonacci chain. The ratio of the lengths of two consecutive patches goes to $(1+\sqrt{5})/2$. The number of intervals in the n th patch is the Fibonacci number F_n .

For the products of the transfer matrices one can introduce

$$M^{(n)} = \prod_{j=1}^{F_n} T_{j \rightarrow} M^{(n+1)} = M^{(n)} M^{(n-1)}. \quad (2.43)$$

Because ω belongs to the spectrum if in the limit the trace of $M^{(n)}$ remains between -2 and $+2$, one has to investigate this asymptotic behavior. Denote the trace of $M^{(n)}$ by $2x_n$. For 2×2 matrices with determinant equal to $+1$, as we have here for transfer matrices and their products, one has the relation

$$A^2 B = A \operatorname{Tr}(AB) - B.$$

Then every product of transfer matrices can be reduced to one without squares, i.e., their traces can be expressed as

$$x_0 = \frac{1}{2} \operatorname{Tr}(T_b), \quad x_1 = \frac{1}{2} \operatorname{Tr}(T_a), \quad x_2 = \frac{1}{2} \operatorname{Tr}(T_a T_b). \quad (2.44)$$

For example,

$$x_3 = \frac{1}{2} \operatorname{Tr}(T_a T_b T_a) = \frac{1}{2} \operatorname{Tr}(T_a) \operatorname{Tr}(T_a T_b) - \frac{1}{2} \operatorname{Tr}(T_b).$$

In general, one gets

$$x_{n+1} = 2x_n x_{n-1} - x_{n-2}. \quad (2.45)$$

This is called the trace map, devised by Kohmoto *et al.* (1983). It can be used to study the spectrum. It is a non-linear mapping in three dimensions, but the orbits are restricted to a two-dimensional surface, because there is an invariant

$$I = x_n^2 + x_{n-1}^2 + x_{n-2}^2 - 2x_n x_{n-1} x_{n-2}. \quad (2.46)$$

Therefore the analysis can be performed on the surface $I=\text{constant}$. For other chains with more than two intervals, similar trace maps have been constructed. The trace map can be used to determine the spectrum. One scans the values of ω^2 for which the values of x_n remain bounded.

Another way to use the self-similarity is to consider successive approximants. By replacing the irrational internal components of the higher-dimensional lattice by rational ones, one causes the intersection of the periodic structure to become itself periodic. If one replaces the value τ by F_{n+1}/F_n in the Fibonacci case, one obtains a periodic chain with $N_n = F_{n+1}$ sites in the unit cell. The dispersion curves then form bands, and in each band one has a fraction $1/N_n$ of the states. This means that the integrated density of states (IDS) has $N_n - 1$ plateaus: it is constant in the gaps. The IDS curves then tend to a limit curve, which in 1D is generally a Cantor function (see Fig. 12).

Luck and Petritis (1986) considered the equation

$$(\Lambda u)_n + z u_n = 0, \quad (\Lambda u)_n = \frac{u_{n+1} - u_n}{\alpha_n} - \frac{u_n - u_{n-1}}{\alpha_{n-1}}, \quad (2.47)$$

where u_n is the displacement and z the square of the frequency in reduced units. The force constants are $\alpha_1=1$ and $\alpha_2=\rho < 1$. Using the transfer matrix technique and the trace map for the Fibonacci chain starting from $(1, 1-\rho z/2, 1-z/2)$, they determined the spectral properties numerically. They showed that, for small frequency ($z \ll 1$), the integrated density of states is barely distinguishable from that of the linear chain with a force constant equal to the average, which is

$$I(z)_{\text{av}} = \frac{1}{\pi} \cos^{-1} \left(1 - \frac{z \hat{\alpha}}{2} \right).$$

For high frequencies (near the top), scaling in the spectrum is observed. The top part of the spectrum will reappear up to a change of scale after six iterations of the inflation rule, i.e., when one compares the spectra of two finite clusters, one corresponding to $\sigma^{(p)}$ and one to $\sigma^{(p+6)}$, if σ is the substitution rule for the Fibonacci chain. The scale factor is related to an eigenvalue of the linearized trace map near a six cycle. If this eigenvalue is $\Lambda(z)$, the scale factor for the spectrum is $6 \ln(\tau)/\ln \Lambda(z)$. A careful analysis of the low-frequency part by means of the escape time (the number of steps in the trace map that lead to a point beyond a certain distance) shows that there are gaps at every scale and no absolute continuous part of the spectrum. This is in agreement with the conjecture that all states are critical, which can be proven numerically by means of a study of the moments of the eigenvectors $\{u_n\}$. The plot of the moment μ_∞ shows a peaked structure and self-similarity.

Lu *et al.* (1986) arrived at comparable conclusions. They used the transfer-matrix technique to study the spectrum numerically. They also noticed that at low fre-

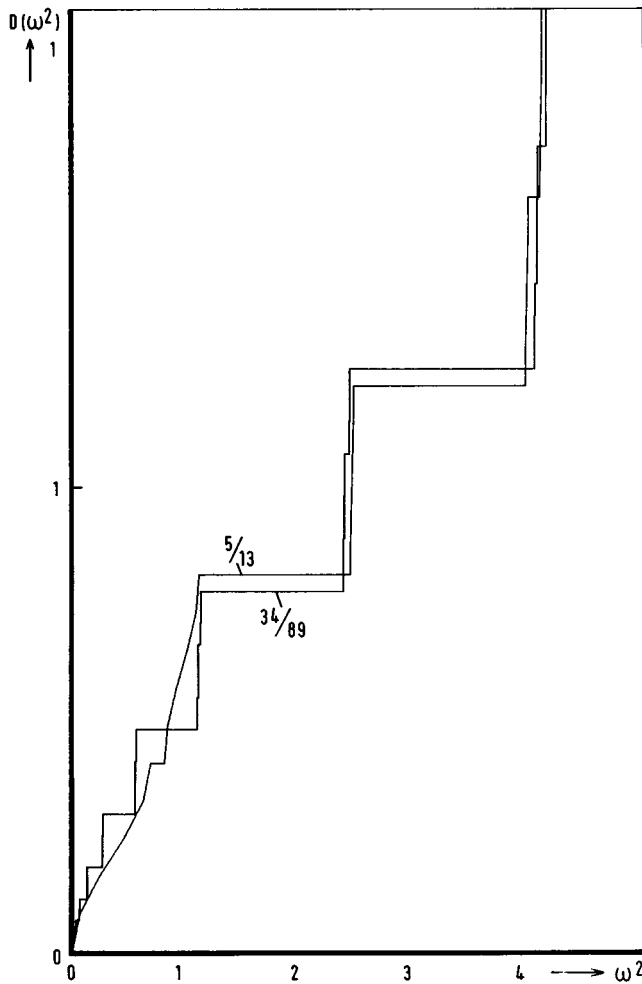


FIG. 12. The integrated density of states in the Fibonacci chain. The functions converge to a Cantor function. There are plateaus for all values of ω in a gap. Because there is a fraction $1/N$ in each band for a period N approximant, the values of the integrated density of states (IDS) in the gaps is $mL/N \pmod{Z}$, if the incommensurability is approximated by L/N . In the limit gaps occur for all values mQ of the IDS.

frequencies there was not much difference in the integrated density of states from that of a periodic chain. They also found self-similarity in the spectrum, especially at higher frequencies, and showed the IDS to be a Cantor function. Moreover, they studied the opening of gaps when the ratio of the force constants was brought from unity down and were able to calculate this with a renormalization procedure. In the case of Fibonacci chains, the big gaps seemed to correspond to repetition of small units.

Ashraff and Stinchcombe (1989) studied the dynamic structure factor

$$S(q, \omega) = \lim_{\eta \rightarrow 0} \lim_{N \rightarrow \infty} \text{Im} G_N(q, \omega - i\eta)$$

for the Green's function G_N . They used a renormalization procedure for this study. Because the atoms are positioned at the sites of a Fibonacci chain, which enter through the expression

$$G_N(q, \omega) = \frac{1}{N} \sum_{lm} G_{lm}(\omega) \exp(iqr_{lm}),$$

the function $S(q, \omega)$ is not trivial, even for equal force constants. This reflects the fact that neutron scattering proceeds partly via the eigenvectors of the vibrations, and partly via the static structure. In the (q, ω) plane one sees ridges emanating from points $(Q, 0)$, where the Q 's are the positions of the Bragg peaks. The multitude of phonon branches in the (q, ω) plane resembles closely that of incommensurate crystal phases in the region where the modulation is described by discommensurations (Currat and Janssen, 1988), in contrast to that in the sinusoidal region, where the proliferation of branches is less visible.

Benoit *et al.* (1990) also calculated the differential cross section, this time by means of the spectral-moments method. From calculations on big samples they came to the following conclusions. If one calculates the cross section at constant distance from a Bragg peak, one always finds a maximum in ω at the same position. This ω value is linear in the distance to the peak. Therefore, near Bragg peaks, there is linear dispersion. Moreover, the intensity is proportional to the intensity of the static structure factor at the peak. For small frequencies, the excitations behave like (extended) Bloch waves, but in fact the IDS is a Cantor function. The spectral-moments method introduces a (small) imaginary part in the frequency (like η in the dynamic structure factor above). This can be seen as a finite lifetime of the phonon. The result for the calculation is that narrow gaps are washed out. Eigenvectors are not found by this method, but one can calculate the displacement-displacement correlation function. This shows that, for frequencies near the top, the states are rather localized. The localization is increased by increasing the value of η .

E. Electrons in quasicrystals

The model calculations for lattice vibrations in quasi-periodic systems and the characteristic features of these excitations agree very well with those for electrons in such aperiodic structures. This was already known for incommensurate crystal phases. The spectra and wave functions of electrons in a crystal in an external magnetic field can be studied on the model system that leads to the Harper or almost-Mathieu equation

$$\psi_{n-1} + \psi_{n+1} + \lambda \cos(\alpha n + \phi) \psi_n = E \psi_n. \quad (2.48)$$

Here ψ_n is the wave function on the site n in a chain, whereas $\alpha/2\pi$ is an irrational number. It has been shown that, for almost all values of α , the spectrum is absolute continuous and the wave functions extended for $\lambda < 2$, while for $\lambda > 2$ there is a point spectrum and the wave functions are localized. For $\lambda = 2$ the spectrum is singular continuous and the wave functions are critical. This is very much the same as the situation for the modulated-spring model with sinusoidal modulation of amplitude

(δ) equal to unity (de Lange and Janssen, 1981; Janssen and Kohmoto, 1988). The almost-Mathieu equation is one of the few examples in which these results have been proven. A general review of such quasiperiodic Hamiltonian operators was given by Simon (1983).

The situation seems to be more complicated for the incommensurate Kronig-Penney model (de Lange and Janssen, 1983), for which the Schrödinger equation reads

$$-\frac{\hbar^2}{2m} \frac{\partial^2}{\partial x^2} \psi(x) + \sum_n \mu \delta(x-x_n) \psi(x) = E \psi(x), \quad (2.49)$$

where m is the electron mass, μ is the strength of the δ potential, and the positions x_n form an incommensurately modulated chain, for example, $x_n = na + \epsilon \cos(an + \phi)$. Simultaneously extended, localized, and pseudo-localized (critical) states have been found numerically (de Lange and Janssen, 1984).

The first model for electrons in a quasicrystal was the tight-binding model on a Fibonacci chain, for which the discrete Schrödinger equation reads

$$t_n c_{n-1} + t_{n+1} c_{n+1} + \epsilon_n c_n = E c_n. \quad (2.50)$$

Here c_n is the wave function on the site n , ϵ_n a site-dependent potential, and t_n the hopping frequency between sites n and $n-1$. Usually one takes either t_n or ϵ_n to be independent of n and the other to be a function of n that takes two values in the sequence of a Fibonacci chain. This model and some generalizations were studied extensively, mainly by numerical methods (Kohmoto *et al.*, 1983; Ostlund *et al.*, 1983; Kohmoto and Oono, 1984; Ostlund and Pandit, 1984; Niu and Nori, 1986; Sire and Mosseri, 1989).

One of these methods involves the use of a transfer matrix and the trace map. The Schrödinger equation for the Fibonacci tight-binding model can be written as

$$\begin{pmatrix} c_{n+1} \\ c_n \end{pmatrix} = \begin{pmatrix} E - \epsilon_n & -t_n \\ t_{n+1} & t_{n+1} \\ 1 & 0 \end{pmatrix} \begin{pmatrix} c_n \\ c_{n-1} \end{pmatrix} \equiv T_n \begin{pmatrix} c_n \\ c_{n-1} \end{pmatrix}. \quad (2.51)$$

This equation then can be transformed to a trace map in the same way as was discussed for the phonon problem.

The results of various models agree in that the spectrum is singular continuous of zero measure, that there is a scaling invariance of the spectrum as a function of energy, and that the wave functions are neither extended nor localized, but are critical, sometimes with self-similarity properties. The scaling indices agree with the eigenvalues of the linearized trace map around an n cycle, a periodic orbit with period n , where n depends on the model and the energy that is being considered. This scaling behavior has been studied by means of multifractal analysis known from dynamical systems. Reviews of these scaling properties have been given by Hiramoto and Kohmoto (1989, 1992).

Generalizations of the Fibonacci tight-binding model include generalized Fibonacci chains (Holzer, 1988; Sire

and Mosseri, 1989; Severin and Riklund, 1989), the Fibonacci Kronig-Penney model, chains with a periodic potential different from that in the almost-Mathieu equation,

$$V(x) = \lambda \tanh[\mu \cos(2\pi x)] / \tanh \mu,$$

chains with three or more values for the hopping or site-energy terms, and chains with a deterministic order different from quasiperiodic systems, such as Thue-Morse or Rudin-Shapiro chains.

These chains can, like the Fibonacci chain, be obtained by a substitution rule. One starts with two or more letters and iterates the substitution of a given word for each letter. For example, for the Fibonacci chain one starts with two letters (A and B) and replaces in every step A by AB and B by A . The result in the limit of an infinite number of iterations is a deterministic chain. Whether or not the result is quasiperiodic depends on the substitution. The electron spectra for such systems have been studied by Niu and Nori (1990), Dulea *et al.* (1992a, 1992b) Deng *et al.* (1993), and Janssen (1994).

For such substitutional chains, and for chains obtained from a circle map, there are rigorous results (e.g., Suto, 1987, 1990; Bovier and Ghez, 1993, 1995).

For tight-binding models in two and three dimensions, there are only numerical results. These are based on diagonalization of huge but sparse matrices or on renormalization methods. Two-dimensional models are tight-binding Hamiltonians on the standard octagonal or the Penrose tiling (Sire and Bellissard, 1990; Fu *et al.*, 1991; Liu and Ma, 1991; Liu *et al.*, 1992; You *et al.*, 1992). The density of states shows a very rich structure with many pseudogaps. This is similar to the situation for phonons, as we shall see in the ensuing sections.

In three dimensions, researchers have studied, besides simple models (Niizeki and Akamatsu, 1990; Kasner *et al.*, 1991), more realistic models, in the sense that the structure as determined with x rays or neutrons can be taken into account (Hafner and Krajci, 1993a, 1993b). The electronic structure and transport properties of three-dimensional quasicrystals and their approximants have been studied by Fujiwara and co-workers (Fujiwara, 1993; Fujiwara *et al.*, 1994; Trambly de Laissardière and Fujiwara, 1994), and the electronic structure of AlZnMg has been studied by Hafner and Krajčí. These materials show a pseudogap near the Fermi surface, which is related to the stability of quasicrystals. This kind of pseudogap does not have a counterpart in the phonon problem, to which we now return.

F. Two-dimensional phonon models

For higher-dimensional systems, there are not so many results and practically no rigorous ones. In two dimensions, there are numerical calculations for the three "standard" quasiperiodic tilings of rank two: the octagonal, the Penrose, and the dodecagonal tilings.

Simple models consider scalar phonons, which are excitations with just one degree of freedom per site, for

example, a displacement perpendicular to the plane. These can be compared directly with a tight-binding model:

$$m\omega^2 u_{nm} = \sum_{n'm'} \alpha(nm, n'm') u_{n'm'} . \quad (2.52)$$

In general, the displacement is a vector.

A simple two-dimensional quasiperiodic structure can be built with quasiperiodic linear chains, such as a periodic or quasiperiodic array of Fibonacci chains. If the couplings are separable, i.e., when

$$m\omega^2 u_{nm} = (H^x u)_{nm} + (H^y u)_{nm} , \quad (2.53)$$

with

$$(H^x u)_{nm} = \alpha_{nm}(u_{nm} - u_{n-1m}) + \alpha_{n+1m}(u_{nm} - u_{n+1m}) ,$$

and

$$(H^y u)_{nm} = \beta_{nm}(u_{nm} - u_{nm-1}) + \beta_{nm+1}(u_{nm} - u_{nm+1}) ,$$

the frequencies of the two-dimensional system are

$$\omega^2 = \omega_x^2 + \omega_y^2 , \quad (2.54)$$

expressed in the frequencies of the chains with coupling constants α_{nm} and β_{nm} . The density of states (DOS) then is the convolution

$$\text{DOS}(\omega^2) = \int dz \text{DOS}_x(z) \text{DOS}_y(\omega^2 - z) . \quad (2.55)$$

For a vector model with decoupling between x and y displacements, the density of states is the sum of the individual densities of states.

Odagaki and Nguyen (1986) studied clusters from a Penrose tiling with kites and darts. The equations of motion involving scalar phonons were solved for

$$m\ddot{u}_i = - \sum_j k_{ij}(u_i - u_j) , \quad (2.56)$$

where the coupling constant k_{ij} takes only two values, one for a short edge and one for a long one. The coupling constant is nonzero only for atoms connected by an edge. Spectra were calculated for clusters up to 391 sites as a function of the ratio of the coupling constants. However, because of the smallness of the sample, it is difficult to make statements about the gap structure.

A model starting from atoms at the vertices of a Penrose pattern with rhombuses and with a Lennard-Jones potential was studied by Janssen (1988). First the system was relaxed to a minimal-energy configuration. This turned out to be a quasiperiodic structure, again with pentagonal symmetry, but with deformed tiles. The Fourier module was the same as that for a Penrose tiling, but the intensities were different. Such a structure is not a modulated quasicrystal but a modulated tiling. For an $8/5$ periodic approximation ($\tau \approx 8/5$) of the modulated tiling, with two types of springs (along the edges of the rhombuses and between atoms a distance $\tau-1$ apart), a

highly structured density of states was found, suggesting a large number of van Hove singularities. It was observed that there were states with a high degree of localization at higher frequencies.

Ashraff *et al.* (1990) studied 2D quasiperiodic systems consisting of a periodic or quasiperiodic array of Fibonacci chains with scalar phonons. The integrated density of states still showed plateaus, at values $\text{Frac}(m\tau)$ for integer m . At low frequencies the density of states was almost linear. For increasing values of the ratio of the spring constants, more and more gaps appeared. The dynamic structure factor showed a structure like that for a Fibonacci chain if one runs along the (1,1) direction in reciprocal space. The scalar phonons in a Penrose tiling by Robinson triangles cannot be expressed in terms of phonons in lower-dimensional systems. Numerically, the spectrum was calculated for clusters of 539 sites as a function of the ratio between the force constants along short and long bonds. For certain intervals in this ratio there were gaps in the spectrum.

Liu *et al.* (1992) studied vectorial phonons (i.e., where the displacements are two-dimensional vectors) numerically in the standard octagonal tiling, using the recursion method (Haydock *et al.*, 1972, 1975). They claim that there is an anomaly at low frequencies, but this is not confirmed by other model calculations.

Vector phonons in the standard octagonal tiling were also studied by Los *et al.* (1993a). Their model consisted of atoms on the vertices of the standard (Beenker or Ammann) octagonal tiling. The atoms were connected by springs along the edges, the small diagonals of the rhombuses, and the diagonals of the squares. The potential energy is

$$V = \frac{\alpha}{4} \sum_i \sum_{j(i)} [|\vec{r}_i + \vec{u}_i - \vec{r}_j - \vec{u}_j| - |\vec{r}_i - \vec{r}_j|]^2 . \quad (2.57)$$

Here, the summation runs over all pairs connected by one of the above-mentioned bonds. The quasiperiodic system is approximated by a systematic series of periodic approximants, obtained by replacing $\sqrt{2}$ in the perpendicular coordinates of the four-dimensional lattice by $1/1, 3/2, 7/5, 17/12, \dots$. This results in a square unit cell with $7, 41, 1393, 8119, \dots$ sites, respectively. For these approximants, the dynamic matrix is diagonalized using a variation on the Lanczos method, which makes use of the sparseness of the dynamical matrix. In this way one finds the spectrum and eigenvectors, and from that the density of states. There is a fairly rapid convergence. One can already see the essential features in the 41 approximant.

The density of states in this model shows a great deal of structure (Fig. 13). There are many pseudogaps, and at higher frequencies there are also real gaps. There are many singularities. Pseudogaps occur at low frequencies, but their depth decreases rapidly for frequencies tending to zero. Near zero, the deviations from linear behavior are extremely small. This is proven also by the calculation of the vibrational specific heat, which does not differ from that of a square lattice with appropriate force constants.

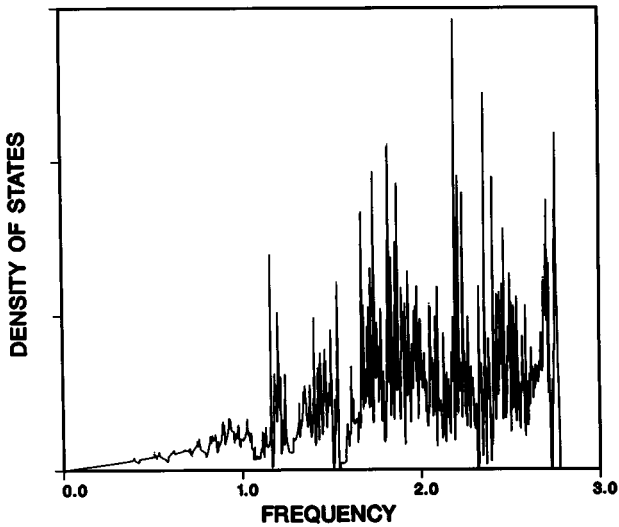


FIG. 13. Density of states for the two-dimensional standard octagonal tiling. It shows many pseudogaps and gaps and is very spiky. (Frequency in a.u.)

Dispersion curves have been calculated as well (Fig. 14). They show an interesting scaling behavior. If one compares the dispersion curves for different approximants, they are practically identical, apart from a scale factor of $1+\sqrt{2}$ in the frequency. This implies that the observed horizontal optical branches are present at arbitrarily low frequencies. This scaling behavior is found again when one calculates the bandwidths. A multifractal analysis shows that the bandwidths, defined as the difference between the maximum and the minimum of the i th eigenvalue in the Brillouin zone, go exponentially to zero as i increases. Moreover, the analysis shows that there is a distribution of scaling exponents. This is an indication of a singular continuous spectrum. At low frequencies, however, the scaling exponent barely deviates from unity, which would be the value for an absolute continuous spectrum. The corresponding eigenvectors are like Bloch waves. Numerically, it is almost impossible to find the critical character for long-wavelength phonons.

If one randomizes the octagonal tiling, by allowing for a number of phason jumps, much of the structure disappears. There are no longer gaps or pseudogaps in the density of states.

G. Icosahedral structures

An important class of three-dimensional quasicrystals is formed by those with icosahedral symmetry. This means that the symmetry group of the diffraction pattern is the symmetry group $5\bar{3}m$ of the icosahedron, or the dodecahedron. It is a group with 120 elements generated by a fivefold rotation, a threefold rotation, and the total inversion $-E$. The rotation subgroup of order 60 has, besides the unit element, 24 fivefold rotations, with axes pointing to the vertices of the icosahedron, 20 threefold rotations, with axes to the centers of the tri-

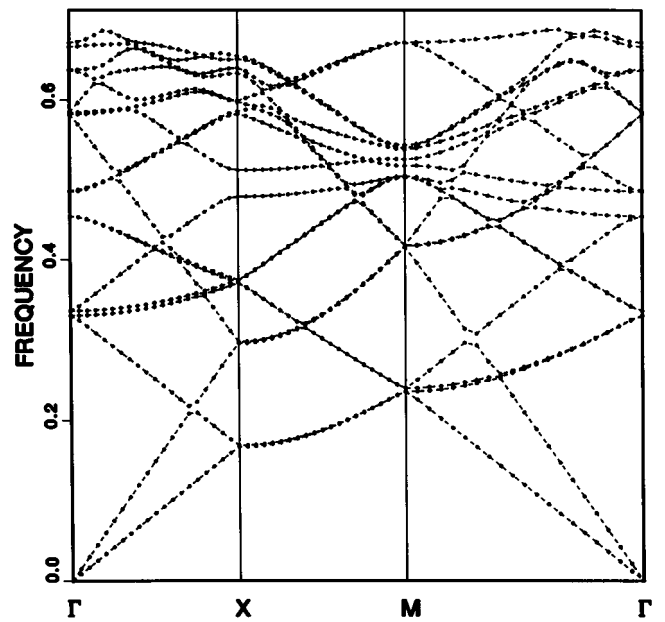


FIG. 14. Dispersion curves for an approximant to the octagonal tiling. The next approximant has almost the same dispersion curve, up to a scale factor in the frequency (a.u.).

angles of the icosahedron, and 15 twofold rotations, with axes through the midpoints of the edges.

The Fourier module of these structures is of rank six: all diffraction spots can be labeled with six integer indices. Six basis vectors can be chosen along the fivefold axes. With respect to a cubic basis in reciprocal space, these six basis vectors can be chosen as

$$\begin{aligned} \vec{a}_1^* &= b(1, \tau, 0), & \vec{a}_2^* &= b(-1, \tau, 0), & \vec{a}_3^* &= b(0, 1, \tau), \\ \vec{a}_4^* &= b(\tau, 0, 1), & \vec{a}_5^* &= b(\tau, 0, -1), & \vec{a}_6^* &= b(0, 1, -\tau), \end{aligned} \quad (2.58)$$

with $\tau = (\sqrt{5} + 1)/2$. With respect to this basis, every diffraction spot has integer coefficients h_i such that

$$\vec{k} = b[h_1 - h_2 + (h_4 + h_5)\tau, h_3 + h_6 + (h_1 + h_2)\tau, h_4 - h_5 + (h_3 - h_6)\tau] \quad (2.59)$$

is an arbitrary diffraction vector.

The basis of the Fourier module can be seen as the projection of a six-dimensional reciprocal lattice with basis vectors

$$\begin{aligned} (\vec{a}_1^*, \vec{a}_1^*), & \quad (\vec{a}_2^*, -\vec{a}_2^*), & \quad (\vec{a}_3^*, -\vec{a}_4^*), \\ (\vec{a}_4^*, -\vec{a}_6^*), & \quad (\vec{a}_5^*, -\vec{a}_3^*), & \quad (\vec{a}_6^*, -\vec{a}_5^*). \end{aligned} \quad (2.60)$$

The symmetry group of the embedded six-dimensional periodic structure is then a six-dimensional superspace group with a point group generated by

$$\begin{pmatrix} 1 & 0 & 0 & 0 & 0 & 0 \\ 0 & 0 & 1 & 0 & 0 & 0 \\ 0 & 0 & 0 & 1 & 0 & 0 \\ 0 & 0 & 0 & 0 & 1 & 0 \\ 0 & 0 & 0 & 0 & 0 & 1 \\ 0 & 1 & 0 & 0 & 0 & 0 \end{pmatrix}, \quad \begin{pmatrix} 0 & 0 & 0 & 0 & 0 & 1 \\ 1 & 0 & 0 & 0 & 0 & 0 \\ 0 & 0 & 0 & 0 & 1 & 0 \\ 0 & 0 & -1 & 0 & 0 & 0 \\ 0 & 0 & 0 & -1 & 0 & 0 \\ 0 & 1 & 0 & 0 & 0 & 0 \end{pmatrix}, \quad (2.61)$$

and the central inversion. Not all icosahedral reciprocal lattices belong to the same Bravais class. The given basis $\vec{a}_1^* \dots \vec{a}_6^*$ gives the primitive icosahedral lattice in 6D. Besides that, there are two other Bravais classes: the body-centered and the face-centered icosahedral lattices. They are characterized, respectively, by $\Sigma h_i = \text{even}$ and $h_i + h_j = \text{even}$ (for all i, j). All icosahedral quasicrystals found up till now have a symmorphic space group, either $P\bar{5} \bar{3} m$ or $F\bar{5} \bar{3} m$.

Special planes in the reciprocal space are those through a number of axes. An important plane is the xy plane. The x and y axes are twofold axes, and in the plane lie a threefold axis and a fivefold axis.

The direct lattice corresponding to the six-dimensional reciprocal lattice can, by a shear transformation, be deformed such that three independent vectors belong to the physical space. Then the intersection of the periodic 6D structure with the physical space is a periodic lattice. Such a structure is an approximant. When this shear gives a basis that is obtained from the one given above by replacing the value τ for the internal components by the ratio of two consecutive Fibonacci numbers ($\tau \approx 3/2, 5/3, 8/5$, etc.) the three-dimensional structure has a cubic lattice. Because of the shear, the symmetry is lowered to tetrahedral. These tetrahedral approximants have indeed been found. When one applies a shear to deform an icosahedral phase to a tetragonal periodic-lattice phase, in between the structure is still quasiperiodic of rank six, but the icosahedral symmetry is broken. The structure is a tetrahedral quasicrystal.

H. Three-dimensional models

A number of model calculations have been performed for three-dimensional quasicrystals. Some of the features found in one and two dimensions can also be found in three-dimensional systems, but usually in a less pronounced fashion. Janssen (1988) studied a three-dimensional icosahedral Penrose tiling with atoms in the vertices. The atoms interacted with identical harmonic springs along the edges of the constituent rhombohedra,

and there was only one degree of freedom per site (scalar phonons). The same icosahedral Penrose tiling was studied by Los and Janssen (1990), this time with vectorial phonons. If the j th atom in the structure is displaced by a vector \vec{u}_j , the potential energy is

$$V = \frac{1}{4} \sum_i \sum_{j(i)} \alpha_{ij} [(\vec{u}_i - \vec{u}_j) \cdot \hat{r}_{ij}]^2, \quad (2.62)$$

with spring constants depending on the distance. The masses are taken to be equal. A more general interaction, which allows for other than pair interactions, is (Los *et al.*, 1993a, 1993b)

$$V = \frac{1}{4} \sum_i \sum_{j(i)} [\alpha_{ij} u_{ij\parallel}^2 + \beta_{ij} u_{ij\perp}^2]. \quad (2.63)$$

Not only the perfect icosahedral Penrose tiling was studied, but also a version of it that was randomized by allowing a finite density of phason jumps. A seemingly more realistic model was studied by Los and Janssen (1990). It mimicked icosahedral AlMnSi and was the icosahedral Penrose tiling decorated according to a model given by Janot *et al.* (1989). The interactions as characterized by the spring constants derived from a Lennard-Jones potential as used in intermetallic compounds (Hafner, 1980) with a core distance that ensured stability of the structure.

More realistic interactions derived from pseudopotentials were used by Hafner and co-workers. Hafner and Krajci (1990) studied a model for AlZnMg based on the icosahedral Penrose tiling. This structure was left free to relax to a minimum in the potential energy. This yielded a modulated tiling, a quasiperiodic structure with deformed rhombohedra but still with icosahedral symmetry, as in the modulated Penrose tiling (Janssen, 1988). The interaction constants were derived as the second derivatives of the pseudopotentials in this relaxed position. A similar model, starting from an icosahedral Penrose tiling with a decoration proposed by Henley and Elser, was discussed by Hafner and Krajci (1993a, 1993b). A model for AlCuLi based on the same icosahedral Penrose tiling with decoration and with force constants given by a pseudopotential in a relaxed structure was described by Windisch and Hafner (1994).

Poussigue *et al.* (1994) presented a model for AlMn. Again, the starting structure was an icosahedral Penrose tiling. It was also supposed to model AlMnPd because the latter, although face centered icosahedral, can be obtained from a simple icosahedral structure by chemical ordering. The icosahedral-Penrose-tiling model used a decoration proposed by Duneau and Oguey. The interaction was a long-range pair potential in which strength decreased with increasing distance. Similar results were also obtained for a dynamical model based on the three-dimensional quasiperiodic Danzer tiling (Danzer, 1989; Kasner *et al.*, 1991).

The quasiperiodic structures have been studied by means of approximations. Los *et al.* (1993a, 1993b) used both a cluster method (a finite piece of quasicrystal with

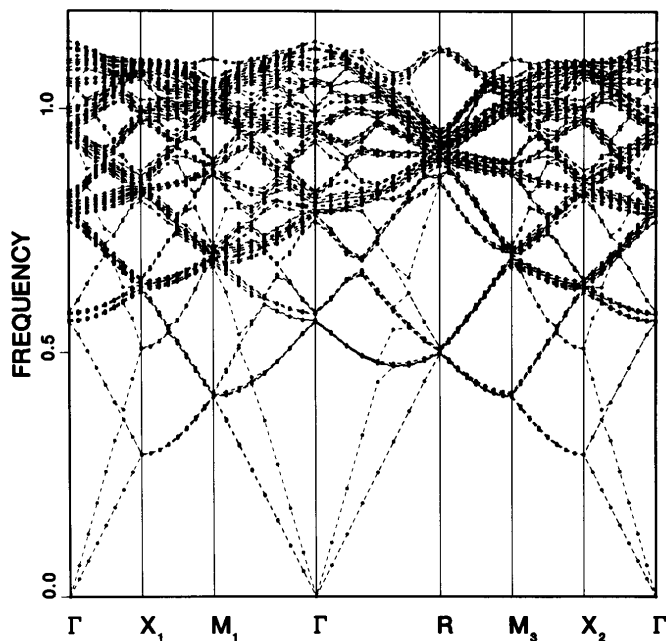


FIG. 15. Dispersion curves in the Brillouin zone of an approximant to the three-dimensional Penrose tiling. There is a strong bunch of very flat optical bands. In going to the next approximant one finds exactly the same picture, up to a scale factor in the frequency. In the quasiperiodic limit the optical bands are expected to occur at arbitrarily low frequencies (a.u.). After Los *et al.*, 1993b.

up to 16 009 atoms and with free or fixed boundary conditions) and approximants. The latter approximation consisted of replacing the coordinate τ in perpendicular space by the ratio F_{n+1}/F_n of two consecutive Fibonacci numbers. This yielded a periodic structure with cubic unit cell. The approximants were denoted by this ratio (1/1, 2/1, 3/2, 5/3, 8/5, ...). The other authors all used periodic approximants as well. The behavior of the quasiperiodic system was considered to be that of the limit of these approximants.

The calculations for the vibrational density of states were confirmed by Cordelli and Gallo (1995). These authors used a spring potential in the cluster approximation. They considered periodic approximants to an icosahedral 3D model structure and to a model for AlPdMn based on experimentally determined positions.

For the cluster method and for the periodic approximants one has to diagonalize a very large dynamical matrix or carry out an analogous procedure. Los *et al.* used the sparseness of the dynamical matrix and performed the calculations by a variation on the Lanczos method, one without reorthogonalization. Hafner *et al.* (1990) used the recursion method (Haydock *et al.*, 1972, 1975). This did not directly give the eigenvectors, but one could calculate the dynamic structure factor. Poussigue *et al.* (1994) used the spectral-moments method, which has similar possibilities (Benoit, 1987, 1989; Benoit *et al.*, 1992).

The density of states shows a large number of peaks.

In principle, there is an infinite number of van Hove singularities. Introduction of deviations from perfect quasiperiodicity by means of randomization tends to blur these details. The dynamical structure factor shows acoustic branches starting from the strong Bragg peaks, but at higher frequencies these branches broaden. There is a clear scaling behavior (Fig. 15). At low frequencies, there are pseudogaps at ever lower frequencies, if one goes to higher-order approximants, but the size of these pseudogaps tends to zero. The optical branches in the approximants run very flat. Moreover, the dispersion curves in successive approximants scale with a constant factor. This implies that these “optic” branches occur at arbitrarily low frequencies. Their contribution to the function $S(\vec{q}, \omega)$, however, decreases, such that at low frequencies near strong Bragg peaks the acoustic branches dominate. The character of the modes can be given by their participation ratio. Especially at higher frequencies, there are modes with a low participation, but such modes also occur for relatively low frequencies.

One expects that the hierarchical structure of quasicrystals, with their usually imperfect scaling symmetry, will be reflected in the eigenvectors. Indeed, a multifractal analysis of the eigenvectors gives an indication of this phenomenon. For one-dimensional models, eigenvectors may be strictly self-similar. In higher dimensions, one sees a distribution of exponents with which the local amplitudes of an eigenvector tend to zero. The vibrations of hierarchical clusters in icosahedral quasicrystals have been considered by Janot (1994). The author analyzed the icosahedral phase of AlMnPd as self-similar clusters of clusters with length scales inflated by a factor of τ^3 . Within this scheme, he derived the eigenmodes, which appeared as standing modes within the structural units generated at each inflation step. This is in agreement with the scaling of the dispersion curves as found in Los *et al.* (1993b, 1993c).

We now summarize the conclusions from the following publications: Los and Janssen (1990), Hafner and Krajci (1992, 1993a, 1993b), Los *et al.* (1993b, 1993c), Poussigue *et al.* (1994), and Windisch and Hafner (1994).

(a) *The density of states* for the 1/1 approximant is the well-known curve for face-centered cubic structures. Starting from the 2/1 approximant, the density-of-states curve is very different. It shows many peaks, corresponding to van Hove singularities. In the calculations of Hafner and Krajci (1992, 1993a, 1993b) and Windisch and Hafner (1994), various bands are clearly visible, and there is a spiky structure near the maximum frequency (Fig. 16). In those of Los and Janssen (1990), Los *et al.* (1993b, 1993c), and Poussigue *et al.* (1994), the structure is more smeared out (Figs. 17 and 18). Also, in experiment one sees less structure than in the figures in Hafner and Krajci (1992, 1993a, 1993b) and Windisch and Hafner (1994). This might also be due to the disorder that occurs in real samples. The density of states is sensitive to the presence of disorder (Hafner, and Krajci, 1992, 1993a, 1993b; Windisch and Hafner 1994). A small amount of phason disorder wipes out most of the details. Also, the type of interaction is important. For

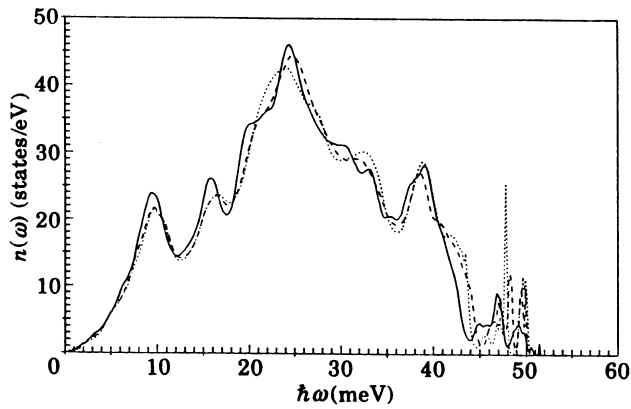


FIG. 16. Density of states for three approximants to the icosahedral AlZnMg, as given in Hafner and Krajci (1993b): the approximants are the 2/1 (dotted), 3/2 (dashed), and 5/3 (solid).

pure two-body interactions there is a broad distribution. Introducing bending forces besides stretching forces shifts the peak to higher frequencies (Los and Janssen, 1990; Los *et al.*, 1993b, 1993c)—see Fig. 19.

(b) *The dynamical structure factor.* $S(\vec{q}, \omega)$ shows pronounced acoustic branches starting with zero frequency from strong Bragg peaks. These ridges in the $S(\vec{q}, \omega)$ surface are narrow near zero frequency. This means that, in this regime, the acoustic propagating waves are well defined. The Bragg peak positions correspond to Γ points in the six-dimensional reciprocal space. In going from one strong peak to another, one passes a pseudo-Brillouin-zone boundary (Fig. 20). This corresponds to special points in reciprocal space, i.e., points with a site

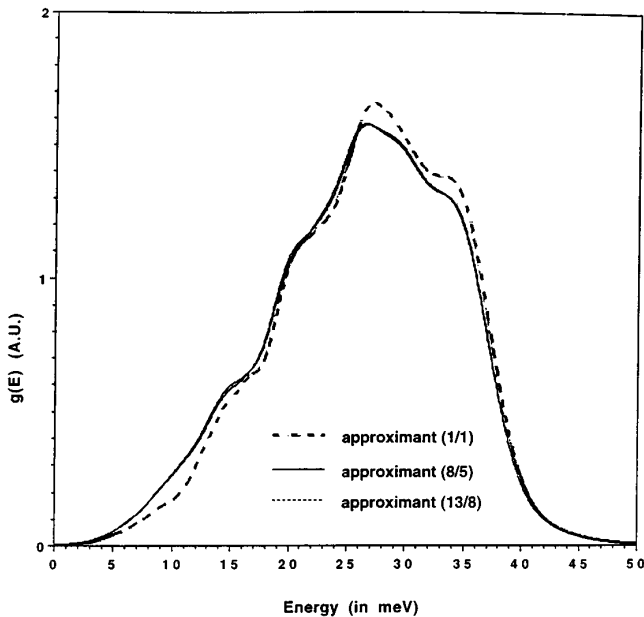


FIG. 17. Weighted density of states for AlMn, as calculated by Poussigue *et al.* (1994) for three approximants to the icosahedral phase.

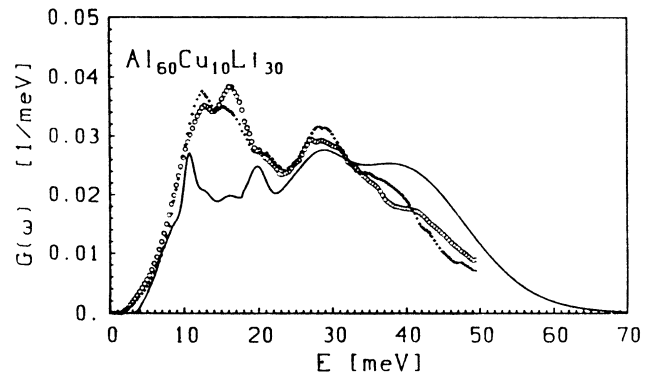


FIG. 18. Comparison of the calculated (solid line) and measured densities of states for AlCuLi in the icosahedral (circles) and R-phases (crosses). The calculations were made by Windisch *et al.* (1994). The measured values are due to Suck, 1990c (see also Fig. 39).

symmetry higher than that of other points that are infinitesimally close. In the 6D reciprocal space, these points form a lattice with a lattice parameter that is twice as small as that for the reciprocal lattice (Niizeki and Akamatsu, 1990). For higher frequencies the branches broaden, due to two effects (Fig. 21). First, there is a collection of very flat bands close together (Los and Janssen 1990; Los *et al.*, 1993b, 1993c). Due to the scaling behavior, these topic branches also occur at lower frequencies, albeit with a much smaller contribution to $S(\vec{q}, \omega)$. The other reason is that for higher frequencies the modes are more localized.

At high frequencies, there are many bands with a weak dispersion, i.e., ridges parallel to the \vec{q} axes. This is similar to the behavior of the $S(\vec{q}, \omega)$ function for IC phases when the modulation is not a small-amplitude

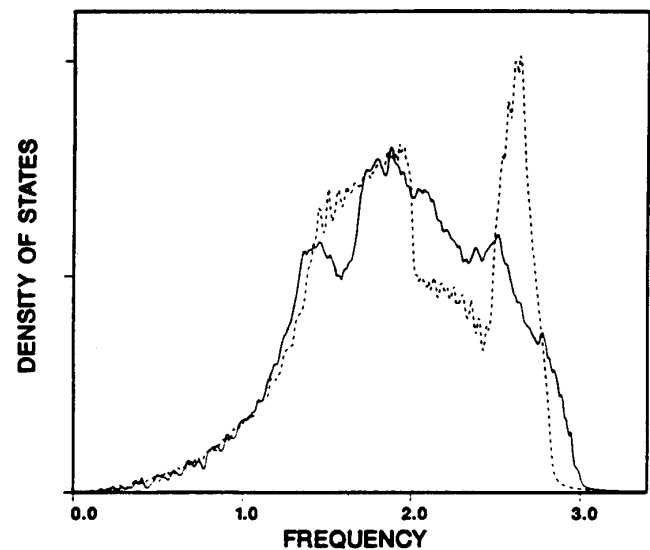


FIG. 19. Density of states for the icosahedral-Penrose-tiling model with only stretching forces (solid line) or with stretching and bending forces (dashed lines) (a.u.).

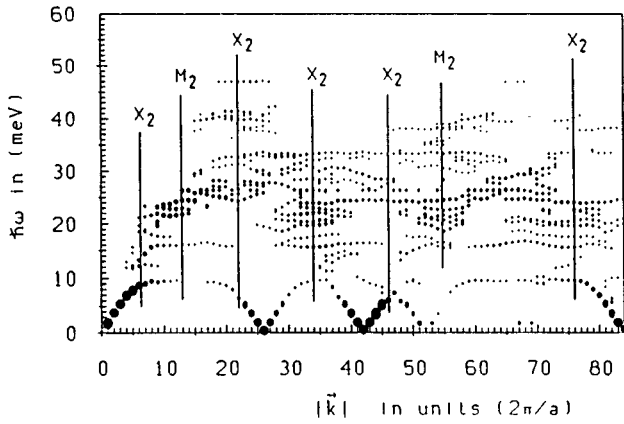


FIG. 20. Dispersion curves are observable in this plot of the dynamic structure factor along the twofold axis of an icosahedral phase. The diameter of the dots is a measure for the modulus of the dynamic structure factor. Compare this with Fig. 1, especially the case of the incommensuration region, and the $S(q, \omega)$ for the Fibonacci chain in Fig. 9 (Hafner and Krajčič, 1993b). The letters indicate the symmetry points in the 6D Brillouin zone.

sinusoidal function, but can be described by discommensurations (Currat and Janssen, 1988). The dynamical structure factor has been calculated for a plane perpendicular to a twofold axis. This plane contains two twofold axes, a threefold, and a fivefold axis.

(c) *The spectrum for one-dimensional systems* is most probably singular continuous. Multifractal analysis in

more than one dimension gives reason to believe that there is a singular continuous component there as well (Los and Janssen, 1990; Los *et al.*, 1993b, 1993c).

(d) *The low-frequency part of the spectrum* shows scaling behavior. This implies an infinity of gaps accumulating at zero frequency. The size of these gaps goes exponentially to zero, so that the relevance for experiment is rapidly lost (Los and Janssen, 1990; Los *et al.*, 1993; 1993c). The fast closing of gaps in the limit of zero frequency allows one to find an average density of states. For sufficiently small values of the frequency, the density of states behaves like ω^{d-1} , where d is the dimension of space. This is the classical behavior that reflects the fact that very long wavelength waves are insensitive to details in the structure. There is no evidence for anomalous behavior, which could lead to observable effects in the lattice specific heat.

(e) *The maxima in the $S(\vec{q}, \omega)$ function* form curves in the (\vec{q}, ω) plane, which can be considered to be dispersion relations. Near the strong Bragg peaks, the dispersion is linear. Moreover, its slope does not depend on the direction. For icosahedral models, the dispersion is isotropic, in agreement with the group-theoretical prediction that materials with icosahedral symmetry should have isotropic elastic constants. Moreover, the frequency for transverse acoustic phonons does not depend on the direction of the polarization vector (Hafner and Krajčič, 1992, 1993a, 1993b; Windisch and Hafner, 1994).

There are bands of optical modes at higher frequencies with little dispersion. The acoustic branches are

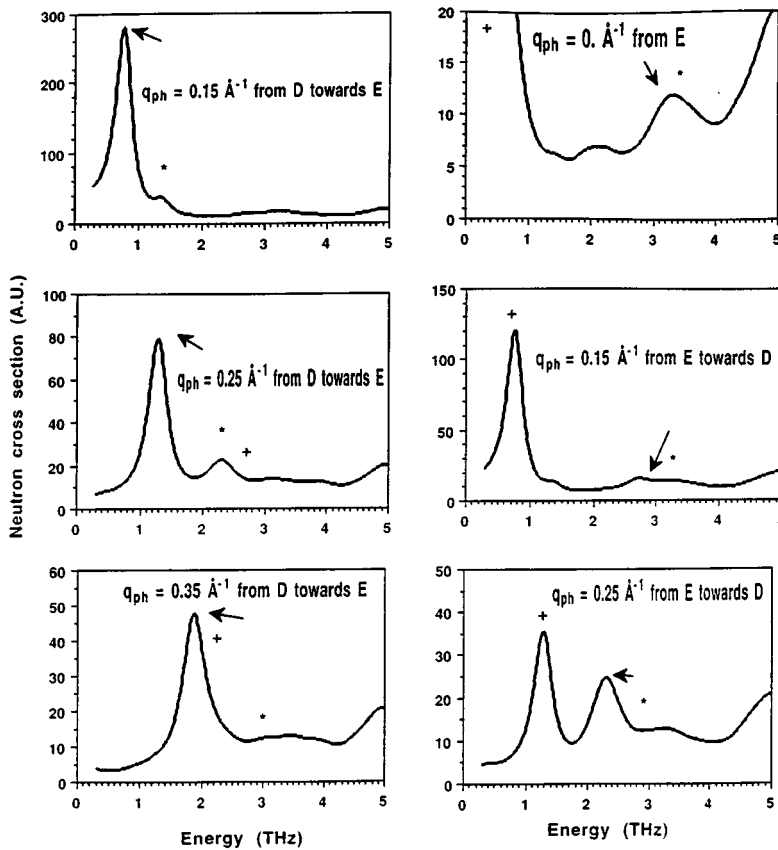


FIG. 21. Calculated inelastic cross section for six values of q along a path from D to E in reciprocal space, i.e., between two strong Bragg peaks. Close to the Bragg peak (small energy) the width is small; for higher energies the width increases. This can be seen also in Figs. 9 and 10.

symmetric around high-symmetry points, which lie on the pseudo-Brillouin-zone boundaries. Such pseudo-zone-boundaries are planes perpendicular to and bisecting the line between two strong Bragg peaks. The frequency maxima in the dispersion curves correspond to peaks in the density of states.

(f) *The character of the eigenstates* has been discussed in recent papers. There is a claim (Hafner and Krajci, 1993a) that there are strictly confined states in quasicrystals, i.e., states that are strictly zero outside a certain region. These are supposed to be connected to specific topological configurations. Whether or not this is true, or whether the effect is an artifact of the finite size of the calculations is an open question.

Another claim (Liu *et al.*, 1992) is that there are states of fracton-like nature. Fractons are the self-similar excitations found in certain fractal models. The inverse participation ratio varies widely over the states. Near the maximum frequency the states have a localized character. Their inverse participation ratio is relatively high. In going to higher approximants this value diminishes, however, which is an indication that the states are not exponentially localized. A multifractal analysis gives an indication that the states are critical (Los and Janssen, 1990; Los *et al.*, 1993b, 1993c).

Near zero wave vector, the states have more the character of Bloch waves. Numerically, it is impossible to show whether or not these states are extended. Because there are (very small) gaps at arbitrarily low frequencies, the situation could be analogous to that in one-dimensional models, where the states are in reality critical, but this property becomes unimportant if the wavelength approaches the coherence length. The same physical consideration is valid for localized or pseudolocalized states. Even if the state for an ideal infinite quasicrystal were critical, but with the state decaying exponentially to very small values, the state could not practically be distinguished from really localized states.

(g) *Phason hopping*, a special type of dynamics, may be present. This is not a harmonic motion. The phenomenon is possible because the quasicrystalline ground state is just slightly above an infinity of structures with phason defects, produced by phason jumps. If the barrier between the ground state and one of these nearby states is low enough, phason hopping is possible. Because a phason flip, generally, makes other phason flips easier, these motions may migrate through the structure. A coherent motion of this type is a new type of excitation, typical of quasicrystals. It may be related to the “breather” suggested by Aubry (1993)—a long-lived vibration having large amplitude (see Sec. III.G.3).

III. EXPERIMENTAL RESULTS

A. Neutron scattering from icosahedral quasicrystalline phases measured with a three-axis spectrometer: Introduction

Three-axis experiments provide a unique technique that allows the measurement of phonon dispersion

curves and the determination of their symmetry properties in crystalline solids. One of the main reasons for measuring the dispersion curves for lattice vibrations is to obtain information on the forces between the atoms. In pure Al or in pure Cu, such measurements have shown that nearest-neighbor interactions are dominant, but there is also a weak longer-range force system with interactions extending to at least sixth-nearest neighbors (Yarnell, 1965). In lattice periodic crystals, modes are classified with the irreducible representations of the group of the wave vector. They have specific symmetry properties that can be studied in a neutron-scattering experiment.

The experiment deals with a scattering process in which incoming neutrons with a wave vector k_i (energy E_i) are scattered by the sample through an angle ϕ to an outgoing wave vector k_f (energy E_f). For ordinary lattice periodic crystals, the conservation laws are

$$\vec{k}_i - \vec{k}_f = \vec{H} = \vec{G} + \vec{q}, \quad (3.1)$$

$$|E_i - E_f| = \hbar \omega, \quad (3.2)$$

for the transferred momentum and energy, respectively.

The vectors k_i, k_f, \vec{H} define the scattering geometry and also the so-called scattering plane. The phonon excitations have a wave vector \vec{q} , which in lattice periodic crystals is measured from a zone center (Bragg peak) located at \vec{G} (\vec{G} is a vector of the reciprocal lattice). For aperiodic crystals, this decomposition is not unique, but the differential cross section can still be measured in the plane through k_i and k_f .

In the experiments we shall present here, the scattering plane was chosen so as to measure phonon dispersion curves in a plane where strong Bragg peaks are located. As has been seen in Sec. II, it is here that one expects to see dispersion curves.

For the experiments on icosahedral quasicrystals, a plane was chosen through the main symmetry axes of the icosahedral phase. This plane is shown in Fig. 22. It is defined by two orthogonal twofold axes and contains threefold and fivefold axes, too. Circles locate Bragg reflections; they are labeled following the indexing method for icosahedral quasiperiodic crystals proposed by Cahn *et al.* (1986). If the diffraction peaks are located on positions

$$[h + h' \tau, k + k' \tau, l + l' \tau],$$

with respect to a cubic reference frame, one defines

$$N = h^2 + h'^2 + k^2 + k'^2 + l^2 + l'^2,$$

$$M = h'^2 + k'^2 + l'^2 + 2(hh' + kk' + ll'). \quad (3.3)$$

Notice that N and M do not characterize the points of the Fourier module uniquely. With respect to the basis defined in Eq. (2.58), with $b=1+2\tau$, one has indices h_i ($i=1,2,\dots,6$). Large dark circles indicate high-intensity peaks. The quasicrystalline compounds that have been investigated by means of neutrons have the same point

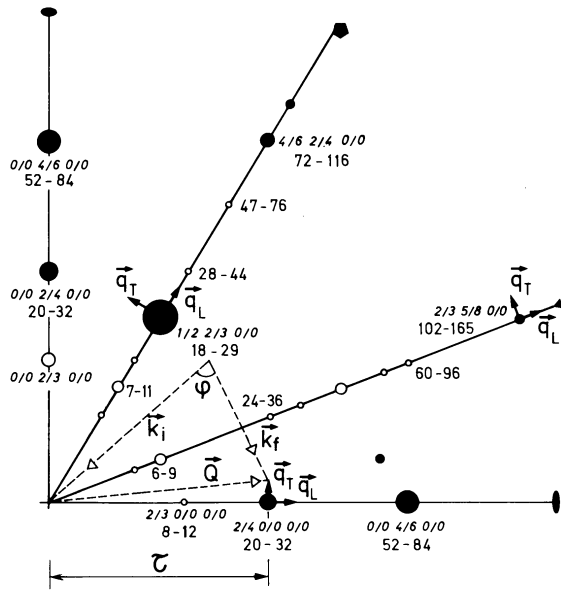


FIG. 22. The scattering plane. Circles locate Bragg reflections. Large dark circles indicate high-intensity peaks around which acoustic modes were measured. Peaks are labeled following the indexing method of icosahedral quasiperiodic crystals by Cahn *et al.* (1986).

group but their space-group symmetry defined in the 6D superspace representation may be different. In Table I we have listed all the Bragg reflections of interest for the experiments described in this section, which are represented by dark circles in Fig. 23. They are all located on the main symmetry axes.

The differential scattering cross section has been given in Eq. (2.30). In lattice periodic crystals, the inelastic neutron dynamical response $S(H, \omega)$ is given by

$$S(\vec{H}, \omega) = \sum_{\nu=1}^{\text{all modes}} S_{\nu}(\vec{H}, \omega), \quad (3.4)$$

where the summation is over all vibrational modes of the crystal. For a single mode one has

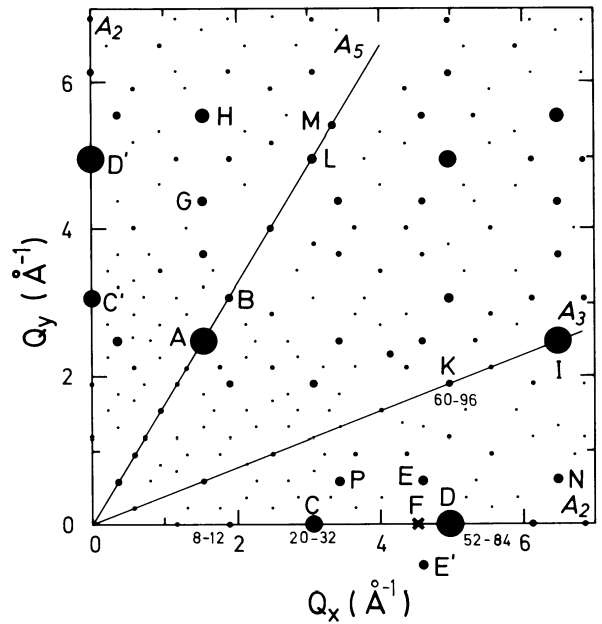


FIG. 23. The reciprocal plane of the AlMnPd phase chosen as the scattering plane for neutron inelastic measurements.

$$S_{\nu}(\vec{H}, \omega) = \langle n(\omega) + 0.5 \pm 0.5 \rangle |F_{\text{in}}(\vec{H})|^2 \delta[\omega \pm \omega_{\nu}(\vec{q})] \times \delta(\vec{H} \pm \vec{q} - \vec{G}). \quad (3.5)$$

In this expression, the first term is the usual Bose factor written for phonon creation (+) and annihilation (-), respectively, and F is the matrix element

$$F_{\text{in}}(\vec{H}) = \sum_{j=1} m_j^{-1/2} \omega_{\nu}(\vec{q})^{-1/2} b_j [\vec{e}_j^{\nu}(\vec{q}) \cdot \vec{H}] \exp(i\vec{H}\vec{r}_j) \times \exp[-W(H)], \quad (3.6)$$

where m_j is the mass of the atom j and b_j its coherent scattering length, which depends on the isotope and on the nuclear spin. The scattering lengths for neutrons vary rapidly from element to element and are much

TABLE I. Indices and labels of the strong reflections shown on the scattering plane of the AlMnPd phase.

N	M	h	h'	k	k'	l	l'	h_1	h_2	h_3	h_4	h_5	h_6	
18	29	1	2	2	3	0	0	1	0	0	0	0	0	A
20	32	2	4	0	0	0	0	1	-1	0	0	0	0	C
26	41	3	4	0	1	0	0	-1	0	1	1	1	1	P
46	73	3	6	0	1	0	0	1	-2	1	0	0	1	E
46	73	1	2	4	5	0	0	2	1	-1	0	0	-1	
52	84	4	6	0	0	0	0	0	0	0	1	1	0	D
60	96	4	6	2	2	0	0	1	1	-1	1	1	-1	K
70	113	1	2	4	7	0	0	1	0	1	0	0	1	H
80	128	4	8	0	0	0	0	2	-2	0	0	0	0	
90	145	5	8	0	1	0	0	0	-1	1	1	1	1	N
90	145	3	4	4	7	0	0	0	1	1	1	1	1	M
72	116	4	6	2	4	0	0	0	0	1	1	1	1	L
102	165	5	8	2	3	0	0	1	0	0	1	1	0	I

smaller than the scattering factors for x rays. Furthermore, this difference is enhanced by the fact that they enter as squared quantities in the formulas for the scattered intensity. This is a reason why large samples are needed for neutron experiments. Neutrons are weakly absorbed by most elements, which allows investigation of large samples. In Eq. (3.6), $W(H)$ is the exponent of the Debye-Waller factor and \vec{e}_j^ν is the eigenvector of the ν th mode. For lattice periodic systems it has 3s components and describes the pattern of the displacements of the s atoms in one unit cell. This displacement field consists of plane waves and is periodic through the lattice. For any \vec{q} in the Brillouin zone, one has 3s dispersion curves, which reach the zone boundary (Bragg plane) generally with a horizontal slope. When \vec{q} is along a high-symmetry direction of the structure, the phonon modes have specific symmetry properties. For a nonsymmorphic space group, degeneracy may occur at the zone boundary and then dispersion curves have non-zero slope at this point.

The occurrence of the scalar product $\vec{e}_j^\nu \cdot \vec{H}$ in Eq. (3.6) allows us, in simple cases, to find a geometry in which the identification of the observed modes, which have to be polarized in the scattering plane, is easy. For small q , the inelastic structure factor of acoustic modes scales with the static structure factor of the Bragg peak from which they emanate. Thus one measures acoustic phonon modes near strong Bragg peaks. Usually we do not work with perfect ideal crystals, and there are all kinds of departures from this perfection, such as anharmonicity, phase-transition precursors effects, electron-phonon interactions, impurities, disorder, and so on. As a consequence, the phonon quasiparticle has a finite lifetime and the plane wave is either damped or diffusive. Thus the scattering function does not remain a delta function. The response function in energy transfer is very often taken to be that of a damped harmonic oscillator, which reads as

$$\frac{\Gamma_\nu(\vec{q}, T)}{[\omega^2 - \omega_\nu^2(\vec{q}, T)]^2 + \omega^2 \Gamma_\nu^2(\vec{q}, T)}. \quad (3.7)$$

Here $\omega_\nu(\vec{q}, T)$ is the quasiharmonic frequency of the oscillator and $\Gamma_\nu(\vec{q}, T)$ its damping. This last parameter can be given by an analytical expression if we have a model that describes the anharmonicity of the system.

In a three-axis experiment, the measured intensity is the convolution product of the dynamic structure factor with the resolution function of the spectrometer. This last function depends on k_i , and k_f , and in the Gaussian approximation the surfaces of equal probability are four-dimensional ellipsoids called “ellipsoids of revolution.” Dorner (1972) has given an explicit expression for the normalization of the resolution function of a three-axis spectrometer. The important point to emphasize here is that, when one measures transverse acoustic modes, the setting of the spectrometer has to be “focalized,” which means that the larger main axis of the ellipsoid has to be roughly parallel to the dispersion curve. One weak point of three-axis measurements is that for longitudinal acoustic modes we cannot work in a “focal-

TABLE II. Atomic coherent scattering length b and nuclear absorption cross section σ .

Element	$b_{\text{coh.}}$ (10^{-12} cm)	σ (10^{-24} cm ²)
Al	0.3449	0.231
Li	-0.203	70.5
Cu	0.7718	3.78
Fe	0.954	2.56
Mn	-0.373	13.3
Pd	0.591	6.9

ized geometry,” so the signal is less well resolved. This is also the case when one measures dispersionless optic modes. In the experimental work that we shall report on in the following subsections, we shall be concerned with these technical constraints, which make the interpretation of the raw data rather delicate.

In lattice periodic crystals that have a nonsymmorphic space group, three-axis experimental results are frequently displayed in the extended-zone scheme. In such a scheme one takes into account the way in which the glide symmetry modifies the relevant phase factor of the mode that propagates with a given q vector. For lattice periodic crystals, the extended-zone scheme representation of the dispersion curves displays the behavior of the inelastic structure factor of the measured modes. For aperiodic crystals, this extended-zone scheme is the natural one, because there is no Brillouin zone, or one may say that its volume is zero.

Up to now, three-axis experimental results have been obtained for only three quasicrystalline icosahedral phases. In shorthand notation, these three phases are AlFeCu, AlLiCu, and AlMnPd. They were studied with coherent neutron scattering experiments that followed the same procedure. Experiments were carried out on monodomain samples of very different size and mosaic spread. As shown in Tables II and III, one can calculate average values of b and σ for the studied phases. Then a simple calculation shows that 7 mm³ of the AlFeCu phase has the same scattering efficiency as 161 mm³ of the AlLiCu phase, or of 20 mm³ of the AlMnPd phase.

We have seen in the theoretical section that, for quasisperiodic structures, strong Bragg peaks act as pseudo-Brillouin-zone centers and, as in a periodic crystal, the degeneracy at Bragg planes (pseudo-zone-boundary) still exists. This degeneracy should open up, on dispersion curves, a gap that has a width proportional to the diffraction amplitude at the corresponding Bragg plane. Furthermore, as we reminded the reader in the experimental introduction, in periodic-lattice crystals the in-

TABLE III. Mean coherent scattering length and mean absorption cross section.

	Mean b_m	b_m^2	Mean σ_m
Al _{60.3} Li _{29.2} Cu _{10.5}	0.230	0.053	21.12
Al ₆₃ Fe ₁₂ Cu ₂₅	0.525	0.275	1.4
Al _{68.7} Pd _{21.7} Mn _{9.6}	0.329	0.108	2.93

tensity of acoustic modes scales with that of the Bragg peaks from which they emanate. Therefore, for each compound studied up to now, the measurements were undertaken mainly around the selected strong Bragg reflections. The scattering intensity was measured along a path in reciprocal space going from one intense Bragg peak to another. We now turn to the specific examples AlCuFe, AlCuLi, and AlMnPd to discuss the experiments in some detail.

B. Results for Al₆₃Cu₂₅Fe₁₂

This compound was investigated by Quilichini *et al.* (1990), using a sample with a volume of 7 mm³. A neutron-diffraction study on a four-circle instrument (5C2 at the ORPHEE reactor, Saclay) permitted a complete structure analysis (Cornier-Quiqandon *et al.*, 1991). To check the icosahedral symmetry, a set of symmetry-related Bragg reflections was measured, and equivalent reflections did indeed have the same intensity. The high quality of the sample was ascertained by studying profiles that corresponded to almost the instrumental resolution obtained by measurements on an ideal single crystal of germanium. Furthermore, a study of the mosaic spread was performed using γ rays from a gold source. Rocking curves of three (20,32) reflections were recorded and showed that the measured full width at half maximum varied from 0.04° to 0.06°; this is roughly one order of magnitude greater than that of a good silicon crystal. These results indicate a perfect quasicrystal without any phason strain, especially when compared to monodomain icosahedral AlLiCu samples, the best of which show a “mosaicity” of about 0.8° and a strong and typical dependence of the reflection profiles on the perpendicular component of the scattering vector H_{\perp} ; this dependence was completely absent for the AlFeCu sample. Data were collected on the intensities of all Bragg peaks up to $H=11.6 \text{ \AA}^{-1}$ in order to make a complete structure analysis. Such an analysis, which is far from trivial for quasicrystalline structures, was first proposed for this compound by Cornier-Quiqandon *et al.* (1991), who specified several steps:

(1) First the 6D space group must be determined. For this icosahedral AlCuFe it was found to be the centered symmorphic icosahedral group $F\bar{5}\bar{3}m$ with a lattice parameter equal to $2a$ ($a=0.63146 \text{ nm}$).

(2) Then a 6D Patterson analysis is carried out, in order to locate the atomic surfaces. There are three such atomic surfaces with full icosahedral symmetry at the nodes $[0,0,0,0,0]$ and at the body center $1/2[1,1,1,1,1]$ of the 6D unit cell. This analysis also demonstrates that atomic surfaces are embedded in 3D hyperplanes parallel to the internal space.

(3) Finally, geometrical shapes and the attributes of the chemical species within these atomic surfaces are determined. This step requires specific models and has not yet been fully carried out. Still, the Patterson analysis leads to an insight into the geometrical properties of these atomic surfaces.

This structural characterization also showed that the sample was a high-quality monodomain quasicrystal. There was no indication of the presence of the microcrystalline phase in the temperature range in which the measurements were performed.

Inelastic measurements, performed at the ORPHEE reactor, were undertaken by Quilichini *et al.* (1990) around strong Bragg reflections of the scattering plane with \vec{q} either parallel to or normal to symmetry axes. Phonon acoustic modes were detected in transverse and longitudinal configurations and found to follow the usual linear dispersion. A systematic data analysis was carried out to account for the convolution of the instrumental resolution with the observed linear dispersion. In the fitting procedure, the phonon response was described by the response function of a damped harmonic oscillator. At room temperature, the signal-to-background ratio became very low for energy higher than about 2.5 THz; therefore the sample was heated up to 400 °C to increase the thermal population and a reasonably good signal up to 3.8 THz was achieved.

The fitted data give evidence for two “regimes.” The first regime corresponds to wave vectors $|\vec{q}|$ smaller than approximately 0.45 \AA^{-1} ; there, the observed modes have no intrinsic width and dispersion curves are linear as in lattice periodic crystals. Furthermore, the slopes of these curves (sound velocities: $v_T=7700 \text{ m/s}$, $v_L=3650 \text{ m/s}$), for both longitudinal and transverse acoustic branches, are independent of the direction of propagation and of the H_b values (Fig. 24). This proves that we have only two elastic constants C_T and C_L , as expected from the icosahedral point-group symmetry, whereas the independence of the results with respect to the chosen Bragg peak supports the idea of a pseudo-Brillouin zone.

The second regime starts from wave vectors greater than 0.4 \AA^{-1} , where the inelastic signal, obtained in transverse geometry, loses its intensity as q increases. Furthermore, this loss is accompanied by a spread of the signal over an appreciable energy range. This was accounted for in the data analysis by introducing an intrinsic phonon linewidth Γ and a decrease of the slope of the dispersion curve, as shown in Fig. 25.

For the longitudinal geometry the signal remains too poor to give reliable results (Quilichini *et al.*, 1992). A general discussion is postponed until after the description of the experimental three-axis data obtained for the three icosahedral phases.

C. Results for Al_{60.3}Cu_{10.5}Li_{29.2}

The properties of AlCuLi were reported on by Goldman *et al.* (1991, 1992). The inelastic measurements were carried out on single grains of icosahedral AlLiCu and the related cubic R phase. A 0.4 g single grain of Al_{60.3}Cu_{10.5}Li_{29.2} with an approximate volume of 192 mm³ was characterized by electron microscopy, neutrons, and x-ray Laue photographs. The size and the shape of diffraction spots indicated that the entire grain contributed to the diffraction. However, the mosaic spread was rather broad and equaled 1.2° (full width at

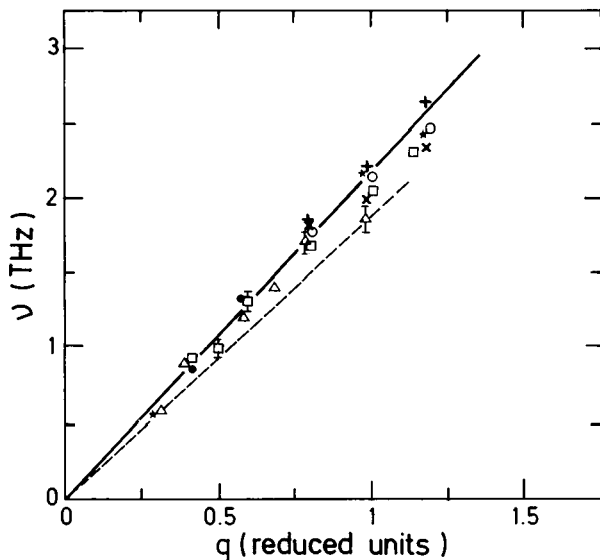


FIG. 24. Transverse acoustic dispersion curve in the linear regime for icosahedral $\text{Al}_{63}\text{Cu}_{25}\text{Fe}_{12}$; q (reduced unit) $=q(\text{\AA}^{-1}) \times a/2\pi$ ($a=16.944 \text{ \AA}$, where a is a pseudocubic lattice parameter). Pseudoindices H, K, L , are calculated using $H=h+h'\tau$, $K=k+k'\tau$, $L=l+l'\tau$, where τ is the golden mean). Notation: \bullet 2/4, 0/0, 0/0; \triangle 0/0, 2/4, 0/0; \square 1/2, 2/3, 0/0; $*$ 0/0, 4/6, 0/0; \circ 4/6, 0/0, 0/0; \times 4/6, 2/4, 0/0; $+$ 2/3, 5/8, 0/0. The dashed line gives the sound velocity in pure Al (Stedman and Nilsson, 1966) for the transverse mode with q along [001]. After Quilichini *et al.* (1990).

half maximum). A 1.3 g grain of cubic $\text{Al}_{56}\text{Cu}_{12}\text{Li}_{32}$ was also prepared and characterized. A complete neutron and x-ray structural analysis of this AlCuLi was proposed by de Boissieu *et al.* (1991), who showed that this quasicrystalline structure has a centrosymmetric superspace group $P53m$ and that the asymmetric unit in the unit cell of the periodic superspace contains three atomic surfaces parallel to perpendicular space. These atomic surfaces are located at the node sites $[0,0,0,0,0,0]$, at the mid-edge sites $[1/2,0,0,0,0,0]$, and at the body-center sites $1/2[1,1,1,1,1,1]$.

Recently Elcoro *et al.* (1994) have proposed a general program (QUASI) for the refinement of quasicrystalline structures. In this program, the superspace formalism is used and the contours of each symmetry-independent atomic hypersurface in the internal space are parametrized in terms of linear combinations of radial (surface-harmonic) functions that are invariant for the hypersurface point group in internal space. The program has been used to refine the structure of the same icosahedral quasicrystal of AlCuLi (Elcoro and Perez Mato, 1994), leading to a structural model that confirms the structure proposed by de Boissieu *et al.* (1991), except for some significant variation of the detailed shape of the lithium surface and the chemical disorder of the other two atomic surfaces.

The inelastic neutron experiment was performed at the high-flux reactor of the Institut Laue-Langevin at Grenoble (France) and at the ORPHEE reactor in

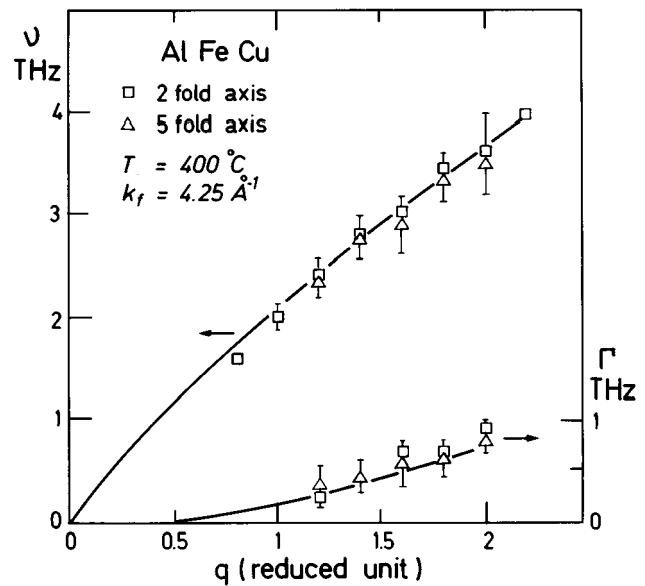


FIG. 25. Dispersion curve of the unique transverse acoustic mode in icosahedral $\text{Al}_{63}\text{Cu}_{25}\text{Fe}_{12}$; dependence on q of the width Γ of this mode; q (reduced unit) $=q(\text{\AA}^{-1}) \times a/2\pi$ ($a=17.09 \text{ \AA}$ at $400 \text{ }^\circ\text{C}$). After Quilichini *et al.* (1992).

Saclay. The scattering plane was as described in the introductory part of this section. The R phase sample was oriented so as to have the analogous plane coincident with the scattering plane. In Fig. 26 one can see the close similarity between the diffraction patterns of the icosahedral and of the R phase. This results from the fact that the dominant scattering clusters in the cubic unit cell of the R phase have icosahedral symmetry.

These inelastic measurements consisted of constant- H energy scans taken along the twofold, threefold, and fivefold directions of the icosahedral sample. Acoustic-like modes were in evidence, as in the experiment on the icosahedral phase of AlFeCu described in the previous subsection. The slopes of the linear dispersion curves for the transverse and longitudinal acoustic branches were isotropic, as expected from the point-group symmetry and in good agreement with ultrasonic measurements obtained by Reynolds *et al.* (1990) on single grains of icosahedral AlLiCu: $v_t=(6.4 \pm 0.1) \times 10^3 \text{ m/s}$, $v_l=(3.8 \pm 0.1) \times 10^3 \text{ m/s}$. In addition, Fig. 27 shows, for the icosahedral phase, the dependence of the phonon integrated intensity (normalized to Q^2) upon the integrated intensity of the zone-center Bragg peak. This shows that the inelastic structure factors of long-wavelength acoustic modes scale to the static structure factor of the Bragg reflections near which they are measured, as expected in lattice periodic crystals. This, again, supports the pseudo-Brillouin-zone concept mentioned above for icosahedral AlFeCu. As can be seen in Fig. 28 and Fig. 29, this concept is nicely illustrated by the dispersion of curves of the longitudinal mode along the fivefold axis (between L and M Bragg peaks) and of the transverse acoustic phonon along the twofold axis (between N and I).

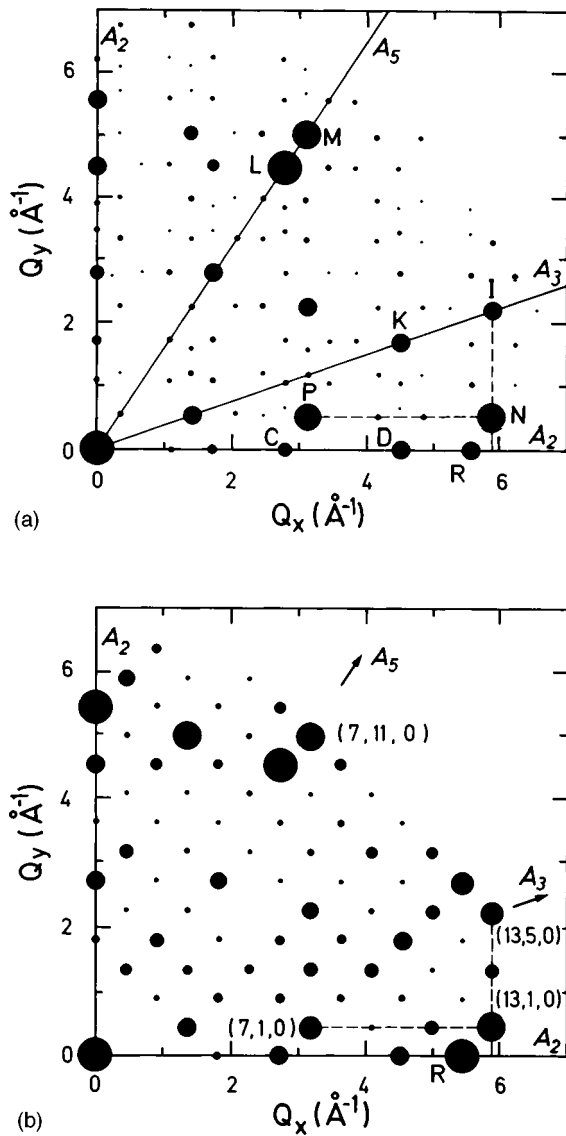


FIG. 26. Twofold planes of AlLiCu investigated by neutron inelastic-scattering measurements: (a) icosahedral phase, and (b) the R phase. The dashed lines denote the directions of inelastic scans for the twofold longitudinal and transverse modes. The arrows in the R -phase plane denote the threefold and the fivefold axes of the icosahedral phase for comparison. After Goldman *et al.* (1992).

Hence one may define pseudo-Brillouin zones in the reciprocal space of the quasicrystalline phase between pairs of strong Bragg reflections. A set of similar measurements at small q was carried out for the R phase. An interesting result was observed for the transverse acoustic modes, which propagate along $[100]$ and $[011]$. There, the elastic anisotropy expected from the cubic symmetry, which predicts two elastic constants C_{44} and $1/2(C_{11}-C_{12})$, was not detected and the transverse sound velocity for the cubic phase was the same as that of the icosahedral phase. So far, it appears that in the long-wavelength limit, longitudinal and transverse phonon dispersion curves for the icosahedral and cubic R phase are quite similar. However, differences were

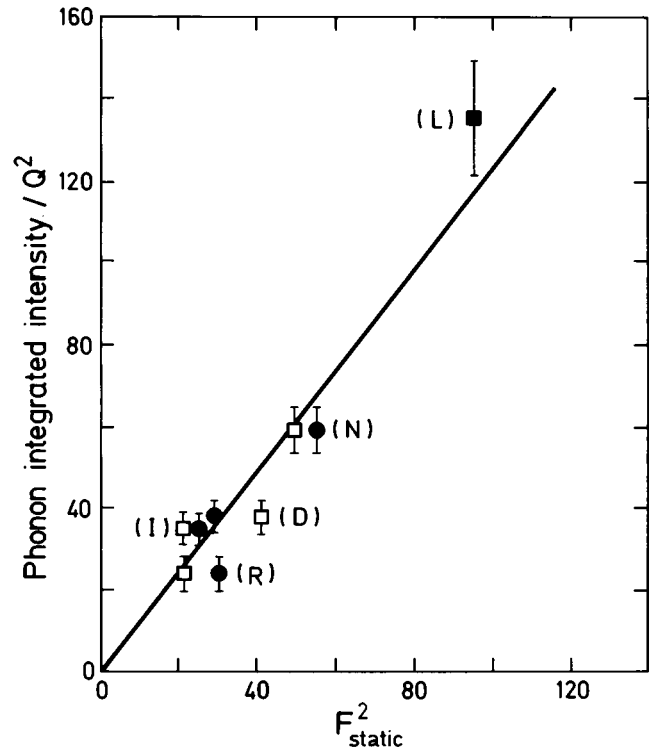


FIG. 27. Dependence of phonon-integrated intensity, measured in icosahedral AlLiCu: \square , upon the integrated intensity of the zone-center Bragg peak; \bullet , upon the static structure factor obtained from Gayle (1987). Letters denote the zone center for the measurements, and the solid line is a guide to the eye. After Goldman *et al.* (1992).

found at higher energies for a phonon wave vector larger than about $0.4\text{--}0.5 \text{ \AA}^{-1}$. In the R phase, longitudinal modes along twofold axes drawn on a special path in the reciprocal space show a dispersive opticlike behavior, while in the quasicrystalline phase the same dispersion curve is rather flat for an equivalent path. This flat dispersion observed at high energy in the icosahedral phase is quite similar to the trend already noticed in the icosahedral phase of AlFeCu and is reminiscent of the behavior of localized modes. Finally, this latter experiment demonstrates the interest of studying approximant phases along with the corresponding parent quasicrystal phases.

D. Results for $\text{Al}_{68.7}\text{Pd}_{21.7}\text{Mn}_{9.6}$

AlMnPd was investigated by de Boissieu *et al.* (1993). An analysis (Boudard *et al.*, 1992) of diffraction data collected with the neutron four-circle spectrometer 5C2 (at the ORPHEE reactor, Saclay) has allowed—with the help of a simple model—description of its structure in the 6D space. The unit cell is cubic and primitive with a parameter $a=6.451 \text{ \AA}$. There is, however, a set of superstructure reflections, whose indices are all half integer. This superstructure is induced by small differences in atomic hypersurface shapes, volumes, and/or the chemi-

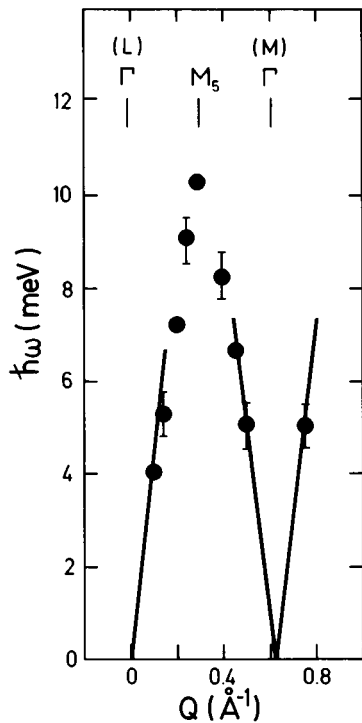


FIG. 28. Longitudinal modes along the fivefold axis between points L and M of the icosahedral AlLiCu phase. After Goldman *et al.* (1991).

cal species involved. The space group is either $\overline{F53m}$ or $F532$, and atomic surfaces are located at the nodes of high symmetry in the 6D cubic unit cell: $[0,0,0,0,0,0]$, $[1,0,0,0,0,0]$, $1/2[1,1,1,1,1,1]$, and $1/2[1,1,1,1,1,1]$ (n_0 , n_1 , bc_0 , and bc_1 , respectively). The authors have proposed that these atomic surfaces be defined as follows:

(1) A core of Mn (radius $0.83a$) surrounded by an intermediate shell of Pd (extending up to $1.26a$) and an outer shell of Al (up to $1.55a$) centered at position n_0 .

(2) A core of Mn (radius $0.52a$) surrounded by a shell of Al (up to $1.64a$) centered at position n_1 .

(3) A ball of Pd (radius $0.71a$) at position bc_1 and a small ball of Al (radius $0.3a$) or an empty volume at bc_0 .

The sample used for the three-axis experiment, performed at the ORPHEE reactor, was a single grain of volume 250 mm^3 , which was grown by a Bridgman technique. It was built up of about 10 slightly misoriented subdomains, each having a mosaic spread of about 0.15° , leading to an overall mosaicity of 1.5° . With such a sample, the measured signal was an order of magnitude greater than that obtained with AlFeCu. The selected strongest Bragg reflections of the scattering plane were nearly the same set as for AlFeCu. They were 52/84 (D, D') and 20/32 (C) on the twofold axes, 18/29 (A) on the fivefold axis, and 102/165 on the threefold axis; for all of them a systematic study of the transverse acoustic and longitudinal acoustic (LA) modes was carried out. As in the other two icosahedral phases, the acoustic dispersion curves show two regimes. For small q values, the modes have no intrinsic width and the branches are linear, giving sound velocities for trans-

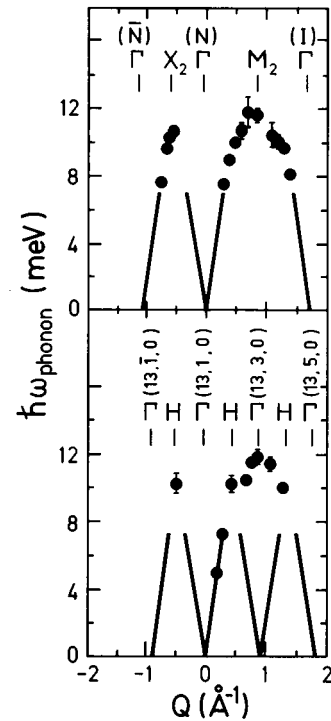


FIG. 29. Transverse phonon modes along the twofold direction of the icosahedral (top panel) and the cubic R phase (bottom panel) of AlLiCu. The Γ points denote the zone-center positions. The straight lines indicate the low-energy acoustic mode. After Goldman *et al.* (1992).

verse and longitudinal modes that are isotropic and in good agreement with values obtained from ultrasonic measurements (Amazit *et al.*, 1992), namely $3593(3) \text{ ms}^{-1}$ and $6520(10) \text{ ms}^{-1}$ for the TA and LA branches, respectively. For larger values of q (q greater than 0.35 \AA^{-1} for the TA modes and q greater than 0.15 \AA^{-1} for the LA modes), modes were fitted to a damped harmonic oscillator, showing, as q increased, a damping parameter Γ that increased, an intensity that decreased, and a quasi-harmonic frequency that seemed to saturate around 3 THz. This is clearly in evidence in Fig. 30, which presents the dispersion curves of the TA modes emanating from D and D' , respectively, and which propagate along a twofold axis. For both curves, it seems that there is a horizontal slope for a q value roughly equal to 1.45 \AA^{-1} ; however, note that the TA branch starting from D has an energy that saturates at almost 4 THz, while the TA branch coming from D' saturates at an energy of 3 THz.

Two paths were studied intensively in this phase; the aim was to observe the behavior of the dispersion curves at what could be a pseudo-Brillouin-zone boundary.

(1) The first path was ($EDE'FE$ in Fig. 23), built with the two symmetry-related Bragg peaks 46/73 and the Bragg reflection 52/84 located on the twofold axis (0.691 \AA^{-1} away from 46/73). Along $DE(DE')$ the wave vector \vec{q} is parallel to a fivefold axis and measurements were performed with a geometry allowing the wave vector to be "focalized" either for the acoustic modes that come

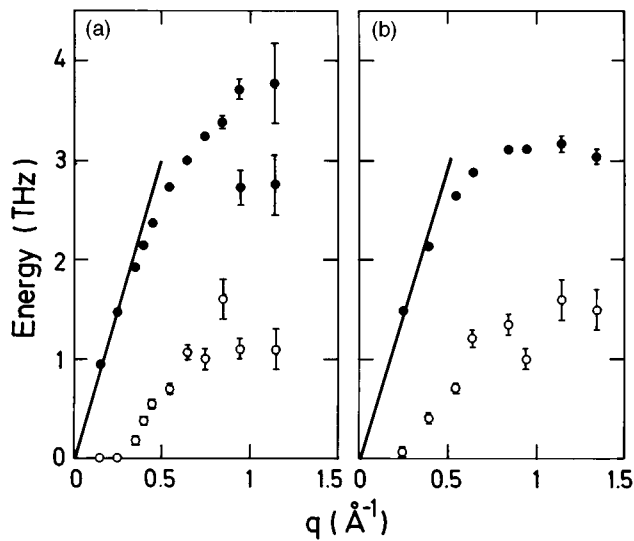


FIG. 30. Dispersion relation (\bullet) and phonon width (\circ) for the transverse acoustic modes that emanate from Bragg reflections: (a) D ; (b) D' . They propagate along twofold axes, which are parallel to two different directions in icosahedral AlMnPd. After de Boissieu *et al.* (1993).

from the 52/84 Bragg reflection or for the acoustic modes that emanate from the 46/73 reflection. This allowed the measured modes to be identified more easily and to give more reliable fitted results. The ratio of the structure factors of D and E reflections is roughly 10; this is also the ratio of the inelastic structure factors of the TA modes that come from D and E , respectively. Along DE (DE'), H is neither parallel nor orthogonal to \vec{q} . Thus both transverse and longitudinal modes are measured. The fitted results are displayed in Fig. 31: one sees that no gap is opened at the middle point between D and E . The dispersion curves cross—which would, in a lattice periodic crystal, suggest that these two modes are of different symmetry. Furthermore, the TA branch that comes from D has a horizontal slope for $q=0.691 \text{ \AA}^{-1}$ ($\parallel DE$, above the weaker Bragg peak E). The results in Fig. 31 may be reminiscent of what is observed in nonsymmorphic crystals for modes having a wave vector parallel to a screw axis when they are pictured in a two-fold extended-zone scheme. Along the direction EE' , we have another example of measured dispersion curves. Here, the wave vector \vec{q} is parallel to a twofold direction. Thus one expects to see the TA modes from E and E' . Experimentally, the situation is slightly more complex, and these TA modes are observed along with modes that come from the D reflection. For instance, at the midpoint F , the spectrometer is set in a longitudinal geometry for the point D ; hence one may measure, in the same scan, TA modes from the E, E' peaks and the LA mode emanating from the D reflection. For all the other points along EE' , the symmetry of the phonon coming from D is not pure. Figure 31 sums up all the results gathered along this ($EDE'FE$) path; in particular, it can be seen that at the midpoint F there is a gap

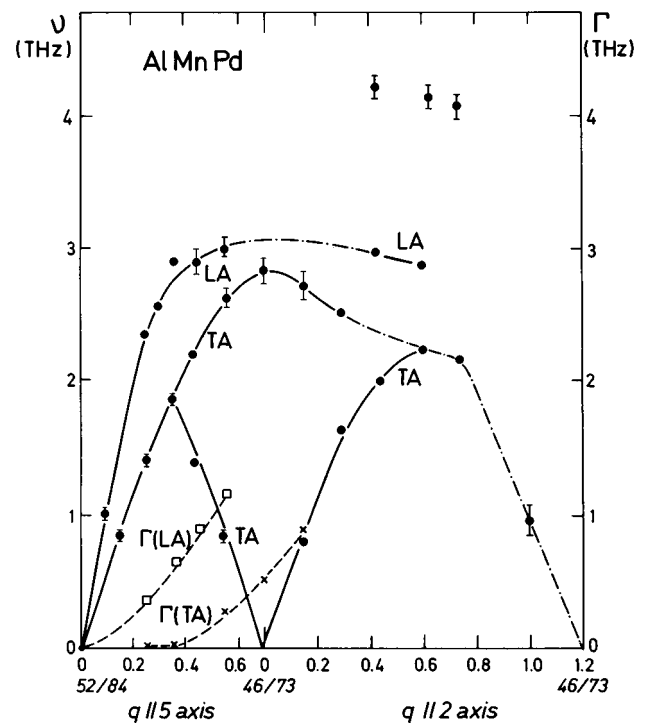


FIG. 31. Dispersion relation between points D (52/84) and E (46/73) of icosahedral AlMnPd. The linear dispersion of transverse and longitudinal acoustic modes is shown as solid lines. Broken lines are a guide for the eye. The damping Γ of the harmonic oscillator used during the fitting procedure is also drawn as a function of q for both transverse acoustic (\times) and longitudinal acoustic (\square) modes. There is a dispersionless optic mode around 4 THz. After de Boissieu *et al.* (1993).

on the TA branches which comes from E and E' , respectively, suggesting that they are truly of the same symmetry.

(2) A second path drawn along $D'H$ (parallel to a threefold symmetry direction) between the two Bragg reflections 52/84 and 70/113 at a distance of 1.64 \AA^{-1} was intensively studied. In this case the data were collected with constant- H energy scans with a constant $k_i=3.85 \text{ \AA}^{-1}$, giving an energy resolution roughly equal to 1 THz. This large value of the incident neutron wave vector k_i was necessary to fulfill the momentum-transfer condition in this region of the scattering plane. Along this path, the TA and LA modes that propagate along the threefold direction were studied, and it was seen that they present the two energy regimes described above. In the nonlinear regime of the dispersion curve, only the TA mode can be followed. As for the previous path presented above, the measured signal was fitted with a damped harmonic oscillator having, as q increased, an increasing damping, a decreasing intensity, and a quasi-harmonic frequency that also saturated around 3 THz. The dispersion curves of acoustic modes propagating along this $D'H$ direction are shown in Fig. 32. Here the TA modes reach the midpoint between the two Bragg reflections with a horizontal slope, suggesting again that symmetry relations exist between them and that the

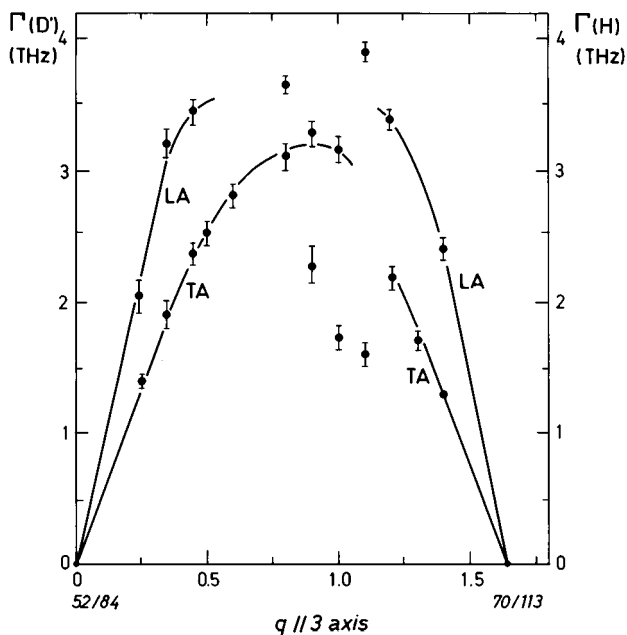


FIG. 32. Dispersion relation along the direction D' (52/84)- H (70/113) of icosahedral AlMnPd. The transverse acoustic mode emanating from $D4$ bends over in the 3-THz energy range. The low-energy mode around 2 THz is an acoustic branch arising from an out-of-plane Bragg reflection. After de Boissieu *et al.* (1993).

midpoint acts as a zone boundary.

Finally, a recent experiment (Boudard *et al.*, 1994), undertaken on a larger sample, has clearly shown the existence of four broad excitations. They are centered at 1.8, 3, 4, and 6 THz and have a width roughly equal to 1 THz. These dispersionless excitations are presented in Fig. 33 and may be referred to as “optic modes.” As will be seen in Sec. III.G, these data are in agreement with the time-of-flight results obtained by Suck (1993a).

E. Conclusions from three-axis experiments

(1) The three quasicrystal phases studied up to now with inelastic neutron scattering and presented in the three preceding subsections are ternary alloys with an aluminum-rich composition. It is interesting here to remind the reader of the early inelastic-neutron work of Stedman and Nilsson (1966) and of Yarnell (1965) on pure aluminum. In Fig. 34 we reproduce the TA mode that propagates along the [100] direction and reaches the X zone boundary at 5 THz, whereas the LA mode saturates at 9.5 THz (Stedman and Nilsson, 1966). Underneath are the corresponding phonon widths. This figure illustrates the great similarity, in the long-wavelength limit, between true acoustic modes of pure aluminum and pseudoacoustic modes of the three quasicrystalline alloys that are discussed in the preceding subsections. With the same experimental technique, Weymouth and Stedman (1970) also reported small Kohn anomalies in pure Al.

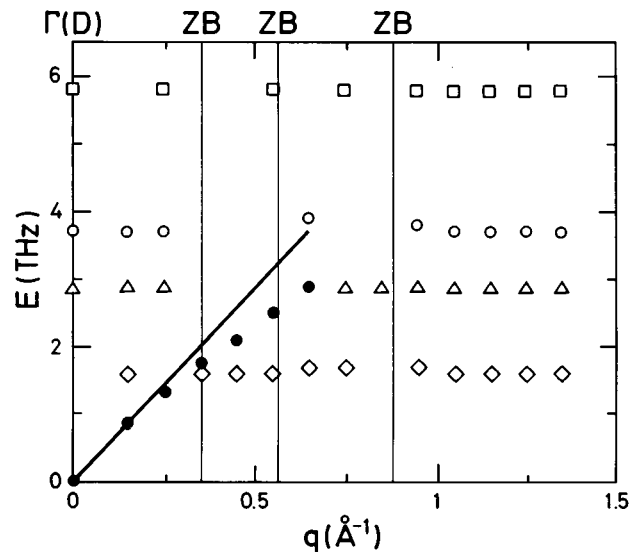


FIG. 33. Dispersion relation for excitations measured around the Bragg peak D (Γ point) in a transverse geometry. The different symbols correspond to the different maxima identified in the measured signal. The full dots are for the acoustic signal. The main pseudo-Brillouin-zone boundaries as determined from the 6D description (de Boissieu *et al.*, 1993) are indicated as ZB . After Boudard *et al.* (1994).

(2) Up to now, three-axis experiments have been undertaken only on icosahedral phases. We have described above the main results obtained for three of them. Consistent with the icosahedral point-group symmetry, acoustic modes with isotropic dispersion have been measured. In the long-wavelength limit they behave as lattice periodic crystals having a linear dispersion, no intrinsic width, and a structure factor that scales with the structure factor of the Bragg reflection from which they emanate. Thus pseudo-Brillouin zones can be defined around strong Bragg peaks, and acoustic modes are propagative modes. In this limit, the vibrational states behave as if they were extended. For larger values of q (smaller wavelength) we are more sensitive to the microscopic details of the structure. In this regime the collected data, if fitted to a damped harmonic oscillator, show a damping factor Γ that increases as q increases; at the same time a decrease of the intensity is observed which seems to be related to a spread of the signal along the energy axis. Many different processes can lead to this broadening of the signal. It may be the signature of some anharmonicity and/or we may have several nearly degenerate modes, which—due to the “pseudolocalization” expected from theoretical predictions—have a weak dispersion and overlap.

(3) Friedel and Denoyer (1987) generalized to quasicrystals the Hume-Rothery criterion and proposed a pseudo-Brillouin zone built with the most intense Bragg reflections. This pseudozone is an approximation that defines the smallest distance between atoms. For AlFeCu and AlMnPd this pseudozone is a triacontahedron generated by 30 vectors $N=20$, $M=32$ [Eq. (3.3)] ($K=3.13 \text{ \AA}^{-1}$ and 3.063 \AA^{-1} for AlFeCu and AlMnPd,

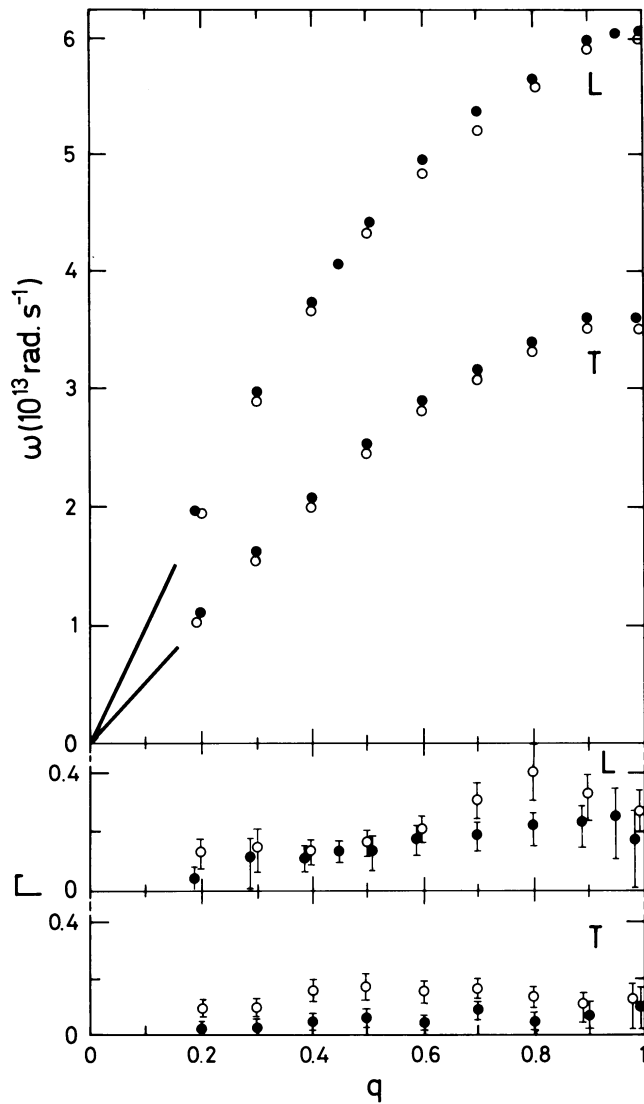


FIG. 34. Dispersion curves for aluminum at 80 K (●) and 300 K (○) along the [100] direction. Underneath are corresponding phonon widths. After Stedman and Nilsson (1966) (9 in units π/a).

respectively) truncated by a dodecahedron generated by 12 vectors $N=18$, $M=29$ ($K=2.96 \text{ \AA}^{-1}$ and 2.913 \AA^{-1} for AlFeCu and AlMnPd, respectively). For AlCuLi the pseudozone is built up with 60 vectors $N=26$, $M=41$ ($K=3.15 \text{ \AA}^{-1}$). Following this simple model we would expect a gap opening at the pseudozone boundary located at about $q=1.5 \text{ \AA}^{-1}$. This pseudozone behavior seems to have been observed in AlMnPd, for the two TA modes that start from the two Bragg reflections on a twofold axis— D and D' —which propagate with a wave vector parallel to a twofold axis (Fig. 30).

(4) The Hume-Rothery rule is a special case, for alloys, of a more general property studied in metals by Peierls (1955). This property has received an important illustration in the so-called “Peierls transition,” or conductor-insulator transition, which occurs in compounds exhibiting charge-density-wave instabilities. For such a transition, a static electronic charge-density wave

develops within the conduction-electron gas and a gap opens at the Fermi surface. The important point to emphasize here, following Peierls’s analysis, is that the lattice is also involved in the transition and, as a result of coupling between lattice and charge density, a lattice distortion generally develops coupled to the charge-density wave. The wave vector of the modulation is $q_\delta=2k_F$, which is not commensurate to the underlying lattice, and therefore the insulating phase is incommensurate. In many metallic layered dichalcogenides, such as 2H-TaSe₂ and 2H-NbSe₂, where such a transition is known to occur, a mode softening at the large Kohn-like anomaly has been measured by inelastic-neutron scattering (Moncton *et al.*, 1977). For the sinusoidal regime in the incommensurate phase, the phason and amplitudon modes have also been seen with the same experimental technique (Pouget *et al.*, 1991).

(5) In contrast to quasicrystals, for this class of compounds and for incommensurate dielectric materials it is possible to define an average structure. Therefore an average Brillouin zone exists in which dispersion curves may be represented. This gives a frame of reference for studying how modes of the periodic-lattice crystalline state are modified in the incommensurate phase. Inside this average Brillouin zone one expects that gaps will open at $1/2(G+m q_\delta)$ ($m=2,3,4,\dots$), where q_δ is the wave vector of the first-order satellite reflection, the largest gap occurring at $1/2 q_\delta$. In addition, in the simple case in which the modulated distortion is well approximated by a sinusoidal function ($\lambda=2\pi/q_\delta$), coupling terms between modes of the average structure are induced by this new periodicity and give rise to a “rearrangement” of low-frequency dispersion curves. More specifically, we observe two branches connected to the fluctuations of the phase and of the amplitude of the modulation, the phason and the amplitudon, respectively. If the higher-order satellites at $q_{2\delta}, q_{3\delta}, \dots$ become large enough, they act as second-order parameters. In this soliton (discommensuration) regime the distortion is no longer sinusoidal, and more coupling terms are allowed. Therefore the original scheme of dispersion curves of the average phase is quite modified. In such a nonlinear regime there is no sliding phason, but, as stated by Currat and Janssen (1988), phasons are more like jumps of atoms between atomic positions across an energy barrier. Thus there are several points in common between incommensurate crystal phases and quasicrystals, and these similarities show up as well in the lattice dynamics.

(6) For the icosahedral quasicrystalline phases, the dispersion curves obtained by three-axis measurements may be represented in a pseudozone scheme centered around a strong Bragg peak. Inside such a pseudozone, gaps located at Bragg planes (Brillouin planes) are expected, and we may think that, in analogy to the soliton regime in incommensurate structures, the complex picture reflected in the dispersion curves results from coupling terms in the potential energy, which are induced by several periodicities that are not commensurate. One may ask: is the semiconductor behavior observed in qua-

quasicrystalline alloys connected with a mechanism whereby lattice and electron density are coupled?

F. Ultrasonic and Brillouin measurements

1. Introduction

Group-theoretic arguments lead to the conclusion that icosahedral quasicrystals are elastically isotropic. The elastic stiffness is described by a fourth-rank tensor C_{ijkl} , which is invariant for appropriate rotations. The elastic tensor in an icosahedral phase contains only two independent components—associated with the longitudinal and the shear acoustic modes, respectively. As pointed out by Bak (1985, 1986), Lubensky *et al.* (1985) and Lubensky (1988), the behavior of icosahedral quasicrystals in the hydrodynamic regime is based on six continuous variables associated with the phases of the six mass-density waves needed to describe the icosahedral state. The free energy of the icosahedral phase is invariant under the translation operation of a 6D space. This allows us to define six continuous symmetries in the real 3D space that are associated with six hydrodynamic acoustic vibrational modes. Three of these translational symmetries transform as the irreducible vector representation of the icosahedral point group; they can be identified as rigid displacements corresponding to shifts of the 6D crystal along a 3D plane parallel to the real space and give the usual acoustic modes. The three remaining symmetries represent internal rearrangements of the atoms, and they are associated with displacements of the 6D crystal normal to the 3D real space. These last symmetries are similar to the phase shift in incommensurate systems and are the so-called “phasons.” These latter modes are diffusive because atomic distances are not conserved, while acoustic modes are true Goldstone modes. In the expression of the elastic energy of a quasicrystal there are phonon and phason terms, plus a coupled phonon-phason term. Thus we expect, on the one hand, that an experiment carried out on an icosahedral phase in the long-wavelength limit, using, for example, ultrasonic technique, will exhibit elastic isotropy and ultrasonic-attenuation anisotropy, and, on the other hand, that any experiment related to inelastic measurements should give an indication of a quasielastic signal very near elastic peaks. In Secs. III.F.2 and III.F.3 we present ultrasonic data that are available for the two icosahedral phases AlCuLi (Reynolds *et al.*, 1990) and AlMnPd (Amazit *et al.*, 1992). In Sec. III.G we shall describe time-of-flight results, which reveal a quasielastic response that can be related to the phason excitation.

2. Al_{5.1}CuLi₃

Reynolds *et al.* (1990) performed an ultrasonic experiment on a single-grain quasicrystal of composition Al_{5.1}CuLi₃ grown from the melt at a rate of 2 mm/hr. The sample was cut with faces perpendicular to a twofold axis and a fivefold axis. Pulsed longitudinal and transverse sound waves were sent through the samples and velocity measurements for each mode were taken

TABLE IV. Ultrasonic shear velocities measured along the twofold and fivefold axes and corresponding elastic constants for Al_{5.1}CuLi₃ (Reynolds *et al.*, 1990).

Axis	v_l 10 ⁵ (cm/s)	v_t 10 ⁵ (cm/s)	C_{11} (dyn/cm ²)	C_{44} (dyn/cm ²)
2	6.4±0.1	3.8±0.1	1.0	0.35
5	6.5±0.2	3.7±0.2	1.0	0.33

using the transit-time method. It was shown that the longitudinal and the transverse sound velocities (v_l and v_t , respectively) are the same along the twofold and fivefold axes, and that v_t is independent of polarization along the twofold axis. These results are thus consistent with a system whose elastic response can be described by two elastic coefficients, C_{11} and C_{44} . In this experiment the authors were unable to observe the anisotropy of the acoustic attenuation, which is not incompatible with the symmetry, due to experimental limitations. The results are summarized in Table IV ($\rho=2.464$ g/cm³).

3. Al_{68.7}Mn_{9.6}Pd_{21.7}

Amazit *et al.* (1992) made ultrasonic measurements on the large Bridgman-grown sample that was already used in the neutron three-axis experiment described above. The sample was cut with faces perpendicular to a twofold axis and a fivefold axis. Both longitudinal and shear velocities were measured accurately using a resonance method. The resonance frequencies are given by $\nu=n \times v/2l$, where v is the phase velocity of the wave (v_l or v_t), n is an integer, and l the thickness of the sample. In this experiment, the absolute values of v_l and v_t were determined with an accuracy of 2.10^{-3} m/s, and it was shown that when the polarization of the shear waves propagating along a twofold axis is changed the velocity remain the same within an experimental uncertainty of 10^{-4} . Results are summarized in Table V ($\rho=5.08$ g/cm³).

Amazit *et al.* (1992) also undertook differential measurements to investigate with good accuracy the anisotropy of the attenuation. They compared the temperature dependence of the shear-wave attenuation for different polarizations. Significant differences, which confirm theoretical predictions, were observed when measuring the attenuation of shear waves propagating along a twofold axis with a polarization either parallel to another twofold axis or parallel to the fivefold axis. Figure 35 shows that the evolution with temperature of these attenuations is different and that the slopes are not identical. The diminution of the attenuation when tem-

TABLE V. Ultrasonic shear velocities measured along the twofold and fivefold axes, and corresponding elastic constants for Al_{68.7}Mn_{9.6}Pd_{21.7} (Amazit *et al.*, 1992).

Axis	v_l (m/s)	v_t (m/s)	C_{11} (GPa)	C_{44} (GPa)
2	6512	3595	215	65
5	6530	3590	216	65

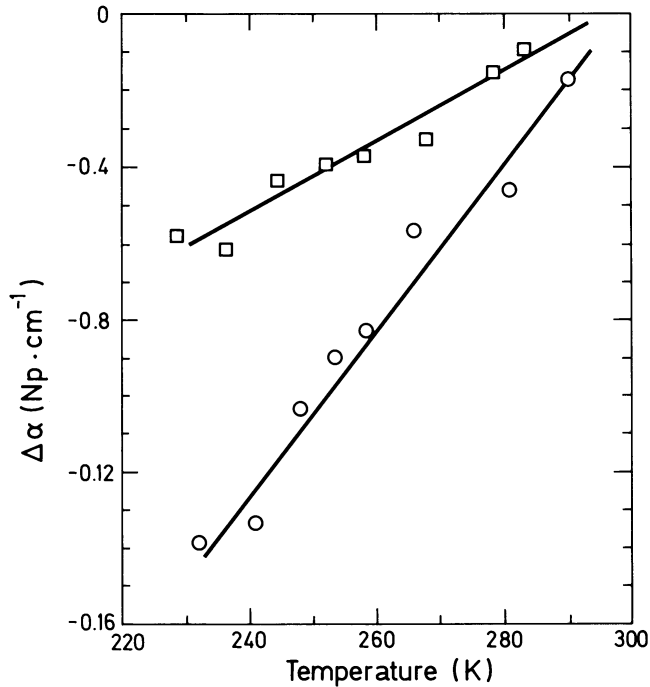


FIG. 35. Temperature dependence of ultrasonic attenuation $\Delta\alpha$ for shear waves propagating along a twofold axis in icosahedral AlMnPd. The polarization is parallel either to a twofold axis (○) or to a fivefold axis (◇). After Amazit *et al.* (1992).

perature is decreased suggests that this attenuation must be related to a thermally activated process.

So far, the ultrasonic technique is the only one that can be used for high-accuracy measurements of long-wavelength excitations in a quasicrystalline alloy.

4. Brillouin spectroscopy experiments

Brillouin spectroscopy experiments are rather difficult for alloys. The penetration of light into an opaque material is determined by its conductivity. It is well known that for a metal it is very hard to detect bulk phonon modes, and only surface phonons will be observed in a Brillouin experiment on a quasicrystal. Up to now Vanderwal *et al.* (1992) have performed the only Brillouin measurements to be published in the literature. They studied acoustic surface waves in the quasicrystal $\text{Al}_{63.5}\text{Cu}_{24.5}\text{Fe}_{12}$. The sample used in this experiment was polycrystalline and mechanically polished. Backscattering geometry was employed with a tandem Fabry-Perot interferometer operating in a five-pass configuration, along with standard optics and an argon-ion laser. The spectrum consists of a sharp peak at the frequency of the Rayleigh wave (ν_R), followed by a shoulder extending towards the high-energy side, where bulk waves are allowed. It was proposed that a continuum of coupled shear and longitudinal bulk acoustic phonons (called Lamb waves) modulated the sample surface, giving rise to scattering. From these data the bulk longitudinal acoustic-wave velocity v_l was shown to be 7191 m/s

TABLE VI. Sound velocities in AlFeCu for the surface Rayleigh, and transverse and longitudinal acoustic modes (m/s) and corresponding elastic constants (Vanderwal *et al.*, 1992).

v_R (m/s)	v_t (m/s)	v_l (m/s)	C_{11} (dyn/cm ²)	C_{12} (dyn/cm ²)
3529	7191	3809	2.3×10^{12}	1.0×10^{12}

(smaller than in the neutron experiment). Then the bulk transverse-wave velocity v_t was calculated using the following equation:

$$\left[2 - \left(\frac{v_R}{v_t}\right)^2\right]^4 = 16 \left[1 - \left(\frac{v_R}{v_l}\right)^2\right] \left[1 - \left(\frac{v_R}{v_t}\right)^2\right]. \quad (3.8)$$

In this equation, v_R is the Rayleigh surface-wave velocity. Assuming elastic isotropy, the elastic constants are calculated from the velocities ($\rho=4.5$ g/cm³). The experimental results obtained for the AlFeCu sample are presented in Table VI.

In this work, the corresponding values of v_R , v_l , and v_t for pure aluminum were also measured to be 2845 m/s, 6393 m/s, and 3022 m/s. From these data it was concluded that the quasicrystal behaves very much like a metal for surface Brillouin scattering measurements.

G. Time-of-flight experiments

1. Introduction

In a triple-axis experiment one measures the wavelength of the neutron, while in a “time-of-flight” experiment one determines its velocity. From the incident-neutron flux, a six-chopper device allows one to obtain narrow monochromatic bursts. An appropriate choice of phase differences between the windows of the six disks leads to selected incident wavelengths in the range 1–10 Å. After scattering, the final energy of neutrons is determined by measuring the time of flight (Δt) of the neutron over a well known flight path (L) between sample and detector [$E_f=0.5m_n(L/\Delta t)^2$]. The angular position 2θ of the detector yields the final momentum. Then one obtains the scattering function $S(\vec{H}, \omega)$.

2. Generalized vibrational density of states and total dynamic structure factor

Since the first work by Miceli *et al.* (1986) on AlMn, dynamical properties of alloys presenting an icosahedral phase have been studied on powder samples by Suck *et al.* (1987) using the thermal time-of-flight spectrometer IN4 and the cold-neutron time-focussing time-of-flight spectrometer IN6 of the high-flux reactor at the Institut Laue-Langevin in Grenoble. These experimental data were compared to those obtained using the same experimental technique for metallic glasses and crystalline phases having closely related composition. All the systems investigated are listed in Table VII.

The generalized vibrational density of states (GVDOS) under investigation is the weighted sum of the Fourier transform of the normalized velocity autocorrelation functions; it reads as

TABLE VII. List of alloys with noncrystallographic point symmetry studied with neutron time-of-flight technique.

$\text{Al}_{80}\text{Mn}_{20}$	Miceli <i>et al.</i> , 1986	icosahedral, crystallized
$\text{Pd}_{58.8}\text{Si}_{20.6}\text{U}_{20.6}$	Suck, 1987	glassy, icosahedral, crystallized
$\text{Al}_{74}\text{Mn}_{20}\text{Si}_6$	Suck, 1988	icosahedral, crystallized ($\alpha+\beta$)
$\text{Al}_{65}\text{Cu}_{20}\text{Fe}_{15}$	Suck, 1990	melt spun, slow-cooled and annealed
$\text{Al}_{57}\text{Li}_{32.2}\text{Cu}_{10.8}$	Suck <i>et al.</i> , 1990	$T2$ phase, R phase (slow-cooled and annealed)
AlMn	Suck <i>et al.</i> , 1990	decagonal, crystalline (μ phase)
$\text{Al}_{75}\text{Cu}_{15}\text{V}_{10}$	Suck and Guentherodt, 1990	glassy, icosahedral, crystallized
$\text{Al}_{62}\text{Cu}_{25.5}\text{Fe}_{12}$	Klein <i>et al.</i> , 1993	icosahedral, tetragonal
$\text{Al}_{71}\text{Pd}_{19}\text{Mn}_{10}$	Suck, 1993a	icosahedral

$$G(\omega) = \frac{\sum_{i=1}^m \exp^{-2W(\vec{H})} c_i \frac{\sigma_i^{\text{sc}}}{M_i} g_i(\omega)}{\sum_{i=1}^m \exp^{-2W(\vec{H})} c_i \frac{\sigma_i^{\text{sc}}}{M_i}}, \quad (3.9)$$

where $\exp^{-2W(\vec{H})}$ is the Debye-Waller factor, c_i is the relative concentration, σ_i^{sc} is the scattering cross section, and M_i is the mass of the element i in the sample, while g_i is its partial density of states. The total dynamic structure factor $S(H, \omega)$ is then determined. Among the systems listed in Table VII, PdSiU and AlCuV are the only two that can be stabilized in the three states—the glassy, icosahedral, and crystalline phases. They are therefore good candidates for a reasonable comparison of physical properties and especially of atomic dynamics. One could expect drastic changes in the GVDOS in going from an amorphous phase to a long-range-ordered phase, but in both PdSiU and AlCuV the GVDOS of the icosahedral phase and of the glassy phase are strikingly similar. For example, as shown in Figs. 36 and 37 for AlCuV, the GVDOS, which consists of three main bands with maxima near 14.5 meV (for the glassy phase) or 16 meV (for the icosahedral phase), 22 and 29 meV, is changed

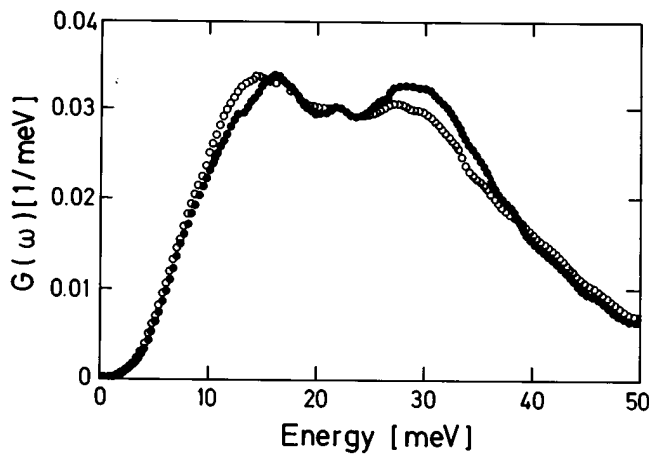


FIG. 36. Generalized vibrational density of states (GVDOS) of the metallic glass (\circ) and of the icosahedral phase (\bullet) in $\text{Al}_{75}\text{Cu}_{15}\text{V}_{10}$. The maxima of the three main bands are near 14.5 MeV (glass), 16 MeV (icosahedral phase), 22 MeV and 29 MeV. After Suck (1990a).

by less than 10% for energies between 6 and 45 meV in going from the glass to the icosahedral phase. The only important changes are the shift of the maximum of the band at lowest energy and a slight decrease of intensity at the low-energy slope. One does not find the spiky structure that appears in the density of states for some icosahedral models. This is perhaps due to the quality of the samples. The density of states is more in agreement with the calculations presented by Poussiguet *et al.* (1994).

On the other hand, it is seen that the GVDOS of the icosahedral alloy and of the crystallized sample present the same three bands, but after crystallization of the icosahedral alloy the first maximum becomes very sharp and there is a drastic loss of low-energy modes. The presence of low-energy modes in the GVDOS of disordered solids is normal (Buchenau *et al.*, 1988), but is

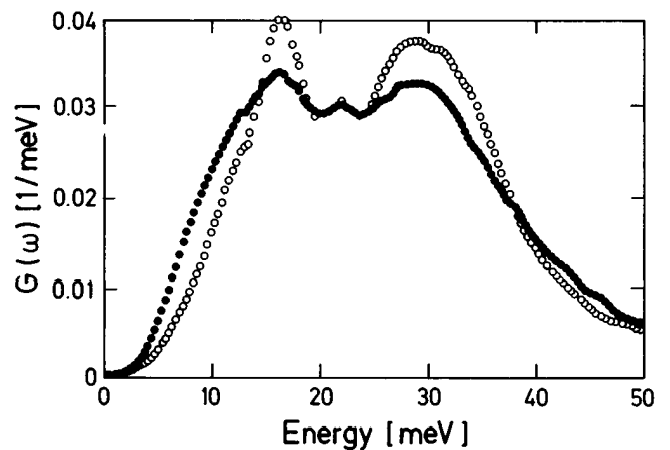


FIG. 37. GVDOS of the icosahedral alloy $\text{Al}_{75}\text{Cu}_{15}\text{V}_{10}$ (\bullet) and of the crystalline sample $\text{Al}_2\text{Cu}, \text{Al}_3\text{V}$ (\circ). The maxima of the three main bands remain the same after crystallization of the icosahedral alloy, but the first maximum becomes sharp and a drastic loss of low-energy modes is observed at the transition from the icosahedral phase to the crystallized sample. After Suck (1990b).

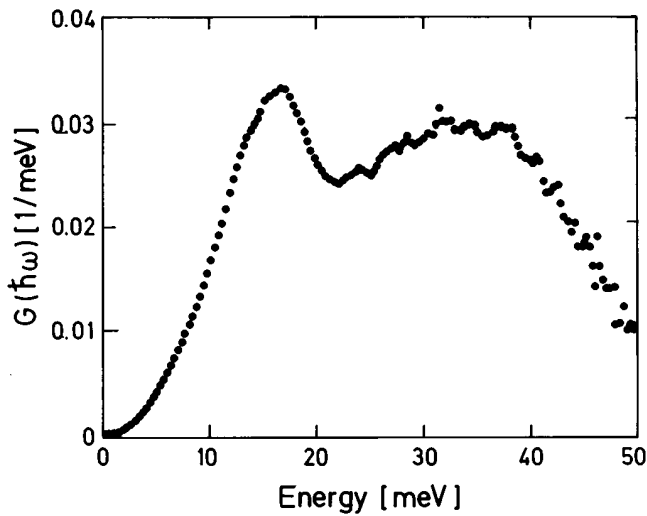


FIG. 38. GVDOS of slowly cooled icosahedral $\text{Al}_{71}\text{Pd}_{19}\text{Mn}_{20}$ measured at 120 K with thermal-neutron energy-loss spectroscopy. The region between 0 and 8 MeV is bridged by a Debye model fitted to the measured data. After Suck (1993a).

quite unexpected for quasicrystals. In thermodynamically stable icosahedral alloys such as AlFeCu or AlMnPd these low-energy modes do not show up. It was concluded that low-energy modes are found in metastable icosahedral alloys obtained by a rapid quench where disorder (phason strain, lattice defects, fluctuating decoration) is known to occur. Let us consider the GVDOS for icosahedral $\text{Al}_{71}\text{Pd}_{19}\text{Mn}_{10}$, presented in Fig. 38. It consists of two main broad bands centered near 16 meV and 33 meV separated by a pseudogap near 22 meV; its profile looks very similar to the GVDOS obtained for the other icosahedral phases. The lowest-energy band is easily related to the modes measured in the three-axis experiment on the monodomain sample of

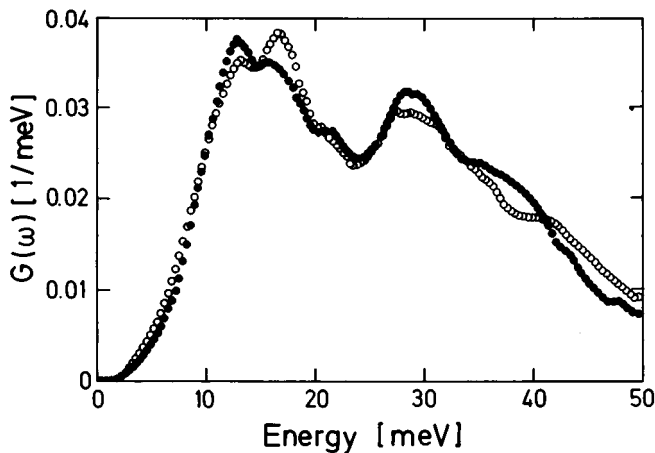
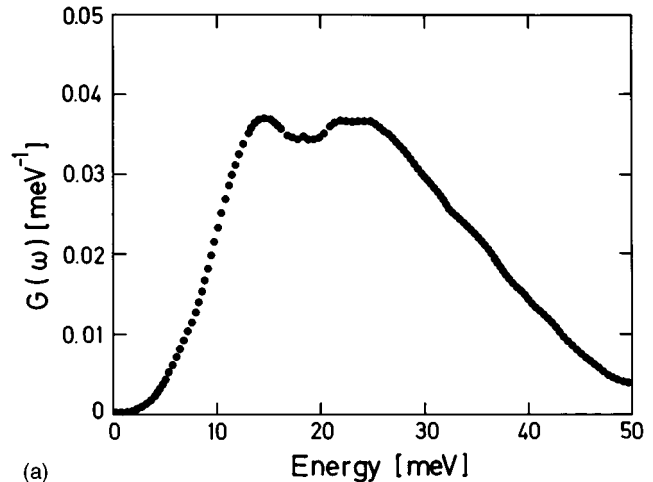


FIG. 39. GVDOS of $\text{Al}_{57}\text{Cu}_{10.8}\text{Li}_{32.2}$ (T_2 phase) (\circ) and $\text{Al}_{56}\text{Cu}_{12}\text{Li}_{32}$ (R phase) (\bullet). Two main bands are clearly distinguishable with a shallow pseudogap near 23.5 MeV. Only the band at lower energy transfers is well resolved in this experiment. After Suck (1990c).

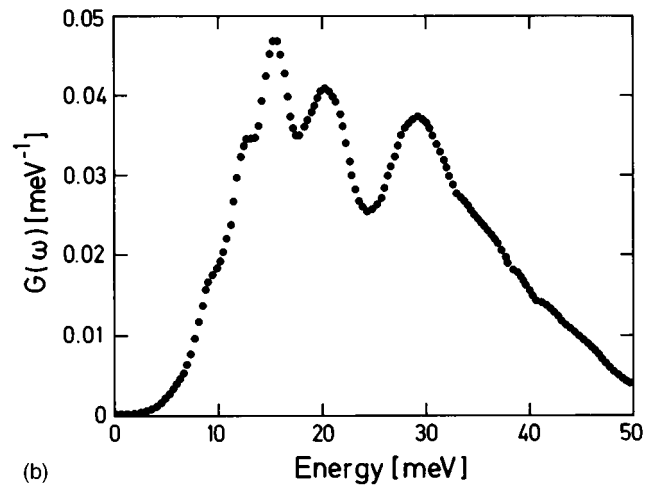
this same phase, whereas the second broad maximum clearly relates to the recent evidence of optic modes found by Boudard *et al.* (1994).

When we further compare the GVDOS of the crystalline and of the icosahedral states of the alloys AlLiCu and AlFeCu , displayed in Figs. 39 and 40, respectively, we see that while the peak positions remain the same in the icosahedral and the crystalline phases, the broad band at lowest energies becomes a sharp peak for the crystal, in spite of the fact that there is a large number of atoms in the unit cell (160 atoms for $R\text{-AlCuLi}$).

In conclusion, we have seen that, in agreement with the theoretical prediction presented in Sec. II, the GVDOS of each icosahedral alloy measured with a time-of-flight spectrometer has a profile that is broad and with little structure. In contrast, the GVDOS of approximant crystalline phases, when available, have a profile that is strongly structured. The low-energy modes are present in the GVDOS of icosahedral phases that are not perfect.



(a)



(b)

FIG. 40. GVDOS measured with inelastic cold-neutron scattering in neutron energy gain at 280 K: (a) icosahedral $\text{Al}_{62}\text{Cu}_{25.5}\text{Fe}_{12.5}$; (b) tetragonal $\text{Al}_{70}\text{Cu}_{20}\text{Fe}_{10}$. After Klein *et al.* (1993).

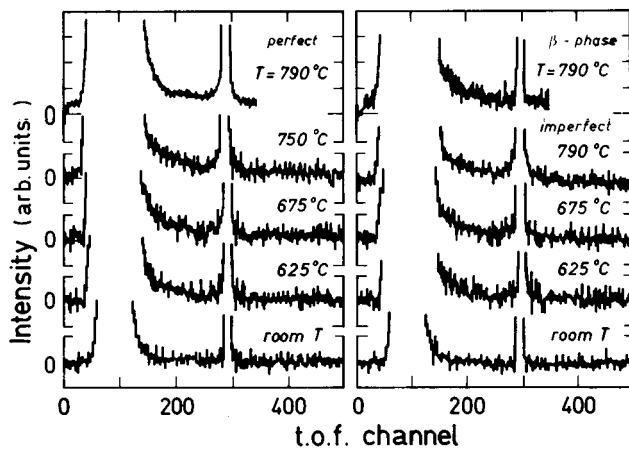


FIG. 41. Time-of-flight spectra on an enlarged scale to bring out the low-intensity features in AlFeCu. The maximum of the (triangular) elastic peak (channel 279) is not shown. The broad peak between channels 50 and 150 corresponds to phonons in neutron energy gain. The Lorentzian at the foot of the elastic peak is the signature of phason hopping, which has disappeared completely at room temperature. After Coddens *et al.* (1991).

3. “Phason hopping”

Recent experiments with the time-of-flight spectrometer MIBEMOL of the Léon Brillouin Laboratory in Saclay (Coddens *et al.*, 1991) gave the first evidence of another type of excitation, a dynamical phason mode. A first series of experiments was carried out on three nonisotopic samples with compositions $\text{Al}_{62}\text{Cu}_{25.5}\text{Fe}_{12.5}$ (perfect sample), $\text{Al}_{63}\text{Cu}_{24.5}\text{Fe}_{12.5}$ (imperfect sample), and $\text{Al}_{50}\text{Cu}_{25}\text{Fe}_{25}$ (β phase). The perfect sample exhibited sharp Bragg peaks with widths that were given by the experimental resolution and was stable in the icosahedral phase within the entire temperature range (20 °C–800 °C). The imperfect sample was annealed for one hour at 800 °C and two hours at 600 °C. This sample remained perfect down to 700 °C, but exhibited a morphological evolution between 700 °C and 650 °C. The samples were encapsulated in Nb cylinders and mounted in a furnace. The experiments were carried out with incoming neutrons having a wavelength of 7 Å and an energy resolution of 77 μeV full width at half maximum (FWHM). Runs were made at 790, 750, 675, 625 °C, and at room temperature. The results are presented in Fig. 41.

They clearly exhibit a quasielastic component at the foot of the elastic peak for the two icosahedral samples; this component disappears completely for T lower than 600 °C. For the crystalline sample no quasielastic signal could be observed in the entire temperature range of the experiment. This quasielastic response is well fitted by a Lorentzian function having a FWHM Γ equal to 95 meV. This signal has tentatively been associated with “phason hopping” of a relaxation time $\tau=7$ ps. For the well-known model of atomic jumps between equivalent sites separated by a distance d , the incoherent scattering function is given by

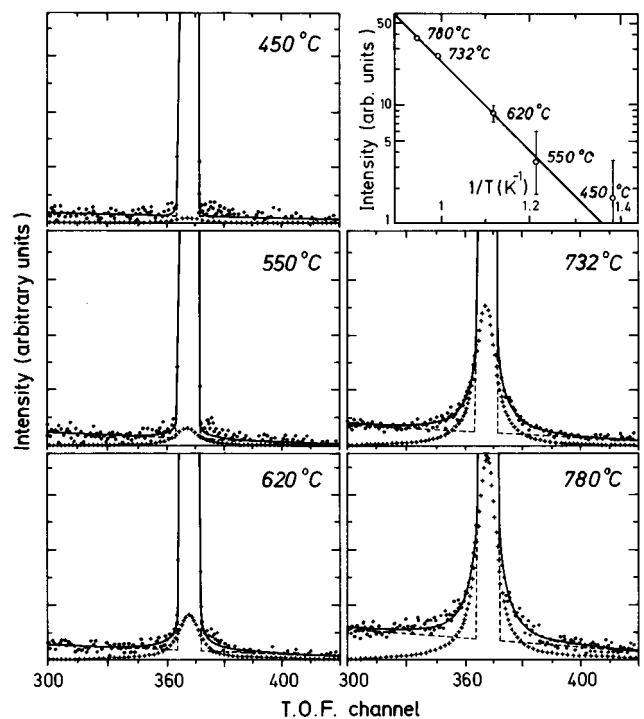


FIG. 42. Temperature dependence of the quasielastic scattering for the ^{65}Cu sample (see text). The inset shows the Arrhenius plot for the total intensity I . After Coddens *et al.* (1993).

$$S(\vec{H}, \omega) = 0.5[1 + j_0(Hd)]\delta(\omega) + 0.5[1 - j_0(Hd)]L(\omega)\exp(-2W), \quad (3.10)$$

where \vec{H} is the scattering vector, j_0 the zeroth-order spherical Bessel function, $\exp(-2W)$ the Debye-Waller factor, and $L(\omega)$ a Lorentzian function. The quasielastic signal was further studied in a detailed experiment (Coddens, 1993; Coddens *et al.*, 1993); using the method of isotopic substitution—which allows separation of the contributions of different atomic species. The nominal sample composition was $\text{Al}_{62}\text{Cu}_{25.5}\text{Fe}_{12.5}$. Several samples were used, with each natural atomic species being replaced by a pure isotope. Data were collected for samples prepared with ^{54}Fe , ^{57}Fe , ^{63}Cu , ^{65}Cu , and $^{65}\text{Cu}/^{57}\text{Fe}$, and they demonstrate that the signal was entirely due to Cu motion. These results also indicated that the width Γ of the quasielastic response is H independent, which means that it does not correspond to long-range translational diffusion. An effective jump distance $d=3.9$ Å was determined from the position of the intensity maximum. This is close to a second-neighbor distance Cu-Cu of 4.06 Å given by diffraction data. Furthermore, Γ was shown to be temperature insensitive, while the intensity I followed an Arrhenius law (Fig. 42).

This is opposite to the normal situation and characteristic of cooperative motion, i.e., of assisted hopping. Aubry (1993) has suggested that “breathers” could be responsible for such hopping. Breathers are localized long-lived vibrations that have a large amplitude. They are encountered in anharmonic systems as solutions of nonlinear dynamical equations. These breathers are re-

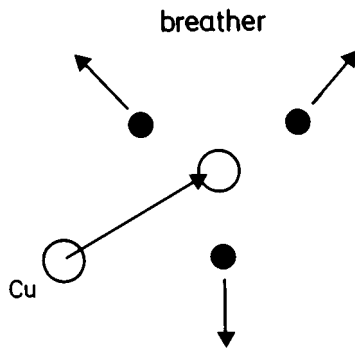


FIG. 43. Hopping of the Cu atom assisted by a breather. The observed displacement of Cu atoms in the icosahedral phase AlFeCu requires an abnormally large displacement of neighboring Al atoms.

possible, in the system, for regions in which the thermal energy is self-localized. Their density is temperature dependent, so the experimental quasielastic response will have an intensity that increases as the temperature is raised, whereas its width is nearly constant. It is this localized thermal energy that will assist the hopping of Cu atoms above the energy barrier, which would otherwise be too high (Fig. 43).

Hopping is a dynamic phason phenomenon, in contrast to the static phason strain in many quasicrystals. Because the hopping occurs between two almost degenerate levels, this possibility is perhaps supported by a study of the acoustic shear waves at high frequency, in which Vernier *et al.* (1993) showed the existence of tunnelling states in AlMnPd. Although there is not yet an unambiguous explanation for these results, the correspondence between Vernier's and Coddens *et al.* (1991) results shows that the dynamics of quasicrystals are richer than those of lattice periodic crystals.

IV. CONCLUDING REMARKS

In recent years we have seen a rapid increase in our knowledge of systems with a high degree of order but without lattice periodicity. In particular, incommensurate crystal phases and quasicrystals have been studied. For the latter, increasing quality and size of available samples have made it possible to study the lattice dynamics. Experimental advances have been paralleled by the development of theoretical models. In this way we have reached the stage of basic understanding. Although many details still remain to be investigated, and only samples of a specific class—the icosahedral quasicrystals—have been studied, we believe that the principles are now understood. It turns out that quasicrystals have, like IC phases, much in common with lattice periodic systems. On the other hand, there are fundamental differences.

For IC phases several examples have been observed of phase transitions via a soft mode, additional optically active modes, and modes that are characteristic of IC

phases: the phasons and amplitudons. The effects of quasiperiodicity in quasicrystals are usually more pronounced, but modes equivalent to soft modes, amplitudons, and phasons do not occur.

Model studies of lattice dynamics in quasicrystals have been carried out on one-dimensional chains, two- and three-dimensional tilings, and three-dimensional model systems with icosahedral symmetry. Only in one-dimensional systems has it been possible to prove mathematically certain properties. In the models one finds propagating waves. In the 1D case it has been shown that the spectrum is singular continuous, generally speaking, and the wave functions are critical. In higher dimensions the long waves behave like extended states, but for higher frequencies the character is closer to that of a critical or pseudolocalized state. For the dynamic structure factor this implies that, for low frequencies, there are well-defined and narrow ridges along dispersion curves, which broaden for higher frequencies. The density of states shows many peaks, corresponding to generalized van Hove singularities.

These theoretical findings are in agreement with experiments carried out by means of inelastic neutron scattering. The samples under investigation were icosahedral phases of AlCuFe, AlMnPd, AlCuLi, and AlMn. The main features of the experiments are understood.

There remain several open questions. The character of the spectrum for 2D and 3D systems has been studied only numerically. Mathematical analysis is still missing here. In models on tilings, one finds self-similarity properties of the states. It is unclear to what extent these are determined by the scaling properties of the underlying tiling. There is some evidence for the role of phason hopping in dynamical processes, but this point still has to be investigated theoretically.

In experiment, the existence or nonexistence of gaps in the dispersion curves is not clear. This is partly due to the still rather small size of the samples. Size has also made it hitherto impossible to investigate other quasicrystal systems. A good candidate without icosahedral symmetry is the decagonal phase, but here one has to wait for an improvement in quasicrystal growing techniques.

In model calculations, the properties of approximants other than the simplest ones do not differ much from those of the quasicrystal. It would be worthwhile to study a series of approximants by experimental means as well.

For lattice periodic systems, lattice-dynamics studies are simplified enormously by the use of the lattice periodicity. The character of the spectrum and the wave functions are fully understood. The quasiperiodic systems are beginning to be understood, but this remains a rich field for research. Just as quasiperiodic systems have forced crystallographers to reconsider the fundamentals of their field, these systems show remarkable properties in their physics as well.

ACKNOWLEDGMENTS

One of us, M.Q., warmly thanks S. Aubry, G. Coddens, G. Heger, B. Hennion, J. M. Luck, and B. Perrin

for fruitful discussions and is grateful to M. de Boissieu, M. Boudard, M. Cornier-Quiquandon, A. Goldman, J. M. Perez-Mato, and J. B. Suck for having been able to profit greatly from their work.

REFERENCES

- Amazit, Y., M. de Boissieu, and A. Zarembowitch, 1992, *Europhys. Lett.* **20**, 703.
- Ashraff, J. A., J. M. Luck, and R. B. Stinchcombe, 1990, *Phys. Rev. B* **41**, 4314.
- Ashraff, J. A., and R. B. Stinchcombe, 1989, *Phys. Rev. B* **39**, 2670.
- Aubry, S., 1993, Rapport d'activité du Laboratoire Léon Brillouin 1992–1993, p. 104.
- Aubry, S., and P. Y. Le Daeron, 1983, *Physica D* **8**, 381.
- Audier, M., and P. Guyot, 1990, in *Proceedings of the Anniversary Adriatico Research Conference on Quasicrystals*, edited by M. V. Jaric and S. Lundqvist (World Scientific, Singapore), p. 74.
- Bak, P., 1985, *Phys. Rev. Lett.* **54**, 1517.
- Bak, P., 1986, *Phys. Rev. B* **32**, 5764.
- Benoit, C., 1987, *J. Phys. C* **20**, 765.
- Benoit, C., 1989, *J. Phys.: Condens. Matt.* **1**, 335.
- Benoit, C., G. Poussigüe, and A. Azougarh, 1990, *J. Phys.: Condens. Matt.* **2**, 2519.
- Benoit, C., E. Royer, and G. Poussigüe, 1992, *J. Phys.: Condens. Matt.* **4**, 3125.
- Bernard, L., R. Currat, P. Delamoye, C. M. E. Zeyen, S. Hubert, and R. de Kouchkovsky, 1983, *J. Phys. C* **16**, 433.
- Blinç, R., J. Dolinsek, P. Prelovsek, and K. Hamano, 1986, *Phys. Rev. Lett.* **56**, 2387.
- Boudard, M., M. de Boissieu, A. I. Goldman, B. Hennion, R. Bellissent, M. Quilichini, R. Currat, and C. Janot, 1994, in *Neutrons in Disordered Materials*, Proceedings of Euroconference 94, edited by M. Dahlborg and U. Dahlborg (*Physica Scripta* **T57**, 84).
- Boudard, M., M. de Boissieu, C. Janot, G. Heger, C. Beeli, H.-U. Nissen, H. Vincent, R. Ibberson, M. Audier, and J. M. Dubois, 1992, *J. Phys.: Condens. Matt.* **4**, 10 149.
- Bovier, A., and J. M. Ghez, 1993, *Commun. Math. Phys.* **158**, 45.
- Bovier, A., and J. M. Ghez, 1995, *J. Phys. A* **28**, 2313.
- Buchenaus, U., H. M. Zhou, N. Nucker, K. S. Gilroy, and W. A. Phillips, 1988, *Phys. Rev. Lett.* **60**, 1318.
- Cahn, J. M., D. Shechtman, and D. Gratias, 1986, *J. Mater. Res.* **1**, 13.
- Cailleau, H., 1985, in *Incommensurate Phases in Dielectrics*, edited by R. Blinç and A. P. Levanyuk (North-Holland, Amsterdam), p. 71.
- Calvayrac, Y., A. Quivy, M. Bessière, M. Cornier-Quiquandon, and D. Gratias, 1990, *J. Phys. (Paris)* **51**, 417.
- Coddens, G., 1993, *Ann. Chim. Mater. (France)* **18**, 513.
- Coddens, G., R. Bellissent, Y. Calvayrac, and J. P. Ambroise, 1991, *Europhys. Lett.* **16**, 271.
- Coddens, G., C. Soustelle, R. Bellissent, and Y. Calvayrac, 1993, *Europhys. Lett.* **23**, 33.
- Cordelli, A., and P. Gallo, 1995, *J. Phys.: Condens. Matt.* **7**, 1245.
- Cornier-Quiquandon, M., A. Quivy, S. Lefebvre, E. Elkaom, G. Heger, A. Katz, and D. Gratias, 1991, *Phys. Rev. B* **44**, 2071.
- Cullum, J. K., and R. A. Willoughby, 1985, *Lanczos Algorithms for Large Symmetric Eigenvalue Computation*, Progress in scientific computing Vol. 3 (Birkhäuser, Boston).
- Currat, R., and T. Janssen, 1988, *Solid State Physics: Advances in Research and Applications, Volume 41*, edited by H. Ehrenreich and D. Turnbull (Academic, San Diego), p. 202.
- Danzer, L., 1989, *Discrete Math.* **76**, 1.
- de Boissieu, M., M. Boudard, R. Bellissent, M. Quilichini, B. Hennion, R. Currat, A. I. Goldman, and C. Janot, 1993, *J. Phys.: Condens. Matt.* **5**, 4945.
- de Boissieu, M., C. Janot, J. M. Dubois, M. Audier, and B. Dubost, 1991, *J. Phys.: Condens. Matt.* **3**, 1.
- de Lange, C., and T. Janssen, 1981, *J. Phys. C* **14**, 5269.
- de Lange, C., and T. Janssen, 1983, *Phys. Rev. B* **28**, 195.
- de Lange, C., and T. Janssen, 1984, *Physica A* **127**, 125.
- Deng, Wenji, Shizhong Wang, Youyan Liu, Dafang Zheng, and Nanzhi Zou, 1993, *Phys. Rev. B* **47**, 5653.
- Dénoyer, F., G. Heger, M. Lambert, M. Audier, and P. Guyot, 1990, *J. Phys. (Paris)* **51**, 651.
- Dorner, B., 1972, *Acta Crystallogr. Sect. A* **28**, 344.
- Dubois, J. M., C. Janot, C. Dong, M. de Boissieu, and M. Audier, 1991, *Phase Transit.* **32**, 3.
- Dulea, M., M. Johansson, and R. Riklund, 1992a, *Phys. Rev. B* **45**, 105.
- Dulea, M., M. Johansson, and R. Riklund, 1992b, *Phys. Rev. B* **46**, 3296.
- Elcoro, L., and J. M. Perez-Mato, 1994, *Acta Crystallogr. Sect. B* **50**, 294.
- Elcoro, L., J. M. Perez-Mato, and G. Madariaga, 1994, *Acta Crystallogr. Sect. A* **50**, 182.
- Frenkel, Y. I., and T. Kontorova, 1938, *Zh. Eksp. Teor. Fiz.* **8**, 1340.
- Friedel, J., and F. Dénoyer, 1987, *C. R. Acad. Sci. II, Mec. Phys. Chim. Sci. Univers Sci. Terre (France)* **305**, 171.
- Fu, Xiujun, Youyan Liu, Bolin Cheng, and Dafang Zheng, 1991, *Phys. Rev. B* **43**, 10 808.
- Fujiwara, T., 1993, *J. Non-Cryst. Solids* **153/4**, 390.
- Fujiwara, T., G. Trambly de Laissardière, and S. Yamamoto 1994, in *Quasicrystals and Imperfectly Ordered Crystals*, edited by K. H. Kuo and S. Takeuchi (Trans Tech, Switzerland), p. 387.
- Gayle, F. W., 1987, *J. Mater. Res.* **2**, 1.
- Goldman, A. I., C. Stassis, R. Bellissent, H. Moudden, N. Pyka, and F. W. Gayle, 1991, *Phys. Rev. B* **43**, 8763.
- Goldman, A. I., C. Stassis, M. de Boissieu, R. Currat, C. Janot, R. Bellissent, H. Moudden, and F. W. Gayle, 1992, *Phys. Rev. B* **45**, 10 280.
- Hafner, J., 1980, *Phys. Rev. B* **21**, 406.
- Hafner, J., and M. Krajčič, 1990, *Europhys. Lett.* **13**, 335.
- Hafner, J., and M. Krajčič, 1992, *Europhys. Lett.* **21**, 31.
- Hafner, J., and M. Krajčič, 1993a, *J. Phys. Condens. Matt.* **5**, 2489.
- Hafner, J., and M. Krajčič, 1993b, *Phys. Rev. B* **47**, 11 795.
- Haydock, R., V. Heine, D. Bullet, and M. J. Kelly, 1980, in *Solid State Physics: Advances in Research and Applications, Volume 35*, edited by H. Ehrenreich and D. Turnbull (Academic, San Diego) p. 215.
- Haydock, R., V. Heine, and M. Kelly, 1972, *J. Phys. C* **5**, 2845.
- Haydock, R., V. Heine, and M. Kelly, 1975, *J. Phys. C* **8**, 2591.
- Hiramoto, H., and M. Kohmoto, 1989, *Phys. Rev. B* **40**, 8225.
- Hiramoto, H., and M. Kohmoto, 1992, *Int. J. Mod. Phys. B* **6**, 281.
- Hofstadter, D. R., 1976, *Phys. Rev. B* **14**, 2239.

- Holzer, M., 1988, *Phys. Rev. B* **38**, 1709.
- Janot, C., M. de Boissieu, J. M. Dubois, and J. Pannetier, 1989, *J. Phys. Condens. Matt.* **1**, 1029.
- Janot, C., 1994, *Int. J. Modern Phys. B* **8**, 2245.
- Janssen, T., 1988, in *Quasicrystalline Materials*, edited by C. Janot and J. M. Dubois (World Scientific, Singapore), p. 327.
- Janssen, T., 1994, *Europhys. Lett.* **25**, 533.
- Janssen, T., and R. Currat, 1987, in *Incommensurate Crystals, Liquid Crystals and Quasi-crystals*, edited by J. F. Scott, and N. A. Clark (Plenum, New York), p. 19.
- Janssen, T., and M. Kohmoto, 1988, *Phys. Rev. B* **38**, 5811.
- Janssen, T., and J. Los, 1991, *Phase Transit.* **32**, 29.
- Janssen, T., and J. A. Tjon, 1982, *Phys. Rev. B* **25**, 3767.
- Kasner, G., D. Wegener, and H. Böttger, 1991, *Z. Phys. B* **83**, 259.
- Kitaev, A. Yu., 1988, *JETP Lett.* **48**, 298.
- Klein, T., G. Pares, J.-B. Suck, G. Fourcaudot, and F. Cyrot-Lackmann, 1993, *J. Non-Cryst. Solids*, **153/154**, 562.
- Kohmoto, M., and J. R. Banavar, 1986, *Phys. Rev. B* **34**, 563.
- Kohmoto, M., L. P. Kadanoff, and C. Tang, 1983, *Phys. Rev. Lett.* **50**, 1870.
- Kohmoto, M., and Y. Oono, 1984, *Phys. Lett.* **102A**, 145.
- Liu, Youyan, and Penghui Ma, 1991, *Phys. Rev. B* **43**, 1378.
- Liu, Z., Z. Zhang, Q. Jiang, and D. Tian, 1992, *J. Phys.: Condens. Matt.* **4**, 6343.
- Los, J., and T. Janssen, 1990, *J. Phys.: Condens. Matt.* **2**, 9553.
- Los, J., T. Janssen, and F. Gähler, 1993a, *Int. J. Mod. Phys. B* **7**, 1505.
- Los, J., T. Janssen, and F. Gähler, 1993b, *J. Phys. I (Paris)* **3**, 107.
- Los, J., T. Janssen, and F. Gähler, 1993c, *J. Phys. I. (Paris)* **3**, 1431.
- Lubensky, T. C., 1988, in *Aperiodicity and Order*, edited by M. V. Jaric (Academic, Orlando), p. 99.
- Lubensky, T. C., S. Ramaswamy, and J. Toner, 1985, *Phys. Rev. B* **32**, 7444.
- Lu, J. P., T. Odagaki, and J. L. Birman, 1986, *Phys. Rev. B* **33**, 4809.
- Luck, J. M., and D. Petritis, 1986, *J. Stat. Phys.* **42**, 289.
- Miceli, P. F., S. E. Youngquist, D. A. Neumann, H. Zabel, J. J. Rush, and J. M. Rowe, 1986, *Phys. Rev. B* **34**, 8977.
- Moncton, D. E., J. D. Axe, and F. J. DiSalvo, 1977, *Phys. Rev. B* **16**, 801.
- Moussa, F., P. Launois, M. H. Lemée, and H. Cailleau, 1987, *Phys. Rev. B* **36**, 8951.
- Niizeki, K., and T. Akamatsu, 1990, *J. Phys.: Condens. Matt.* **2**, 2759.
- Niu, Q., and F. Nori, 1986, *Phys. Rev. Lett.* **57**, 2057.
- Niu, Q., and F. Nori, 1990, *Phys. Rev. B* **42**, 10 329.
- Odagaki, T., and D. Nguyen, 1986, *Phys. Rev. B* **33**, 2184.
- Ostlund, S., and R. Pandit, 1984, *Phys. Rev. B* **29**, 1394.
- Ostlund, S., R. Pandit, D. Rand, H. J. Schellnhuber, and E. D. Siggia, 1983, *Phys. Rev. Lett.* **50**, 1873.
- Peierls, R. E., 1955, *Quantum Theory of Solids* (Clarendon, Oxford).
- Pouget, J. P., B. Hennion, C. Escribe-Filippini, and M. Sato, 1991, *Phys. Rev. B* **43**, 8421.
- Poussiguet, G., C. Benoit, M. de Boissieu, and R. Currat, 1994, *J. Phys.: Condens. Matt.* **6**, 659.
- Quilichini, M., G. Heger, B. Hennion, S. Lefebvre, and A. Quivy, 1990, *J. Phys. (Paris)* **51**, 1785.
- Quilichini, M., B. Hennion, G. Heger, S. Lefebvre, and A. Quivy, 1992, *J. Phys. (Paris) I* **2**, 1785.
- Reynolds, G. A. M., B. Golding, A. R. Kortan, and J. M. Parsey, 1990, *Phys. Rev. B* **41**, 1194.
- Severin, M., and R. Riklund, 1989, *Phys. Rev. B* **39**, 10 362.
- Shechtman, D., I. Blech, D. Gratias, and J. W. Cahn, 1984, *Phys. Rev. Lett.* **53**, 1951.
- Simon, B., 1983, *Adv. Appl. Math.* **3**, 463.
- Sire, C., and J. Bellissard, 1990, *Europhys. Lett.* **11**, 439.
- Sire, C., and R. Mosseri, 1989, *J. Phys. (Paris)* **50**, 3447.
- Stedman, R., and G. Nilsson, 1966, *Phys. Rev.* **145**, 92.
- Suck, J.-B., 1988, in *Quasicrystalline Materials*, edited by C. Janot and J. M. Dubois (World Scientific, Singapore), p. 337.
- Suck, J.-B., 1990, in *Phonons 89: Proceedings of the Third International Conference on Phonon Physics . . . Heidelberg, 21–25 August, 1989, Federal Republic of Germany*, edited by S. L. Hunklinger and G. Weiss (World Scientific, Singapore), p. 397.
- Suck, J.-B., 1993a, *J. Non-Cryst. Solids* **153/154**, 573.
- Suck, J.-B., 1993b, *J. Non-Cryst. Solids* **156/158**, 872.
- Suck, J.-B., H. Betscher, H. Rudin, P. Grütter, and H. J. Güntherodt, 1987, *Phys. Rev. Lett.* **59**, 102.
- Suck, J.-B., and H. J. Güntherodt, 1990, in *Phonons 89: Proceedings of the Third International Conference on Phonon Physics . . . Heidelberg, 21–25 August, 1989, Federal Republic of Germany*, edited by S. L. Hunklinger and G. Weiss (World Scientific, Singapore), p. 573.
- Suck, J.-B., C. Janot, M. de Boissieu, and B. Dubost, 1990, in *Phonons 89: Proceedings of the Third International Conference on Phonon Physics . . . Heidelberg, 21–25 August, 1989, Federal Republic of Germany*, edited by S. L. Hunklinger and G. Weiss (World Scientific, Singapore), p. 576.
- Süto, A., 1987, *Commun. Math. Phys.* **111**, 409.
- Süto, A., 1990, in *Number Theory and Physics*, edited by J. M. Luck, P. Moussa, and M. Waldschmidt (Springer, Berlin), p. 162.
- Toda, M., 1966, *Prog. Theor. Phys. Suppl.* **36**, 113.
- Trambly de Laissardière, G., and T. Fujiwara, 1994, in *Quasicrystals and Imperfectly Ordered Crystals*, edited by K. H. Kuo and S. Takeuchi (Trans Tech, Switzerland), p. 417.
- Tsai, A. P., A. Inoue, and T. Matsumoto, 1987a, *J. Mater. Sci. Lett.* **6**, 1403.
- Tsai, A. P., A. Inoue, and T. Matsumoto, 1987b, *Jpn. J. Appl. Phys.* **26**, L1509.
- Tsai, A. P., A. Inoue, Y. Yokoyama, and T. Matsumoto, 1990, *Philos. Mag. Lett.* **61**, 9.
- Vanderwal, J. J., P. Zhao, and D. Walton, 1992, *Phys. Rev. B* **46**, 501.
- Vernier, N., G. Bellessa, B. Perrin, A. Zarembowitch, and M. de Boissieu, 1993, *Europhys. Lett.* **22**, 187.
- Weymouth, J. W., and R. Stedman, 1970, *Phys. Rev. B* **2**, 4743.
- Windisch, M., J. Hafner, M. Krajčí, and M. Mihalkovič, 1994, *Phys. Rev. B* **49**, 8701.
- Yarnell, J. L., J. L. Warren, and S. H. Koenig, 1965, in *Lattice Dynamics: Proceedings*, edited by R. F. Wallis (Pergamon, New York), p. 57.
- You, J. Q., J. R. Yan, J. X. Zhong, and X. H. Yan, 1992, *Europhys. Lett.* **17**, 231.